The Development of Steady State and Lifetime Fluorescence Instruments for Real Time In Situ Aquatic Chemistry Measurements

by

Schuyler Senft-Grupp

S.B., Massachusetts Institute of Technology (2006)

Submitted to the Department of Civil and Environmental Engineering
in Partial Fulfillment of the Requirements for the Degree of

Doctor of Philosophy

at the

MASSACHUSETTS INSTITUTE OF TECHNOLOGY

February 2015

Signature redacted

Signature of Author..... .....
Department of Civil and Environmental Engineering
January 29, 2015

Signature redacted

Certified by.....
Harold F. Hemond
William E. Leonhard Professor of Civil and Environmental Engineering
Thesis Supervisor

Signature redacted

Accepted by..... .....
Heidi Nepf
Donald and Martha Harleman Professor of Civil and Environmental Engineering
Chair, Graduate Program Committee

The Development of Steady State and Lifetime Fluorescence Instruments for Real Time In Situ Aquatic Chemistry Measurements

by

Schuyler Senft-Grupp

Submitted to the Department of Civil and Environmental Engineering on January 29, 2015 in Partial Fulfillment of the Requirements for the Degree of Doctor of Philosophy in Environmental Engineering and Instrumentation

ABSTRACT

The development of three optical instruments for the chemical exploration and characterization of natural waters is described. The first instrument (called LEDIF) employs a novel flowcell, 6 UV LEDs as excitation sources, a wideband lamp, and a spectrometer to measure steady state chemical fluorescence and absorbance. The instrument is packaged aboard an autonomous underwater vehicle (AUV) and demonstrates the ability to map chemical concentrations in three dimensions. The second instrument repackages the sensor components to study dissolved organic matter (DOM) in tropical Southeast Asia peatland rainforests. This instrument is optimized for low power consumption over long deployments to remote locations. Two field trials in Pontianak Indonesia with durations of two and six weeks captured peatland river fluorescence measurements at 20 minute intervals. The results show changes in DOM linked to tidally induced water level fluctuations and provide insight into the complex biogeochemical dynamics of the system.

The third instrument increases the chemical sensitivity and specificity of LEDIF with the addition of fluorescence lifetime sensing capabilities. The development of this sensor for AUV deployment required the engineering of a compact, low power, high speed (GHz) data acquisition circuit board. The resulting circuit digitizes data at a rate of 1 gigasample/second and performs user customizable digital signal processing. This board is used along with a 266 nm Q-switch laser, fast photomultiplier tube (PMT), and computer controlled monochromator to build a small fluorescence lifetime instrument. The instrument is tested with solutions of low concentration pyrene to demonstrate its ability to identify small, long-lived fluorescence signals in the presence of large background fluorescence. Results indicate a pyrene limit of detection below environmentally relevant levels. The final overall instrument dimensions allows it to be packaged for future AUV deployments.

Thesis Supervisor: Harold F. Hemond

Title: William E. Leonhard Professor of Civil and Environmental Engineering

Table of Contents

List of Figures

Acknowledgements

I am incredibly fortunate to have been able to pursue the research presented in this document and none of it would have been possible without the support of many individuals. First and foremost I must thank Prof. Harold Hemond for bringing me into his lab group. In every conversation with Harry you not only learn something new but also get a piece of history or tidbit of lore to go along with it. The rest of the Hemond Lab Group, Amy, Matt, Irene, Kyle, Sarah Jane, and Charu, have also provided immense support with machining and chemistry and MATLAB, and I'll miss grabbing beers at the Muddy with you all.

I also had two great committee members, Prof. Phil Gschwend and Dr. Lewis Girod to prod me forward. As my undergraduate advisor, I remember Phil asking me where I wanted to be in 10 years. I'm still not exactly sure, but wherever it ends up being he did his part to get me there. I met Lewis on my first trip to Singapore where he took time to show us around Sim Lim Square. He continues to be a great resource for all things electronic.

It has been a very rewarding experience working with Dr. Kelvin Ng at NUS in Singapore. Kelvin's knowledge of optics is very impressive and his assistance and guidance made much of this work possible. He was also very helpful in letting me know the best places to eat when I was visiting NUS.

Parsons Lab and Course 1 have been a great place to call home for the past 12 years. Vicki Murphy and Jim Long do an amazing job taking care of all the important things so that everyone else can focus on research. Sheila Frankel and John MacFarlane keep everyone safe and provide help with all things chemistry. In addition, and in no particular order, Prof. Charles Harvey, Laure Gandois, Alex Cobb, Alison Hoyt, Mason Stahl, and Ben Scandella all provided invaluable assistance on various parts of this project.

Lastly I need to thank my family for their constant encouragement and support for me no matter what I'm up to – taking my senior year in upstate NY, driving to the Grand Canyon, or pursuing this PhD.

And finally there's Kristen. You are much more than just a resource – you are my inspiration.

Chapter 1

Introduction

1.1 Understanding Our Environment: Personal Motivation

It is a cliché, although probably true more often than not, that the childhoods of engineers are spent taking objects apart to see how they work. While I definitely disassembled a good number of discarded household appliances, my aspiration to know how things work eventually morphed into the desire to know how we know and measure... everything. In other words, what are sensors and how do they transform an abstract quantity such as temperature, oxygen concentration, or acceleration into a value that we can read off a screen?

I was also keenly interested in studying environmental science. I was fascinated with ecological systems ranging from wildlife predator-prey dynamics to global carbon cycling. Once again my mind was drawn to *how* it is even possible to study these ecological systems when there are massive numbers of critical variables that must be measured (think all the chemical compounds found in a lake) over spatial areas from puddles to oceans and time scales from seconds to geologic eras. The short answer is: one new sensor at a time.

It is for this reason that I have spent the last seven years working on a series of new field deployable aquatic chemistry instruments. It is my hope that these new tools will help scientists answer questions related to the changing environmental system and the role human impacts play.

1.2 The Case for Real Time In Situ Aquatic Chemistry Sensing

The focus of the work presented in this document is the development of sensors that can be used in the field. There are many current excellent instruments for analyzing water samples in a laboratory. However there are numerous reasons why the next generation of instruments should be capable of measuring environment parameters in situ and in real time. The following sections provide further rational.

1.2.1 Chemical Heterogeneity Exists in Water Bodies

Although often the chemical concentrations of large bodies of water (e.g. lakes) are assumed to be well-mixed in the horizontal plane, they often show significant spatial and temporal variation. The sources of chemical heterogeneity are nonuniform inputs, nonuniform transformation rates, and nonuniform physical mixing [1]. Examples of potential nonuniform chemical inputs to lakes include stream inflows, groundwater influx, and sediment point sources. Nonuniform transformation rates can be driven by patchiness of organisms for biologically mediated reactions, by system temperature variations, or by patchy light availability (e.g. clouds, plants) for light mediated reactions. Additionally, these effects can constructively combine to increase the overall heterogeneity of a particular chemical of interest. Since heterogeneity is generally both time- and space-dependent (e.g. a storm runoff event triggers the chemical heterogeneity in space), understanding the heterogeneity requires relatively rapid sensing over a potentially large physical area. Knauer [1] demonstrates that even in small lakes, simple scaling arguments can be used to show that assuming heterogeneous distributions should be the rule rather than the exception.

1.2.2 Identifying Chemical Contamination Sources

Identifying source locations and chemical fluxes of contaminants requires the ability to discern small concentration gradients. In the case of sediment contamination sources, the timescale for mixing is much shorter than the timescale of chemical transport from the sediment to the water column. Therefore the ability to take many measurements at high spatial resolution over large areas is essential. Researchers are currently exploring the use of in situ sensors to perform eddy correlation measurements for determining oxygen and dissolved organic matter sediment fluxes [2]–[4], and the development of new sensors should expand this method to additional analytes. With continuous measurements obtained from roving autonomous underwater vehicles, it may be possible to use large spatial data sets and statistical mapping techniques to identify small concentration gradients which indicate locations of contaminated sediment acting as point sources.

1.2.3 Increased Data Quality

Sample collection and handling produces errors that can be avoided by in situ measurements. The process of obtaining samples in the field and then storing and transporting them alters the sample in ways that can lead to changes in concentration of the chemical of interest. This is especially true of samples taken from deep locations in the water column, which undergo significant changes in pressure, temperature and light exposure. These physical changes can drive chemical phase changes (e.g. volatilization) or increase both chemical and biological reaction rates, in some cases leading to under- or over-estimates of the true chemical composition. Additionally, compounds can be lost through adsorption to the container or lab instruments (e.g. tubing) [5]. In situ sensing techniques, especially optical ones, remove the hurdles of sample collection and minimize the invasiveness of the measurement.

1.2.4 Rapid Emergency Response and Contamination Delineation

Deployable chemistry sensors can play a vital role in rapid response to chemical and biological emergencies. Not only can they help in quickly identifying an emerging problem, but when used on board vehicles, they can quickly delineate the extent of contamination. One of the most notable recent examples of this capability was the mapping of a 35 km oil plume at 1100m depth from the Deepwater Horizon oil spill [6].

1.2.5 New Aquatic Sensing Platforms Require New Sensors

There is currently a significant research effort underway to engineer sensing platforms for both short-term exploration and continuous, long-term observations of water bodies. In the last decade particularly, there has been an increase in the use of autonomous underwater vehicles (AUVs) as part of these sensing campaigns [7]. These sensing platforms include AUVs, autonomous surface vehicles (ASVs), buoys, and moorings working together to gather information (e.g.[8], [9]). These platforms range in size, power availability, depth rating, mission length, and communication capability. Studies using AUVs have been carried out in oceans and in lakes [10], [11]. Although recent research has made AUVs more reliable, cheaper, and easier to use, new and improved sensor packages for these vehicles have been slower to materialize [7].

1.3 Optical Sensing

Given the need for new in situ chemical sensors, there are various technologies available for further development. In situ sensors generally utilize either optical or electrical properties of chemicals to acquire measurements. Optical sensors take advantage of chemical-specific properties such as the ability to absorb light, scatter light, or fluoresce. Electrode sensors, meanwhile, use chemically driven voltage potentials or currents as proxies for concentrations. Examples of this type of sensor include ion selective electrodes, pH probes, and Clark dissolved oxygen electrodes. Of these techniques, optical sensors are the clear choice for organic compounds such as polycyclic aromatic hydrocarbons (PAHs)s, which by definition contain multiple aromatic rings that have a relatively strong ability to absorb and emit light [12].

1.4 Development of New Fluorescence Instruments for In Situ Applications

The research presented in Chapters 2 through 5 document the development of several new optical instruments for in situ study of aquatic chemistry.

Chapter 2 discusses an instrument deployed on a STARFish AUV and used to study the waters of Singapore. A compact, custom flowcell was designed to allow continuous water sampling as the vehicle moves through the water. The flowcell has 6 optical ports for fluorescence excitation sources, and a port for a wideband lamp for absorbance measurements. Resulting fluorescence and absorbance spectra can be measured with a small spectrometer and stored on the instrument's embedded computer. The fluorescence can be used to identify a range of compounds such as humic material and chlorophyll. This work demonstrates the ability to obtain water quality information at high resolution in three dimensions over large areas.

Chapter 3 focuses on a moored instrument used to measure long time series of data. The work targeted the peatland rainforests located in Southeast Asia that are currently undergoing high rates of deforestation. The effect of the deforestation on the degradation of the peat and the amounts and types of dissolved organic matter (DOM) transported via rivers is an ongoing research question. The instrument provides a way to autonomously measure the fluorescence and absorbance of the river water at 20 minute intervals for 6 weeks, and in field trials showed significant tidally linked changes in the water's optical properties. This information can be used

to understand the organic matter dynamics in a complicated hydrological system, and in the future aid in estimates of organic matter transport.

Chapters 4 and 5 discuss the details for a novel fluorescence lifetime instrument. Fluorescence lifetime measurements supply an additional dimension of data (time) to the fluorescence wavelength spectrum, providing increased chemical identification specificity and sensitivity. For these measurements a data acquisition system must capture the fluorescence signal as a function of time, with resolution on the nanosecond scale. There are no off the shelf solutions available with this capability that also meet the size, power, and computing requirements for an instrument deployable on small AUVs. Chapter 4 provides the details and performance for a generalized data acquisition circuit board capable of digitizing an analog input signal at the rate of 1 gigasamples per second. This board has several additional features, such as a high speed trigger, and can be reprogrammed to perform any digital signal processing required for the user's application.

In Chapter 5, the data acquisition board, the flowcell from Chapter 2, and additional hardware are combined to demonstrate a compact fluorescence lifetime instrument capable of deployment aboard small AUVs. The instrument uses a 266 nm Q-switched laser to excite a water sample and a monochromator to scan across fluorescence wavelengths. Solutions of pyrene dissolved in water at environmentally relevant levels are used to quantify the instrument's performance.

1.5 References

[1] K. Knauer, H. Nepf, and H. Hemond, "The production of chemical heterogeneity in Upper Mystic Lake," *Limnol. Oceanogr.*, vol. 45, no. 7, pp. 1647–1654, 2000.

[2] P. Berg, H. Røy, F. Janssen, V. Meyer, B. B. Jorgensen, M. Huettel, and D. De Beer, "Oxygen uptake by aquatic sediments measured with a novel non-invasive eddy-correlation technique," *Mar. Ecol. Prog. Ser.*, vol. 261, no. 2872, pp. 75–83, 2003.

[3] C. Lorrai, D. F. McGinnis, P. Berg, A. Brand, and A. Wüest, "Application of Oxygen Eddy Correlation in Aquatic Systems," *J. Atmos. Ocean. Technol.*, vol. 27, no. 9, pp. 1533–1546, Sep. 2010.

[4] M. P. Swett, "Assessment of Benthic Flux of Dissolved Organic Carbon in Estuaries Using the Eddy Correlation Technique," The University of Maine, 2010.

[5] H. S. Hertz, W. E. May, S. A. Wise, and S. N. Chester, "Trace Organic Analysis," *Anal. Chem.*, vol. 50, no. 4, p. 428A–434A, 1978.

[6] R. Camilli, C. M. Reddy, D. R. Yoerger, B. a S. Van Mooy, M. V Jakuba, J. C. Kinsey, C. P. McIntyre, S. P. Sylva, and J. V Maloney, "Tracking hydrocarbon plume transport and biodegradation at Deepwater Horizon.," *Science (80-.).*, vol. 330, no. 6001, pp. 201–4, Oct. 2010.

[7] T. Dickey, "Progress in multi-disciplinary sensing of the 4-dimensional ocean," in *Proceedings of SPIE*, 2009, vol. 7317, p. 731702.

[8] R. N. Smith, J. Dasa, H. Hei\dharssona, A. M. P. F. A. Ivona, L. D. Cetinićb, M. È. Garneauc, M. D. Howardc, C. Oberga, M. Raganb, E. Seubertc, and others, "The USC Center for Integrated Networked Aquatic PlatformS (CINAPS): Observing and Monitoring the Southern California Bight," *IEEE Robot. Autom. Mag.*, 2010.

[9] I. Vasilescu, C. Detweiler, M. Doniec, D. Gurdan, S. Sosnowski, J. Stumpf, and D. Rus, "AMOUR V: A Hovering Energy Efficient Underwater Robot Capable of Dynamic Payloads," *Int. J. Rob. Res.*, vol. 29, no. 5, pp. 547–570, 2010.

[10] H. F. Hemond, A. V Mueller, and M. Hemond, "Field testing of lake water chemistry with a portable and an AUV-based mass spectrometer.," *J. Am. Soc. Mass Spectrom.*, vol. 19, no. 10, pp. 1403–10, Oct. 2008.

[11] D. A. Caron, B. Stauffer, S. Moorthi, A. Singh, M. Batalin, E. A. Graham, M. Hansen, W. J. Kaiser, J. Das, A. Pereira, and others, "Macro-to fine-scale spatial and temporal distributions and dynamics of phytoplankton and their environmental driving forces in a small montane lake in southern California, USA," *Limnol. Ocean.*, vol. 53, no. 5 part 2, pp. 2333–2349, 2008.

[12] R. P. Schwarzenbach, P. M. Gschwend, and D. M. Imboden, *Environmental Organic Chemistry*, 2nd ed. Hoboken, N.J.: John Wiley & Sons, Inc., 2003.

Chapter 2

A Multi-Platform Optical Sensor for In Situ Sensing of Water Chemistry

by Chee-Loon Ng, Schuyler Senft-Grupp, and Harold Hemond, Published in Limnology and Oceanography: Methods, Vol. 10, 2012.

Author's Note: The work presented in this article was a collaborative effort. The individual authors each had distinct responsibilities and deliverables for the project. Senft-Grupp designed and fabricated all of the custom instrument electronics and was the developer of the sensor operating software, iLEDLIF. Ng was responsible for all optical designs and the majority of chemical testing. Hemond oversaw the project, providing expertise as needed. The design of the physical flowcell was jointly developed by the authors, with multiple versions fabricated both at MIT and NUS.

Abstract

A compact field-deployable optical instrument utilizing fluorescence, absorbance, and scattering to identify and quantify contaminants and natural substances in water bodies is described. The instrument is capable of deployment on autonomous underwater and surface vehicles, manned vehicles, fixed platforms such as buoys, or access points in water supply or drainage networks. The instrument comprises (1) a flowcell, (2) multiple optical systems, (3) a data logger, (4) a power control board and computer, and (5) a battery. The instrument has been packaged in a cylindrical pressure case of 200 mm diameter and 300 mm length for electrically and mechanically seamless insertion as a STARFISH AUV payload module. The same module can be fitted with watertight end caps for use aboard other platforms, or simpler packaging can be employed for use in less demanding environments. For spectrofluorometry, the system uses six (expandable to twelve) electronically-switchable excitation sources, allowing the construction of fluorescence excitation-emission matrices (EEMs). A deuterium-tungsten light source (185 to

1100 nm) is used in making UV-VIS absorbance measurements. Turbidity can be measured by nephelometry, using observations of light scattering at each excitation wavelength. The absorbance and turbidity capabilities provide useful water quality information and can also be used for correction of inner filtering effects. Validation of the instrument includes (1) comparison with a commercial luminescence spectrometer in measuring both standards and field samples, (2) comparisons of observed spectra with published optical characteristics for several chemicals, and (3) field demonstration aboard an AUV.

2.1 Introduction

Understanding the chemistry of natural waters often relies on the collection of samples, followed by transport to a laboratory, followed by chemical analysis. This time consuming and costly process introduces time delay and puts practical limits on the number of measurements that can be obtained in a given water body. Also, uncertainty can be introduced as samples undergo degradation during transport to the laboratory. Finally, low-density data sets obtained via manual sampling may fail to adequately capture spatiotemporal variability, which can sometimes hold the key to understanding biogeochemical processes in water bodies.

Recent developments in environmental *in situ* instrumentation and platforms have begun to address the above limitations. In the last decade particularly, there has been an increase in the use of *in situ* sensors and novel sensor platforms used as part of environmental sensing campaigns [1]. Platforms include autonomous underwater vehicles (AUVs), autonomous surface vehicles (ASVs), buoys, and moorings (e.g. [2], [3]), and range widely in size, power availability, depth rating, mission duration, and communication capability. Chemical studies using AUV platforms have been carried out in oceans, and also more recently in lakes (e.g. [4], [5]). However, although AUV platforms are becoming more available and easier to use, new and improved chemical sensor packages for these vehicles have been slower to materialize [1].

Chemical instrumentation suitable for autonomous *in situ* operation includes but is not necessarily limited to membrane-inlet mass spectrometers [4], optical devices such as fluorometers and spectrophotometers, electrochemical sensors [6], and flow injection analyzers. Each above type of sensor is intrinsically best suited to certain categories of substances (e.g. membrane inlet mass spectrometry for gases but not humic materials, electrochemical sensors for

ionic species but not most organic species). In the present case we focus on optical sensing by means of fluorescence, absorbance, and scattering.

The potential to make optical measurements *in situ* has been enhanced by recent advances in light emitting diodes (LEDs), which are now available at reasonable cost in a wide range of wavelengths, from 245 nm through the infrared region (www.thorlabs.com). This enables LED-excited fluorescence spectrum measurements to be made at a substantial number of excitation wavelengths, thus providing 2-dimensional data sets, often called excitation-emission matrices (EEMs). In this role LEDs offer several advantages over alternate narrowband light sources. Compared to broadband lamps paired with either monochromators or filters, LEDs generally have advantages of lower power usage, higher efficiency, cooler running temperatures, smaller size, and lower cost. Compared to laser sources, LEDs are less expensive and are available in a wider range of wavelengths. The negative aspects of LEDs typically include wider emission bands than those of lasers or sources using a lamp and monochromator; LEDs also often have lower power output and present more difficulty in focusing the beam as compared with laser sources [7]. Compared with EEMs obtained using excitation from a broadband lamp and monochromator, EEMs obtained using LED excitation typically contain a smaller number of excitation wavelengths, specific to the LEDs used. Nevertheless, the advantages of LEDs are compelling. LEDs have now been used in a wide range of optical sensing devices [8]–[14] and researchers have begun to demonstrate field-capable instruments. For example, Obeidat et al. [15] describe a 1.5 kg spectrofluorometer for analyzing plant and animal feed in the field, using excitation sources ranging from 405 to 640 nm; and power is supplied by a laptop computer which also captures, stores and analyzes the resulting EEMs. Other work includes the development of a single UV LED field spectrofluorometer for reagent-based characterization of selenium concentrations in river water [16], and a fiber optic *in vivo* LED fluorescence instrument for real-time medical imaging [17].

Commercial suppliers such as WET Labs, Turner Designs, Seapoints, and YSI produce optical sensors specifically designed for measurements in natural waters, including spectrometers for absorbance measurements, turbidity sensors, and fluorometers for measuring specific compounds or chemical groups such as dissolved organic matter, crude oil, rhodamine, and chlorophyll. The sensors generally use a single LED excitation source and an emission detector with a filter, with LED and filter both chosen for the optimum wavelength bands for the

parameter of interest. The output of a single-wavelength-pair fluorometer, however, is intrinsically incapable of identifying or correcting for interferences [18]. Ocean Optics Inc. and StellarNet Inc. both supply spectroscopy accessories such as spectrometers and fiber optics that are generally smaller, easier to use, and less expensive than typical laboratory equipment, and which have been applied to environmental analyses [15]–[17], [19], [20].

To the authors' knowledge, however, no low-cost instrument capable of deployment aboard a small AUV and exploiting both the spectral absorbance and the fluorescence EEM of natural waters yet exists. This paper provides details for a field instrument, named LEDIF, that has been built to address this need, and is made possible by advances in LED technology, advances in commercially available optical components, advances in low-cost single board microcomputers, and a valuable and a growing literature discussing LED-based field instruments. LEDIF measures fluorescence, absorbance, and turbidity of natural waters. It is specifically designed for incorporation as a payload module of a STARFISH developed by National University of Singapore Acoustic Research Laboratory [21] or the MIT Sea Grant Reef Explorer, but with some variation in packaging can be used manually or can be installed on multiple other types of autonomous platforms. Applications include but are not limited to long-term monitoring, guiding rapid response to environmental chemical releases, developing adaptive sampling strategies for autonomous vehicles, and facilitating basic water quality research. This manuscript discusses the design and optical performance of LEDIF; equally important issues of signal processing will be discussed elsewhere.

2.2 Materials and Procedures

2.2.1 Sensor Module Overview

The layout of LEDIF and its typical modes of deployment are shown in 1.1.1.1Figure 2.1. The optical functions of LEDIF rely on a custom designed flowcell fitted with light emitting diodes (LEDs) of different wavelengths, focused on the analytical volume and oriented 90 degrees from the main axis of light collection by a series of adjustable optics. To measure absorbance, a broadband (185 to 1100 nm) light source coupled via an optical fiber illuminates the flowcell at 180 degrees to the light collection system. Turbidity is also estimated within the flowcell by measuring the amount of excitation light scattered at 90 degrees (i.e. nephelometry).

For all measurements (fluorescence, absorbance, and turbidity), light from the flowcell is observed with an Ocean Optics USB4000 spectrometer, and the data are recorded with a single board computer running custom software under a Linux operating system. LEDIF uses switching DC-DC converters to efficiently provide 5 and 12 VDC to various subsystems from either an internal battery or from any external power supply voltage between 12 and 72 volts DC (VDC), a range which encompasses voltages used on a very large number of AUVs.

2.2.2 Flowcell geometry

A compact [~37(W) x 61(L) mm] optical flowcell permits the measurement of a water's fluorescence spectrum, absorbance spectrum, and turbidity within the same analytical volume (1.1.1.1Figure 2.2). The optic junctions for optical attachment use UV transmissive fused silica windows with O-ring seals. Six junctions arranged perpendicular (90 degrees) to the detecting optic junction are used to provide excitation to the analytical volume for fluorescence and turbidity measurements. A similar optic junction arranged directly opposite (180 degrees) to the light-collecting optic junction is used to illuminate the volume for absorbance measurement. A collector lens, with focal length equal to the distance from the lens to the optical intersection with the perpendicular excitation optical paths, is fitted in front of the detecting optic junction to enhance collection of light emitted by fluorescence. Fluid flow into the flowcell occurs via a pathway that contains two 90 degree bends to minimize the entrance of stray light.

2.2.3 Excitation-Emission Optical System

A series of [~12.7(Dia) x 25.4(L) mm to 12.7(Dia) x 50.8(L) mm] LED-based light sources produce optical excitation for the analytical volume. The light produced by the LEDs is focused to the geometrical center of the flowcell, in line with the detection optical path, using compound lenses chosen to accommodate the divergence angle associated with each respective LED. The lenses are mounted inside lens tubes, and optical adjustments are performed using retaining rings, which are locked in place after adjustment to minimize susceptibility to mechanical disturbances. This compact packaging allows each excitation LED to be connected directly to the flowcell without the use of optical fiber, as shown in 1.1.1.1Figure 2.2. For absorbance measurement, the light produced by a broadband (185 to 1100 nm) deuterium-tungsten (12 VDC at 0.6 A) source is focused with a plano-convex lens into an optical fiber, and

the exiting light is collimated with another plano-convex lens and redirected with a right angle prism mirror to the optic junction of the flowcell. A collector lens with a single core fiber is used for the collection of photons from fluorescence and scattering, and for collection of transmitted light in absorbance mode.

2.2.4 Power Control Board

The instrument requires a custom circuit board for power conditioning. 1.1.1.1Figure 2.3 shows the block diagram of the power control board of LEDIF, which powers various loads at 5 or 12 VDC. It provides efficient DC-DC conversion of external power at 12 to 72 VDV (e.g. from a 48 V AUV battery) to 5 VDC and 12 VDC. One 5 VDC output for the embedded computer is always on when the board is powered. Two outputs of 5 VDC at 2.5 A maximum and one output of 12 VDC at 2.5 A maximum are provided; these are used (at less than their maximum current ratings) to power the spectrometer and the deuterium-tungsten light source. Eight current-limited outputs at user selectable 5 VDC or 12 VDC, rated up to 100 mA, are provided for the excitation LEDs. Three 5 VDC software-controlled variable-current outputs are supplied for future expansion, such as alternate broadband light sources for absorbance measurement, or shorter-wavelength excitation sources that may become available in the future.

2.2.5 Computer

The sensor is controlled by an onboard single-board-computer (SBC) manufactured by Technologic Systems (Model TS-7260-64-128F). The TS-7260 uses an ARM9 200 Mhz CPU with 64 MB of RAM, 128 MB of Flash memory, and 2 GB (expandable) USB flash storage, and runs a Debian Linux operating system (OS). The SBC has 3 serial COM ports, 2 USB ports, 1 Ethernet port, 30 digital input/output (DIO) pins, and two analog to digital converter (ADC) pins. The DIO and ADC pins are software controlled. A battery-backed real time clock retains synchronized sensor-host clock information for mission time-stamp. An on-board temperature sensor allows direct measurement of board temperature in the field. The microcomputer uses Ethernet for communication with a host platform such as the STARFISH. In addition, a serial port (RS-232) can be connected to the SBC for software development and diagnostic purposes. The USB 2.0 (12 Mbits/s max) port is used for connection with the 2 GB of flash storage and a COM port is used for communication with the spectrometer (Ocean Optics USB4000). The

microcomputer is connected to the power control board using the added TS-XDIO (PN: OP-XDIO) port. Further technical data can be found at: (http://www.embeddedarm.com/documentation/ts-7260-manual.pdf).

2.2.6 Software

Custom software (iLEDLIF; the extra "L" refers to the capability to control laser-excited instruments as well as LED-excited instruments) was written to control all sensor functionality. iLEDLIF was designed to be easily configurable and to handle asynchronous communication between multiple devices. The software is written in C++ using standard C/C++ libraries, and runs within Debian Linux on the embedded TS-7260 computer. iLEDLIF handles communication with external devices (e.g. spectrometer) over serial, USB, Ethernet, or DIO connections as well as with virtual devices implemented entirely in software (e.g. a data analysis device). On startup iLEDLIF reads an XML configuration file to load the device modules currently connected to the sensor, which allows for easy customization of the sensor hardware (e.g. changing excitation LEDs). Once all device modules have been initialized, iLEDLIF passes commands from the operator or AUV to the specific devices. iLEDLIF also has a built-in scripting language which enables users to generate text files of series of commands without needing to write or compile C++ code. These text files can be written or modified in the field, allowing the operator to automate scanning and spectra storing processes for a specific mission.

2.2.7 Spectrometer

Light transmitted through the sample volume or emitted by fluorescence from the sample volume is quantified by an Ocean Optics USB4000 spectrometer, which uses an uncooled TCD1304AP CCD (charge-coupled device) as its detector and is equipped with: (1) UV4 Quartz windows, (2) variable longpass order-sorting filters to block 2nd and 3rd order light (part number OFLV-4), (3) a cylindrical lens to increase light collection efficiency by the CCD (part number L4), and (4) the widest available entrance slit (200x1000 μm) to provide maximum light throughput. This slit width corresponds to a wavelength resolution of ~7.5 nm. Although the spectrometer is capable of higher resolution using narrower slit settings, this setting is acceptable given the characteristically broad fluorescence emission peaks of most analytes of interest, and the larger slit width allows for greater spectrometer throughput. The detector response is

wavelength dependent; the manufacturer-specified number of received photons per count of output are 130 and 60 at 400 nm and 600 nm, respectively. The optical bench uses a f/4 asymmetrical cross Czerny-Turner design with a SMA 905 inlet fitting, and has a 0.22 numerical aperture at the inlet that is matched to the connecting optical fiber. The integration time for each emission spectrum capture is software selectable from 3.8 ms to 10 s. Further technical information on the spectrometer is available at: (http://www.oceanoptics.com/technical/USB4000operatinginstructions.pdf).

2.2.8 Sample Flow

To minimize power consumption when deployed on an AUV, LEDIF samples water without use of a pump, using ram pressure to drive fluid through the flowcell as the AUV moves. To verify satisfactory flow conditions, three-dimensional transient flow modeling of the (x-z plane) symmetrical liquid chamber (meshed with 212,016 cells of hybrid hex/tet mesh) was performed with Fluent (Version 12) software. The typical (0.21 million cells) mesh captured flow features identical to those obtained with a high density (1.05 million cells) mesh (1.1.1.1Figure 2.4(d) and (e)), showing the adequacy of the chosen mesh density. Flow through a LEDIF mounted aboard a STARFISH was simulated for several vehicle velocities, to visualize the flow and determine if flow was obstructed, as well as to estimate the time required for water parcels both to reach the flowcell and to be flushed out. Each elbow was found to generate a local circulation that reduced the effective cross-sectional diameter of the flowpath. Particles were tracked to determine chemical transport and residence times; typical particle pathlines are shown in 1.1.1.1Figure 2.4(b). The model shows that all tracked particles (335 particles tracked for high density mesh and 91 particles tracked for typical mesh) escape through the outlet, with the maximum transit time for 95% of particles plotted in 1.1.1.1Figure 2.4(c) at various vehicle velocity conditions. Transit time was approximately 0.8 s at the standard 3 knot cruising speed of STARFISH. This value is shorter than a typical measurement duration (several seconds), and therefore it is concluded that the sample flow does not limit data spatial resolution.

2.3 Assessment

The performance of LEDIF was compared with that of a Perkin Elmer (PE) LS-55, a commercially available luminescence spectrometer that uses a pulsed xenon lamp (200 to 800

nm) as the source of excitation, and records emission spectra from 200 to 900 nm. The wavelengths in the PE LS-55 are selected with an excitation monochromator and an emission monochromator. The manufacturer's stated wavelength accuracy is +/-1 nm with a scanning speed of 10 to 1500 nm / minute with 1 nm increments. The signal-to-noise ratio is stated as 2500:1 RMS at the baseline and 750:1 RMS for observing water Raman using 350 nm as excitation (http://www.perkinelmer.com/Catalog/Product/ID/L2250107).

2.3.1 Fluorescence Peak Validation

Fluorescence peaks are assessed by comparing the fluorescence spectrum of an aqueous solution of rhodamine B and chlorophyll a measured with LEDIF against the corresponding spectrum from the PE LS-55 (1.1.1.1Figure 2.5). For spectrum display purposes the emission spectrum intensity of the PE LS-55 is normalized by a factor equal to $I_{LEDIF(Saturation)} / I_{PE(Saturation)} =$ ~63.5. This normalization is for display purposes only and is not an attempt to correct the spectra for differences in wavelength specific response. The emission peaks of rhodamine B and chlorophyll a observed by the two sensors are in agreement within 1 nm; the emission peaks of rhodamine B and chlorophyll a reported by LEDIF were at 575 nm and 677 nm, respectively, agreeing well with values from the literature. For LEDIF, the peak amplitude of 405 nm is higher than 370 nm because the optical output of the 405 nm LED is approximately 4 times that of the 370 nm LED.

2.3.2 Field Samples Comparison

Emission spectra of pore waters collected from multiple depths at a peatland in Brunei are shown in 1.1.1.1Figure 2.6. The fluorescence of these waters is attributed primarily due to high levels (10s of mg/L) of dissolved organic carbon (DOC). Emission spectra from LEDIF at 405 nm excitation and the PE LS-55 at 390 excitation were measured. The fluorescence peak from LEDIF is shifted longer by ~50 nm compared to the PE LS-55. This shift can be attributed to the longer excitation wavelength and the wavelength dependent response of the USB4000 which has not been corrected for with this data. Both LEDIF and the PE LS-55 instruments captured an ~15% increase in fluorescence maxima as the depth from which the samples were collected increased.

2.3.3 Multi-spectral and EEM Demonstration

The ability of LEDIF to capture an emission-excitation matrix is demonstrated by measuring an aqueous solution containing five chemicals, each relevant to natural water studies. 1 ppm naphthalene, 135 ppb pyrene (i.e. at its solubility), 5 ppm of a commercial humic acid, 0.2 ppm rhodamine B, and 5 ppm chlorophyll a were selected to represent, respectively, a semi-volatile pollutant, a higher-molecular-weight semi-volatile PAH, humic material, a widely-used tracer, and algal biomass. 1.1.1.1Figure 2.7 shows the EEM of the mixture: each chemical peak can be clearly identified by inspection. Wavelengths of individual emission peaks of the chemicals were compared with published fluorescence peaks from PhotochemCAD (Du et al. 1998) and found to be in very good agreement (1.1.1.1Figure 2.7). Note that many of the data in Du et al. (1998) are for compounds dissolved in a different solvent, potentially contributing to small differences in the location of fluorescence peaks.

Another meaningful comparison between LEDIF and the PE LS-55 is the instrumental detection limit (IDL). IDL is defined as:

$$IDL = 3\sigma$$

where σ denotes standard deviation of repeated measurements at a single concentration. Using an excitation wavelength of 405 nm for both instruments, the detection limit of rhodamine B was 2.5 ppb and 2.1 ppb for LEDIF and the PE LS-55, respectively. For an excitation wavelength of 370 nm, the detection limit was 4 ppb and 3.2 ppb for LEDIF and the PE LS-55, respectively. For the mixture described above, LEDIF had a detection limit of ~50 ppb naphthalene, ~7 ppb pyrene, ~420 ppb humic acid, ~1 ppb rhodamine B, and ~5 ppb chlorophyll a, with each detection limit being obtained at the optimum excitation wavelength.

2.3.4 Absorbance Measurement

The absorbance spectra at various concentrations of aqueous rhodamine B at its wavelength of maximum absorbance is shown in 1.1.1.1Figure 2.8(a). Based on 1.1.1.1Figure 2.8(b), absorbance as low as 0.01 was adequately measured by LEDIF at this wavelength. The absorbance peak is observed at 552 nm, which falls within the range of 550-554 nm (shaded region) reported by the manufacturer (Panreac). In addition, the profile of the absorbance curve recorded by LEDIF was compared with the graph published by PhotochemCAD using ethanol as solvent (Du et al. 1998) and found to be very similar. Based on linear fitting to the Beer-Lambert

curve and the pathlength (4.0 cm) of LEDIF's flowcell, the molar absorptivity was calculated as 0.17 L mol^{-1} cm^{-1} and the individual measurements at different concentrations are reported as 0.16 L mol^{-1} cm^{-1} (0.2 ppm), 0.19 L mol^{-1} cm^{-1}(1 ppm), and 0.17 L mol^{-1} cm^{-1} (2 ppm).

2.3.5 Turbidity Measurement

Turbidity measurement was demonstrated using a calibration standard made of styrene divinyl benzene copolymer beads in water (AMCO CLEAR®TURBIDITY STANDARD manufactured by GFS Chemicals, Inc). 1.1.1.1Figure 2.9 shows the scattered light spectra using 405 nm excitation and various levels of turbidity, as well as resulting calibration curves for turbidity in the 0-1 Nephelometric Turbidity Unit (NTU) and 0-40 NTU ranges, using a 200 ms integration time. Three ranges of turbidity were tested: (1) 0 to 1 NTU in 0.2 NTU increments, (2) 0 to 10 NTU in 2 NTU increments, and (3) 0 to 40 NTU in 20 NTU increments. These ranges are representative of samples ranging from finished drinking water to many natural waters. 40 NTU does not reflect the upper bound limits of LEDIF, however, as higher turbidities can be measured by using shorter integration times, different excitation wavelengths, or lower optical power. Turbidity as low as 0.1 NTU can be measured, demonstrating a potential application in monitoring processed drinking water, for which a typical upper limit specified by water authorities is 1 NTU.

2.3.6 Pressure and Temperature Effects

Given that LEDIF is intended for in situ deployment, the sensor response as a function of pressure was assessed using chlorophyll-a as an example from 0 to 120 psi gauge pressure. It was found that the effect of pressure on sensor response was less than 2% difference, which is immaterial. There is no evidence that LEDIF response to temperature at any anomalous function and we anticipate this affects LEDIF similar to other instruments. Fluorescence is known in general to decrease with increased temperature [22], although the dependence varies among compounds; Downing et al. [23] have measured the temperature dependence for the case of DOM. The STARFISH vehicle, and likely most other platforms on which LEDIF would be deployed, carries a temperature sensor that may be used for temperature corrections if desired. A second possible temperature effect occurs via mechanisms that cause instrument response to vary with temperature. The USB4000 spectrometer CCD has 13 black pixels that are not exposed to

incoming light, but are read each time that a spectrum is read from the instrument. The average of these pixels corrects for baseline offset for the resulting spectrum, while the variance among these pixels provides an estimate of the noise. These values are used in post processing to correct for temperature effects on the detector. We did not examine temperature effects that may exist due to various temperature coefficients of the LEDs, although users seeking the most precise data in environments of widely varying temperature, such as thermally stratified lake, might wish to measure appropriate correction factors. Typically, LED forward voltage decreases at rate of a few mV (out of several volts) per K.

2.3.7 Field Deployment

Because an AUV host represents one of the more demanding platforms for *in situ* real time measurement, we present data demonstrating the successful operation of LEDIF as a payload for an AUV. 1.1.1.1Figure 2.10 shows a 3D subsurface mapping of chlorophyll a concentration performed with LEDIF aboard STARFISH in the late morning of 20th December 2011 at Pandan reservoir, Singapore. In this demonstration, the vehicle covers an area of 150x80 m with an AUV "lawnmower" mission scheme, operating from the surface to 3 m depth (with 1 m increment) in one mission per depth. Total duration of the experiment, including all 4 missions was 1 hour 26 minutes. The measurements demonstrated the successful operation of LEDIF in the freshwater environment for accessing the aforementioned information rapidly and with spatial resolution of 12 m.

2.4 Discussion

LEDIF is demonstrated to measure fluorescence excitation-emission matrices, optical absorbance, and light scattering for a variety of substances of importance in natural waters. Turbidity as low as 0.1 NTU can be measured, and the instrument can operate autonomously aboard an AUV or surface vessel without requiring a sample pump. LEDIF can be built at moderate cost using mostly commercial off-the-shelf components; the materials bill for the unit tested here is approximately $15,000 Singapore dollars (order of $12000 US dollars at the time of writing). Power consumption (0.5W in standby mode, <10 W in all active measurement modes) is low enough that it imposes only a minor energy burden on an AUV host; in fact, in deployments aboard STARFISH, LEDIF internal battery was paralleled with the vehicle battery

and actually subsidized the vehicle's energy budget. LEDIF software allowed the vehicle to manage operation of the instrument, a feature that is especially favorable where adaptive sampling, plume tracking, real-time monitoring as part of a network, or other advanced operating modes are envisioned. Table 1 shows the size, power consumption, and performance of LEDIF compared to three presently (at time of writing) available filter-type commercial instruments.

2.5 Comments and Recommendations

Because LEDIF relies on the transverse velocity of the host vehicle to create water flow through the flowcell, a pump may be needed to draw sample through the flowcell in the case of some alternate platforms (e.g. certain buoys). The flowcell was demonstrated to withstand >10 bars of pressure without leakage; higher pressure versions are doubtless possible by using thicker quartz windows. If power consumption is of utmost important and the absorption peak of the compound of interest falls within the wavelength range, the deuterium-tungsten lamp can be replaced by multi-wavelength LED. Optical design of a tri-wavelength package was investigated; it is expected that performance will be enhanced by improvements in commercially available LEDs, and will be reported in future work. At least two straightforward means are available for reducing the size and power consumption of LEDIF. For applications in which substantial on-board signal processing is not required, it is possible to replace the microcomputer with a microcontroller. We have demonstrated a version of LEDIF that uses the popular Arduino Uno microcontroller board, which has a 69(L) x 53(W) mm footprint and consumes less than a half of a watt of power at 5 VDC (this number is approximate and can be lower depending on fraction of time spent in sleep mode, frequency of write cycles, etc.). It would also be possible to replace the USB4000 spectrometer with a subminiature spectrometer such as the Ocean Optics STS, whose volume is less than half that of the USB4000 and whose power consumption is only 0.75 watt (vs. 1.25 watts for the USB4000). Low intrinsic power usage, and control by a microcomputer that can enter sleep mode, make LEDIF inherently suited to deployment where little power is available, such as remote installations utilizing solar panels.

2.6 Acknowledgements

Funding for this work was provided by the Singapore National Research Foundation (NRF) through the Singapore-MIT Alliance for Research and Technology (SMART) Centre for Environmental Sensing and Modeling (CENSAM), MIT Sea Grant Project No. 2009-R/RCM-25, and the W. E. Leonhard professorship to Hemond. T. B. Koay, Y. H. Eng, Y. T. Tan, and J. L. Chew at the Acoustic Research Laboratory (ARL) of National University of Singapore (NUS) assisted with field deployment of the sensor onboard their STARFISH AUV. We thank L. Gandois for sharing comparison data from lab-based instrument measurement, and M. Chitre and J. V. Sinfield for advice and helpful discussions. An international Patent Treaty Application has been filed by Ng et al. 2012, based on the claims priority of US Provisional Application 61/477661, 61/494014, and 61/571593 by Ng et al. 2011.

2.7 References

[1] T. Dickey, "Progress in multi-disciplinary sensing of the 4-dimensional ocean," in *Proceedings of SPIE*, 2009, vol. 7317, p. 731702.

[2] R. N. Smith, J. Dasa, H. Hei\dharssona, A. M. P. F. A. Ivona, L. D. Cetinićb, M. È. Garneauc, M. D. Howardc, C. Oberga, M. Raganb, E. Seubertc, and others, "The USC Center for Integrated Networked Aquatic PlatformS (CINAPS): Observing and Monitoring the Southern California Bight," *IEEE Robot. Autom. Mag.*, 2010.

[3] I. Vasilescu, C. Detweiler, M. Doniec, D. Gurdan, S. Sosnowski, J. Stumpf, and D. Rus, "AMOUR V: A Hovering Energy Efficient Underwater Robot Capable of Dynamic Payloads," *Int. J. Rob. Res.*, vol. 29, no. 5, pp. 547–570, 2010.

[4] H. F. Hemond, A. V Mueller, and M. Hemond, "Field testing of lake water chemistry with a portable and an AUV-based mass spectrometer.," *J. Am. Soc. Mass Spectrom.*, vol. 19, no. 10, pp. 1403–10, Oct. 2008.

[5] D. A. Caron, B. Stauffer, S. Moorthi, A. Singh, M. Batalin, E. A. Graham, M. Hansen, W. J. Kaiser, J. Das, A. Pereira, and others, "Macro-to fine-scale spatial and temporal distributions and dynamics of phytoplankton and their environmental driving forces in a small montane lake in southern California, USA," *Limnol. Ocean.*, vol. 53, no. 5 part 2, pp. 2333–2349, 2008.

[6] A. V Mueller and H. F. Hemond, "Extended artificial neural networks: incorporation of a priori chemical knowledge enables use of ion selective electrodes for in-situ measurement of ions at environmentally relevant levels.," *Talanta*, vol. 117, pp. 112–8, Dec. 2013.

[7] E. P. de Jong and C. a Lucy, "Low-picomolar limits of detection using high-power light-emitting diodes for fluorescence.," *Analyst*, vol. 131, no. 5, pp. 664–9, May 2006.

[8] P. B. Oldham, M. E. McCarroll, L. B. McGown, and I. M. Warner, "Molecular fluorescence, phosphorescence, and chemiluminescence spectrometry.," *Anal. Chem.*, vol. 72, p. 197R–209R, Jun. 2000.

[9] R. A. Agbaria, P. B. Oldham, M. McCarroll, L. B. McGown, and I. M. Warner, "Molecular fluorescence, phosphorescence, and chemiluminescence spectrometry," *Anal. Chem.*, vol. 74, pp. 3952–3962, Jun. 2002.

[10] A. M. Powe, K. A. Fletcher, N. N. St. Luce, M. Lowry, S. Neal, M. E. McCarroll, P. B. Oldham, L. B. McGown, and I. M. Warner, "Molecular fluorescence, phosphorescence, and chemiluminescence spectrometry.," *Anal. Chem.*, vol. 76, pp. 4614–4634, Jun. 2004.

[11] R. N. Smith, J. Das, H. Heidarsson, A. Pereira, and G. S. Sukhatme, "Implementation of an embedded sensor network for the coordination of Slocum gliders for coastal monitoring and observation," *Proc. Fourth ACM Int. Work. Underw. Networks - WUWNet '09*, pp. 1–8, 2009.

[12] K. a Fletcher, S. O. Fakayode, M. Lowry, S. a Tucker, S. L. Neal, I. W. Kimaru, M. E. McCarroll, G. Patonay, P. B. Oldham, O. Rusin, R. M. Strongin, and I. M. Warner, "Molecular fluorescence, phosphorescence, and chemiluminescence spectrometry.," *Anal. Chem.*, vol. 78, no. 12, pp. 4047–68, Jun. 2006.

[13] M. Lowry, S. O. Fakayode, M. L. Geng, G. A. Baker, L. Wang, M. E. McCarroll, G. Patonay, and I. M. Warner, "Molecular fluorescence, phosphorescence, and chemiluminescence spectrometry.," *Anal. Chem.*, vol. 80, pp. 4551–4574, Jun. 2008.

[14] A. M. Powe, S. Das, M. Lowry, B. El-Zahab, S. O. Fakayode, M. L. Geng, G. a Baker, L. Wang, M. E. McCarroll, G. Patonay, M. Li, M. Aljarrah, S. Neal, and I. M. Warner, "Molecular fluorescence, phosphorescence, and chemiluminescence spectrometry.," *Anal. Chem.*, vol. 82, no. 12, pp. 4865–94, Jun. 2010.

[15] S. Obeidat, B. Bai, G. D. Rayson, D. M. Anderson, A. D. Puscheck, S. Y. Landau, and T. Glasser, "A multi-source portable light emitting diode spectrofluorometer," *Appl. Spectrosc.*, vol. 62, no. 3, pp. 327–332, 2008.

[16] Y. Suzuki, N. Hashigaya, and S. Kawakubo, "Development of a simple and low-cost device for fluorometric determination of selenium in water samples.," *Anal. Sci.*, vol. 26, no. 6, pp. 719–22, Jan. 2010.

[17] D. Fabila, J. de la Rosa, S. Stolik, E. Moreno, T. Lopez, M. Alvarez, A. Arellano, G. de la Rosa, R. Mercado, and J. Soto, "Development of a spectrofluorometer with USB interface for in vivo measurements in surgical procedures," in *Circuits and Systems for Medical and Environmental Applications Workshop (CASME), 2010 2nd*, 2011, pp. 1–4.

[18] P. Lambert, M. Goldthorp, B. Fieldhouse, Z. Wang, M. Fingas, L. Pearson, and E. Collazzi, "Field fluorometers as dispersed oil-in-water monitors," *J. Hazard. Mater.*, vol. 102, no. 1, pp. 57–79, Aug. 2003.

[19] J. S. Kuo, C. L. Kuyper, P. B. Allen, G. S. Fiorini, and D. T. Chiu, "High-power blue/UV light-emitting diodes as excitation sources for sensitive detection.," *Electrophoresis*, vol. 25, no. 21–22, pp. 3796–804, Nov. 2004.

[20] L. Fiorani and A. Palucci, "Compact laser spectrofluorometer for water monitoring campaigns of Southern Italian regions affected by salinization and desertification processes," *J. Optoelectron. Adv. Mater.*, vol. 10, no. 2, pp. 461 – 469, 2008.

[21] T. B. Koay, Y. T. Tan, Y. H. Eng, R. Gao, M. Chitre, J. L. Chew, N. Chandhavarkar, R. R. Khan, T. Taher, and J. Koh, "STARFISH – A small team of autonomous robotic fish," *Indian J. Geo0Marine Sci.*, vol. 40, no. 2, pp. 157–167, 2011.

[22] J. R. Lakowicz, *Principles of Fluorescence Spectroscopy*, 3rd ed. New York: Springer, 2006.

[23] B. D. Downing, B. a. Pellerin, B. a. Bergamaschi, J. F. Saraceno, and T. E. C. Kraus, "Seeing the light: The effects of particles, dissolved materials, and temperature on in situ measurements of DOM fluorescence in rivers and streams," *Limnol. Oceanogr. Methods*, vol. 10, pp. 767–775, 2012.

2.8 Figures and Tables

Table 1. Comparison of LEDIF with filter-type in situ commercial instruments.

	LEDIF*		Wetlabs EcoFL†		YSI 600 OMS‡		Turner Designs C3™ Submersible Fluorometer§	
Size (volume, cm^3)	6000		396		750		1806	
Voltage (V)	12-7		27-15		External: 12		8-30	
Power (W), max.	2.6 (F‖, T¶), 9.5 (A#)		0.75		—		6	
	Range	LOD	Range	LOD	Range	LOD	Range	LOD
Chlorophyll-a (µg/l)	0 to 1000	5	0 to 125	0.045	0 to 400	0.1	0 to 500	0.025
CDOM (µg/l)	0 to 150000	100	0 to 500	0.275	-	-	0 to 1250	0.15
Uranine (µg/l)	0 to 600	0.2	0 to 400	0.15	-	-	0 to 500	0.01
Rhodamine (µg/l)	0 to 1000	0.3	0 to 230	0.085	0 to 200	1	0 to 1000	0.01

*Standalone (sensor, power, and data logger) system with tri-optical measurement capability.
†ECO FL | WET Labs (http://www.wetlabs.com/eco-fl).
‡YSI 600OMS V2 Sonde-Single-Parameter, Low-Cost Water Quality Monitoring System (http://www.ysi.com/productsdetail.php?600OMS-5).
§Turner Designs C3™ Submersible Fluorometer. (http://www.turnerdesigns.com/products/submersible/c3-submersible).
‖F=Fluorescence.
¶T=Turbidity.
#A=Absorbance.

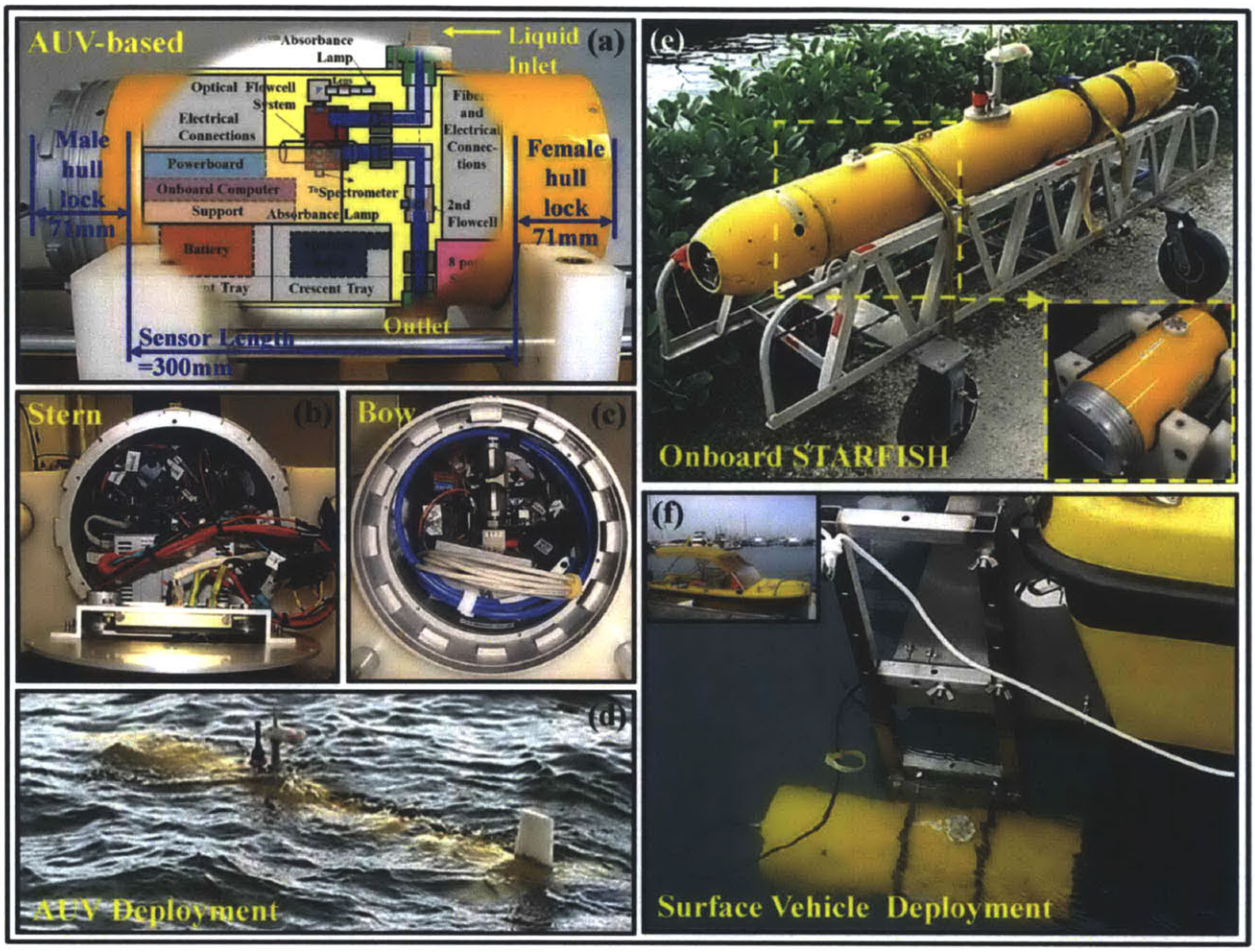

Figure 2.1 The layout of LEDIF and the demonstration of its multi-platform deployment capability: (a, b, and c) Front, stern, and bow views of LEDIF packaged inside the pressure hull, (d) LEDIF aboard STARFISH deployed in the field for sensing of water chemistry, (e) LEDIF integrated to the STARFISH, and (f) LEDIF is end capped for surface vehicles deployment, utilizing a simple interface box for communication and external brackets.

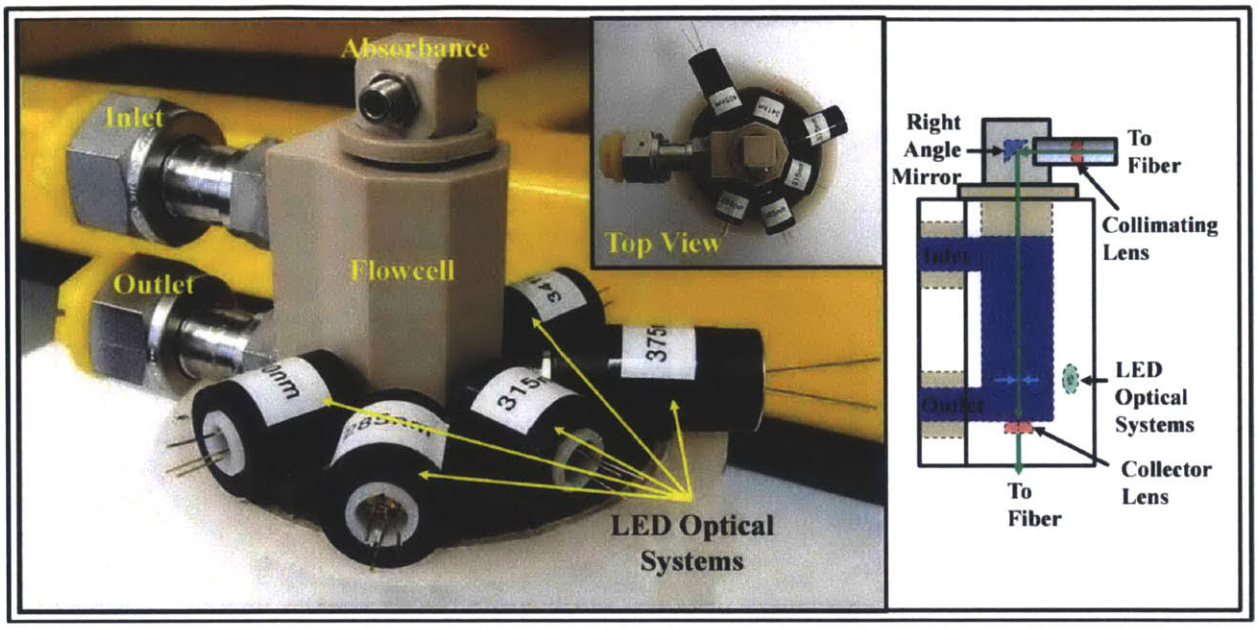

Figure 2.2 LEDIF multi-excitation optical flowcell system.

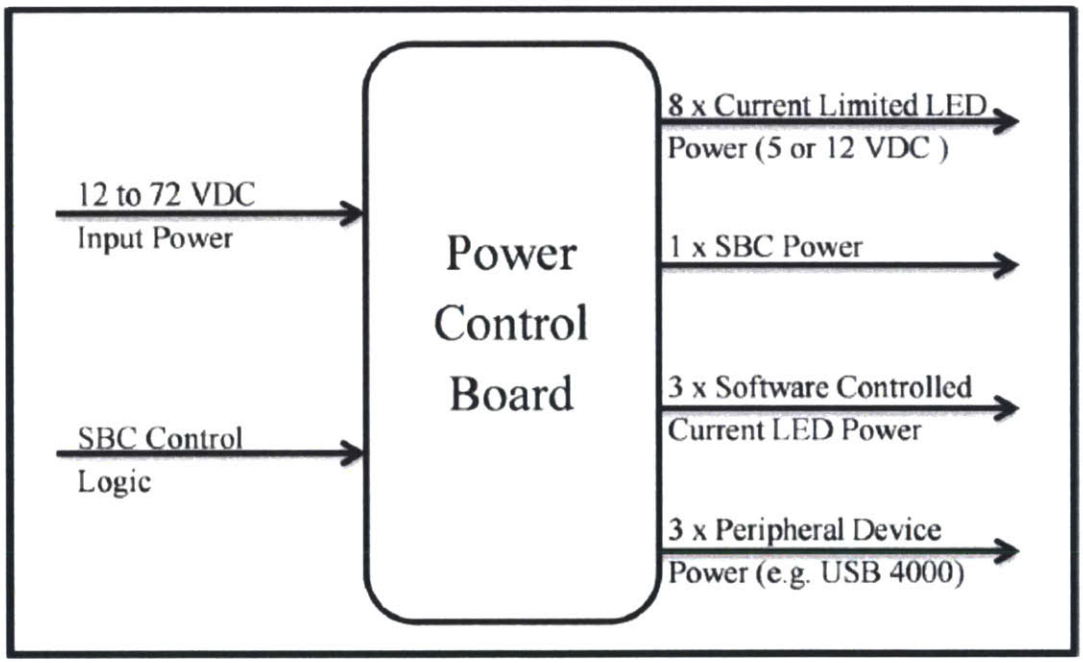

Figure 2.3 Block diagram of LEDIF power control board.

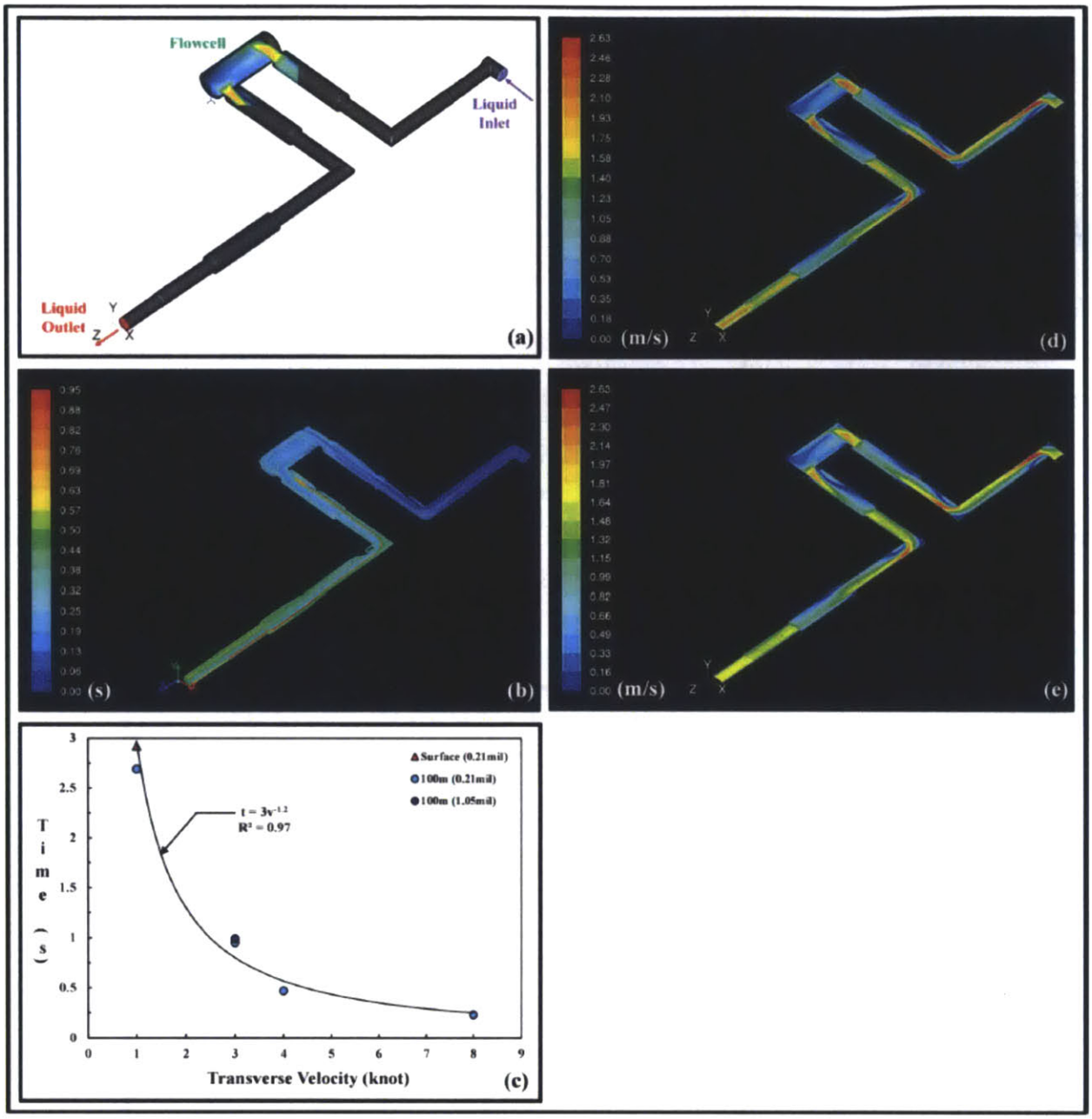

Figure 2.4 3-D transient modeling of through hull flow transportation manifold: (a) Liquid chamber of the through hull flow transportation manifold, (b) Particle pathlines coloured by elapsed time (s) at 100 m depth, 3 knots transverse velocity, (c) Flow retention time at various operating conditions, and Internal velocity contours (m/s) of (d) typical (0.21 million cells) and (e) high density (1.05 million cells) mesh at 100 m depth, 3 knots transverse velocity.

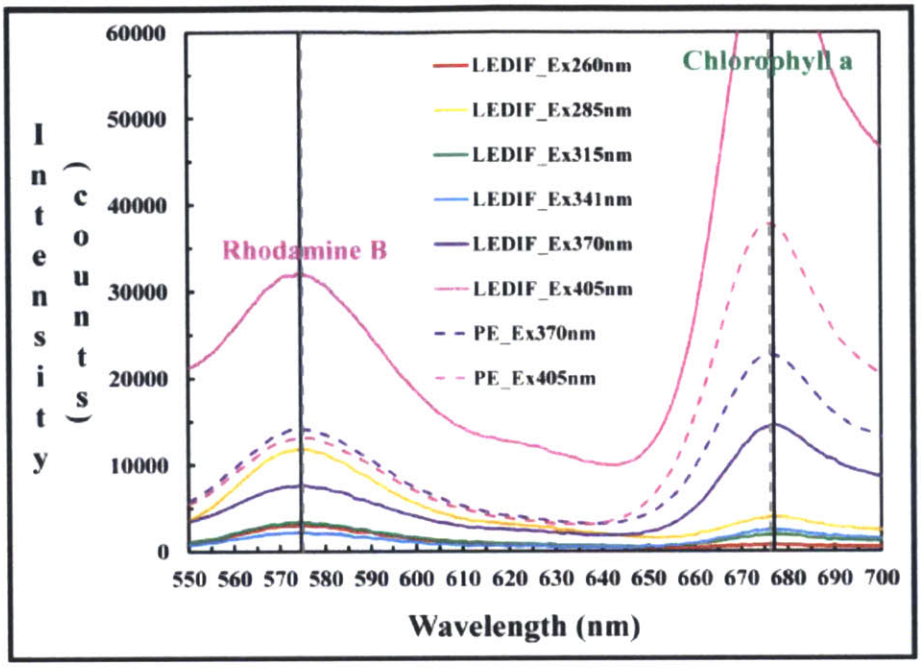

Figure 2.5 Emission peaks comparison between LEDIF and Perkin Elmer LS-55 of a lab mixture (normalized by a factor equal to ~63.5). Note: Symbol legend in instrument excitation wavelength format.

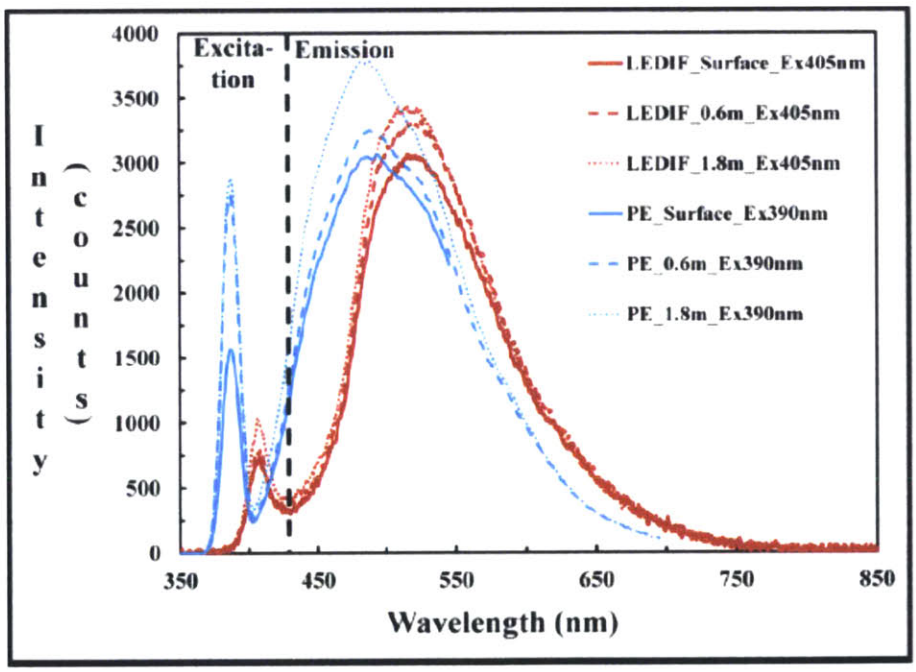

Figure 2.6 Emission spectra from Brunei peatland water samples at various depths, observed using LEDIF and Perkin Elmer LS-55 (normalized by a factor equal to ~8). This shift can be attributed to the longer excitation wavelength and the wavelength dependent response of the USB4000 compared to the PE LS-55.

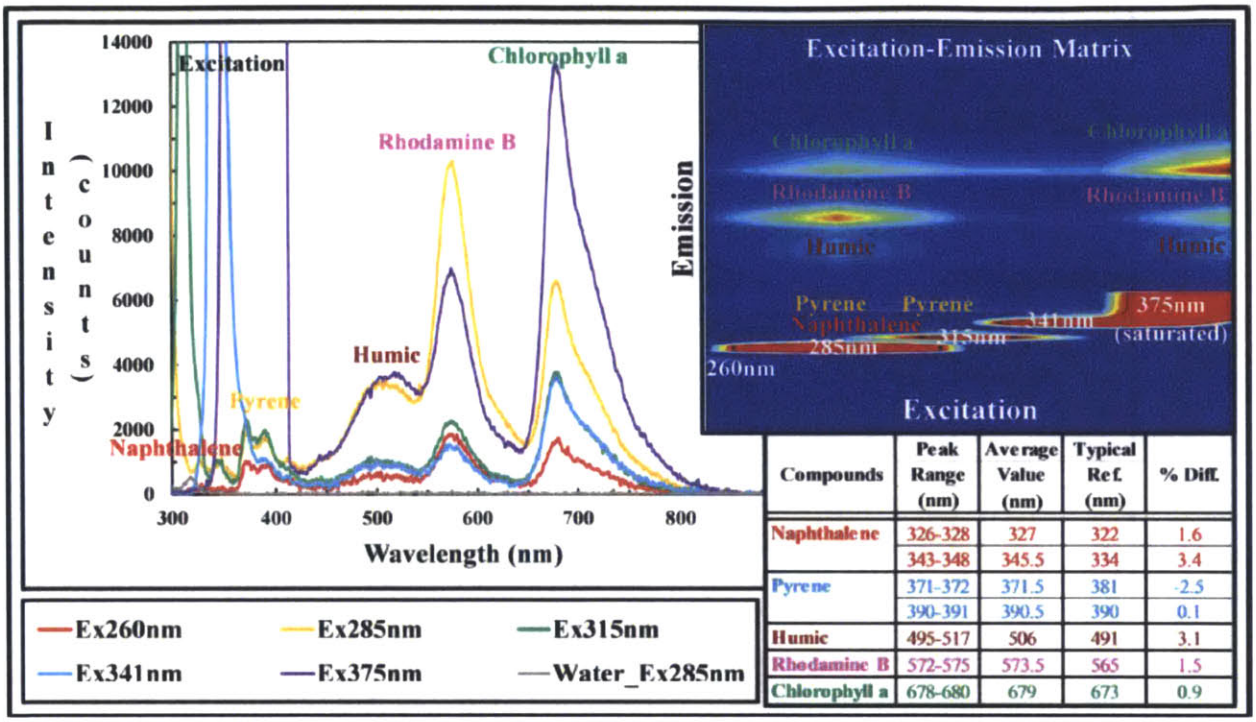

Compounds	Peak Range (nm)	Average Value (nm)	Typical Ref. (nm)	% Diff.
Naphthalene	326-328	327	322	1.6
	343-348	345.5	334	3.4
Pyrene	371-372	371.5	381	-2.5
	390-391	390.5	390	0.1
Humic	495-517	506	491	3.1
Rhodamine B	572-575	573.5	565	1.5
Chlorophyll a	678-680	679	673	0.9

Figure 2.7 Emission spectrum and excitation-emission matrix of a complex lab mixture. The table lists the observed and reference fluorescence emission values.

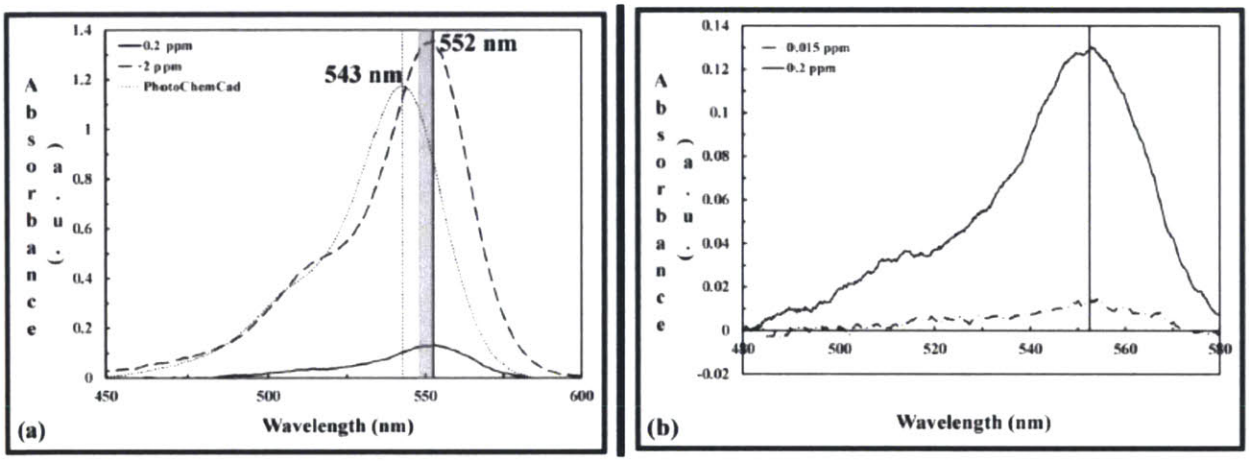

Figure 2.8 The absorbance of rhodamine B (dissolved in water) measured by LEDIF and compared with PhotoChemCAD: (a) At various concentrations, and (b) For low concentration sample, absorbance as low as 0.01 can be accurately measured.

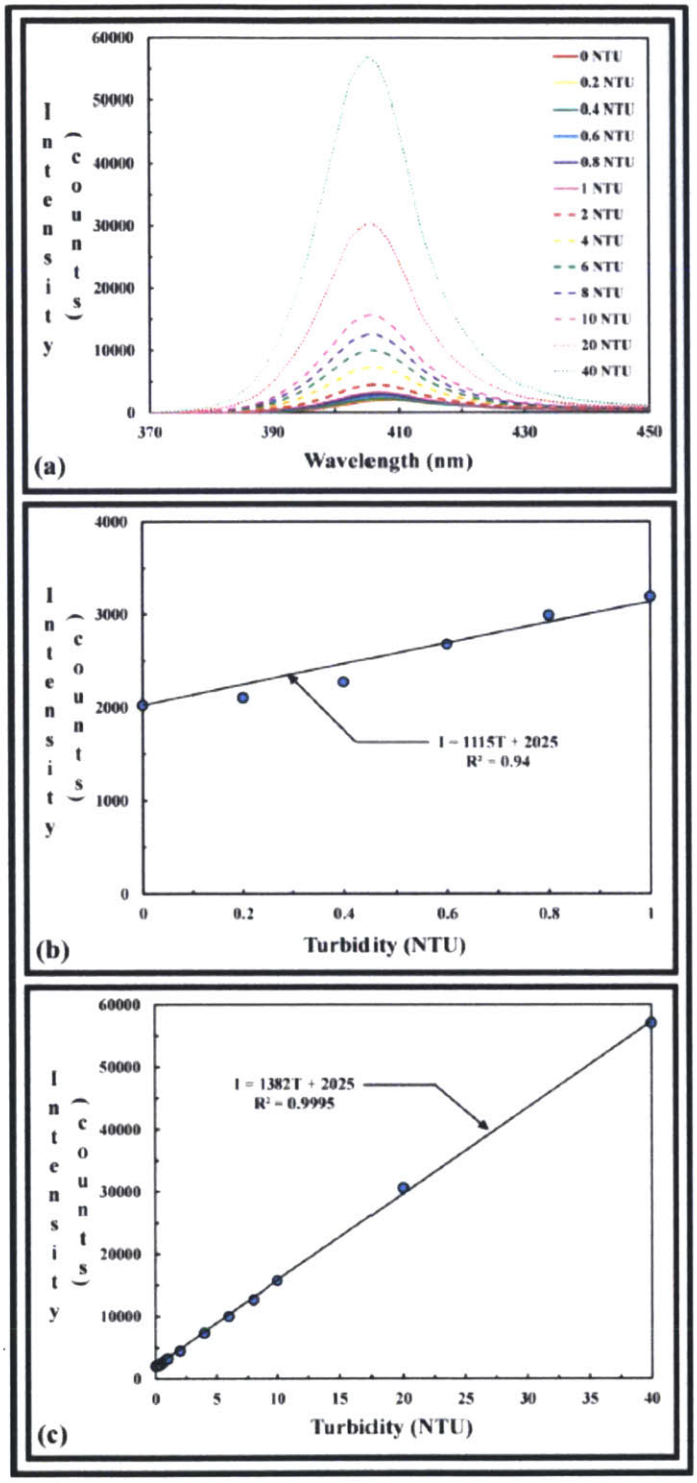

Figure 2.9 Linear calibration curve for turbidity measurement of LEDIF: (a) Measurement of excitation light scattering of known turbidity standards, (b) Turbidity below 1 NTU (typical requirement by water authorities) can be measured for the application of screening processed water, and (c) Scattering of the excitation intensity can be calibrated and described with a single correlation for the turbidity (NTU) measurement.

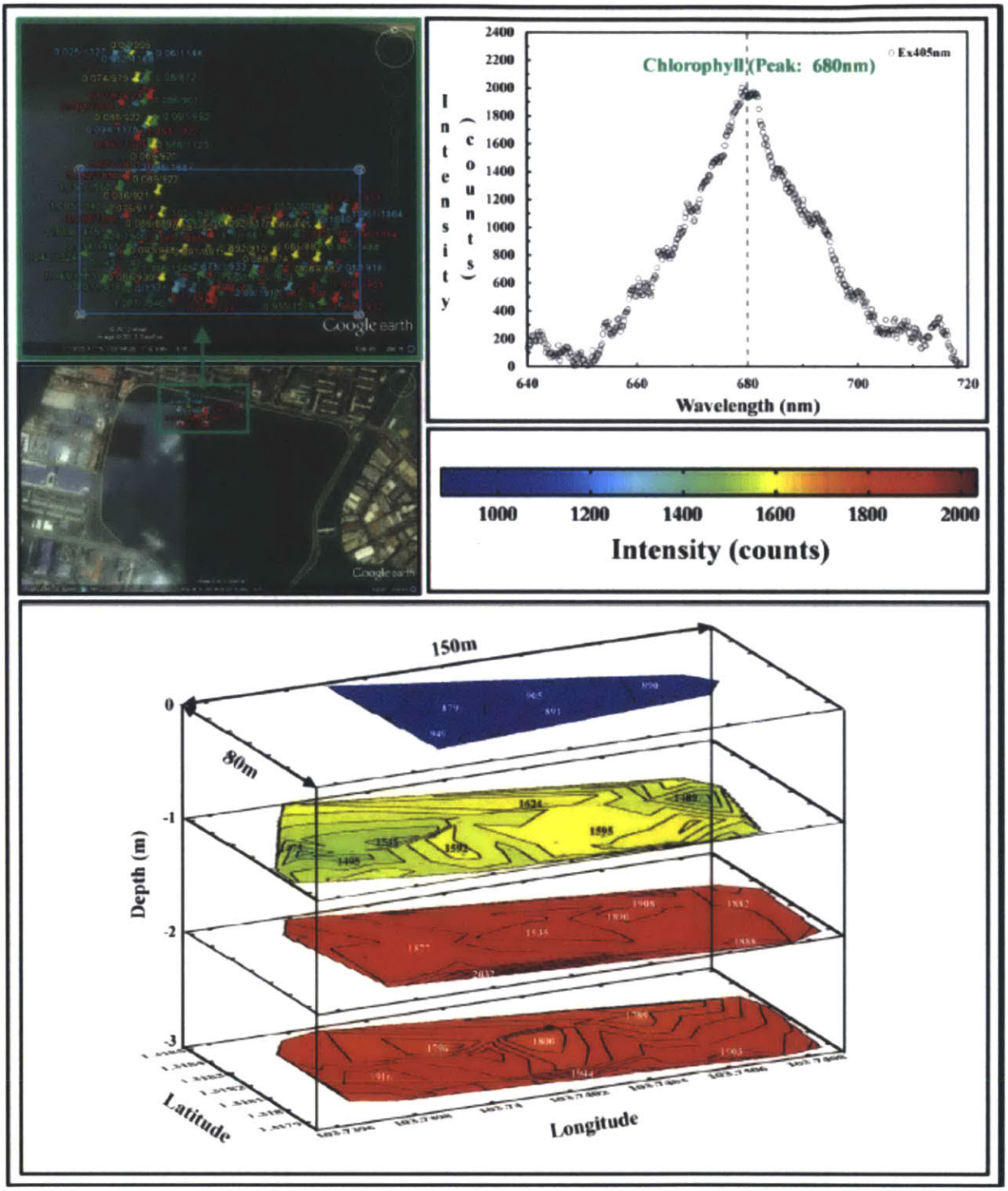

Figure 2.10 3D subsurface mapping of chlorophyll a concentration performed with LEDIF aboard STARFISH in the late morning of 20th December 2011 at Pandan reservoir, Singapore. The measurements demonstrated the successful operation of LEDIF in the freshwater environment for 3D subsurface mapping.

Chapter 3

An In Situ Spectrophotometer and Fluorometer for River DOM Characterization in Peatland Rainforests

Abstract

Peatland rainforests of Southeast Asia are poorly understood ecosystems being rapidly destroyed, however studying these forests is difficult due to their remote locations. An in situ instrument capable of long term deployment to study peatland river carbon transport is described. A combination of fluorescence and absorbance measurements are used to measure the optical properties of the water. Five UV LEDs, between 360 and 430 nm, provide fluorescence excitation, a wideband lamp enables absorbance measurements, and a spectrometer records the resulting spectra. The instrument was successfully deployed in a river near Pontianak Indonesia for two deployments of 2 and 6 weeks. The recorded data show significant changes in bulk fluorescence that are linked to tidally driven changes in water level. An accompanying Monte Carlo model was also developed to simulate the instrument results, specifically the inverse relationship between fluorescence and DOM at the high concentrations (> 30 mg / l) of DOM found in these systems.

3.1 Introduction

The study of water bodies with high levels of dissolved organic matter (DOM) is important for reasons ranging from human health to climate change. Quantifying the transport of organic material from nutrient-rich ecosystems is of particular interest to global climate scientists attempting to estimate current carbon fluxes and study large carbon sinks that could become

future sources of additional atmospheric carbon. A specific example ecosystem is the tropical peatland rainforests of southeast Asia. These tropical rainforests contain an estimated 89 Gt of carbon mass stored as peat [1]. However land use changes, causing an annual deforestation rate of 2.2% of peat swamp forests since 2000 [2], have led to large atmospheric and aquatic carbon fluxes [3].

Gandois et al. [3] used several measurement techniques to characterize the dissolved organic matter (DOM) in peatland pore and drainage water. They compared results between a pristine tropical peat forest and a deforested peatland and estimated a 23% greater river carbon export for the deforested area. The results also showed differences in absorbance and fluorescence spectra for the two sites, determined by differences in fluorescence index (FI), the ratio of fluorescence at two wavelengths of the same spectra, indicating chemically different DOM. FI has been shown to be an indicator of DOM components, knowledge of which is important for understanding its source, transformations, and fate [4].

To further advance the understanding of DOM in tropical peatlands, more measurements over longer time periods are required. The complicated physical nature of the peat, along with tidal influences and intermittent periods of intense rainfall, creates a highly dynamic hydrologic system [5]. To date it is unclear how the hydrology and biochemistry of peat are coupled, and how these interactions change in deforested peatlands. Developing an understanding of these systems and accurately estimating DOC fluxes requires persistent estimates of total DOC and FI of the DOM. However the high DOC concentrations and remote nature of the study sites make it difficult to obtain this necessary data without a custom, in situ instrument.

The objective of this research was to develop a field instrument to record the UV/VIS absorbance and fluorescence spectra of peatland water containing high levels of DOC. The instrument needed to be deployable underwater in remote locations and capable of collecting data continually for several weeks.

3.2 Measuring in situ DOC via Fluorescence

The most common method of measuring DOC in situ relies on the optical properties of water samples. Fluorescence measurements of the water provide estimates of colored dissolved organic matter (CDOM), which is related to the total amount of DOM present. The conversion from CDOM to DOM is specific to the body of water and sources of carbon, but the utility of the

method is generally accepted once site specific conversion curves are developed through more accurate laboratory measurement techniques. Measurements of DOM can be extrapolated to DOC through further laboratory analysis or by estimating the proportion of carbon in organic matter from the literature [6].

There are several commercially available in situ CDOM instruments (e.g WET Labs ECO, Turner Designs C3). These instruments estimate CDOM from fluorescence by exciting the water with light in the 350 nm range and sensing the level of fluoresced light in the 450 nm range. (The actual excitation/emission wavelengths vary between models.) The orientation between the excitation source and detector in most benchtop fluorometers is 90 degrees, but for in situ fluorometers is generally 0 degrees. These sensors typically have a maximum detection limit of approximately 1 mg DOM / l and therefore are not applicable to many highly concentrated water bodies. To the authors' knowledge, there are no commercially available in situ instruments capable of measuring in the range of concentrations often seen in peatland rivers (e.g. 35 mg / l). Estimating DOM at these concentrations becomes difficult because there is no longer a linear or even monotonic relationship between concentration and fluorescence, as high levels of DOM absorb the excitation and fluorescence signals via inner filtering [7]. Additionally, the above mentioned instruments provide only a single fluorescence value making it impossible to estimate the FI of the sample. Deploying an instrument that can record the entire UV/VIS absorbance and fluorescence spectra allows for corrections of inner filtering and the calculation of FI parameters.

3.3 Instrument Description

One requirement of the instrument was that it be capable of measuring high levels of CDOM (up to 60 mg / l) in natural waters, and also that it have capabilities for measuring both absorbance and fluorescence. Additional design constraints were: continuous underwater deployment for a minimum of 1 month, simple data retrieval via a micro secure digital (SD) card, and easy battery replacement in harsh environments (e.g. remote rainforests).

The instrument is comprised of several subsystems that include: 1) narrow wavelength LED fluorescence excitation sources, 2) wideband absorbance lamp source, 3) spectrometer, 4) battery, 5) controller circuit board and data logger and 6) waterproof pressure case. Figure 3.1 shows an overview system schematic.

3.3.1 Optical Configuration

The optical configuration was designed to measure both fluorescence and absorbance. Figure 3.2 shows the orientation of the absorbance and fluorescence light sources to the detector. For absorbance measurements the light source must be oriented 180 degrees from the detector. For fluorescence measurements the source can be oriented at almost any angle to the detector, however the viewing angle of the light source must not overlap the acceptance angle of the detector. In practice, angles between 0 and 90 degrees are most useful. We chose to position the fluorescence light sources at 0 degrees from the detector. This orientation simplified the design of the instrument housing by enabling us to use a single outward facing optical window for both the excitation source and detector.

Orienting the absorbance light source at 180 degrees to the detector required a more complicated design. The light from the lamp is collected by a fiber optic cable. This cable runs inside a copper tube which is curved into a semi-circle at the far end, and connects to the housing through a water tight compression fitting (Figure 3.3). This configuration allows the lamp to be mounted anywhere inside the instrument housing, while emitting light at a precise location in the water in front of the detector.

3.3.2 Control Circuit Board

A single printed circuit board (Figure 3.4) provides a majority of the electronic controls. These include efficiently converting the battery voltage to the required operating voltages, initiating a measurement at set time intervals, communicating with the LED and lamp light sources, communicating with the spectrometer, and storing data on the micro SD card.

The circuit uses a microcontroller to control sensor operation. The microcontroller is an Atmel Atmega348, the same microcontroller used on the Arduino platform, and is preloaded with the Arduino bootloader so it can be programmed similarly to Arduino circuit boards. This microcontroller was chosen due to its ease of coding and programming, and wide availability of open source Arduino code libraries for communication over a serial UART and SPI bus (two different common protocols for communication between integrated circuits), as well as reading and writing to a micro SD card. The chip is a dual inline package (DIP) and can be quickly removed or inserted onto the board. This provides an easy method to upgrade the instrument firmware in the field – the person servicing the instrument can bring a new microcontroller

programmed with updated firmware when she is retrieving the data and changing the battery. The Atmega348 also has several low-power sleep modes that make it ideal for an application such as this that is largely inactive.

The board maintains time using a real time clock (RTC). The RTC (Maxim DS3234) is accurate to 2ppm which corresponds to a potential drift of approximately 1 minute/year. Communication with the chip is over SPI, and includes the ability to program the current date, time, and two separate alarms. For the alarms, when the current time equals the time stored in the alarm register, an interrupt signal is sent from the RTC to the microcontroller to wake it from sleep mode. A 3V coin cell battery is included on the PCB to provide minimal power to the RTC when no other power is connected. An Arduino library has been written to allow for easy use of the RTC.

Power management is a critical function of the circuit board. The main power comes from a 48V battery source which is converted to 5 and 12V with efficient DC-DC converters. These DC-DC converters can achieve almost 90% efficiency when operating near their power capacity, but are very inefficient at low loads. Therefore, when the instrument is in sleep mode the microcontroller disables both of the DC-DC converters and seamlessly switches over to a low voltage (3.7V) Li-ion battery. When the instrument is awake, it uses the main battery to recharge the Li-ion battery. The Li-ion battery can stay permanently installed in the sensor and does not need to be replaced or removed for external recharging. Additionally, when the microcontroller initially wakes up, it measures the voltage of both the main battery and backup battery. This information is logged for performance assessment and can also be used by the microcontroller to adjust the instrument behavior (e.g. decreasing the measurement frequency.)

3.3.3 Fluorescence LED Excitation Sources

For sample excitation, five LEDs at wavelengths of 360nm, 375nm, 390nm, 405nm, and 430nm were chosen based on previous characterization of the organic matter fluorescence and commercially available LED wavelengths [8]. These LEDs are driven by an integrated circuit (IC) designed to deliver a programmable constant current to up to 8 LEDs (TI TLC5916). The IC communicates over SPI and can be programmed to turn on any arbitrary combination of LEDs with individual currents ranging from 4mA to 100mA. (Only one current is programmed at a time, so if the IC is set to deliver 20mA and 3 of the LEDs are enabled, each LED receives

20mA and in total the chip sources 60mA.) The IC uses feedback to monitor the current to each LED, and therefore the LEDs do not need to have the same forward voltage, or for that matter, a known forward voltage to maintain constant light intensity.

The excitation sources and LED driver are soldered onto a small PCB (see Figure 3.5). The layout of the PCB precisely positions the LEDs in a circular formation around a central opening for an optical cable to fit between the LEDs. The optical cable collects the fluorescence and absorbance signals and transmits them to the spectrometer.

3.3.4 Wideband Absorbance Lamp

A wideband lamp is chosen for performing absorbance measurements. The lamp is the Heraeus FiberLight® Miniature UV-Vis Light Source (DTM 6/10), a combination tungsten and deuterium lamp with a spectral distribution between 185 and 1100 nm. The lamp is powered with 12V DC and uses 12 W. Each source can be enabled individually or a shutter can block all light output. This lamp is used in other long term field instruments requiring high reliability and consistent output [9].

3.3.5 Spectrometer

The instrument's spectrometer is an Ocean Optics USB4000. This spectrometer was chosen for its small size, performance, and ease of use, and has been demonstrated to work in similar instruments [10]. The spectrometer communicates over serial RS-232 with the microcontroller. A microcontroller code library has been written to control the spectrometer's various settings and capture spectrum data.

3.3.6 Batteries

The instrument operates off of a 48 VDC source generated from four 12 V batteries wired in series. The sealed lead acid batteries (Industrial Energy IE1290) were chosen for availability (they are widely available around the world), convenience (sealed lead acid batteries can be carried in checked airplane luggage), and cost. Lead acid batteries also come in a variety of sizes that fit into standard 5" PVC pipe. Additionally, at this operating voltage we were able to reuse components and circuits that had already been designed and tested for previous research projects utilizing 48 V [10].

3.3.7 Pressure Housing

The pressure housing is constructed from PVC (Figure 3.6). The top sensing portion contains the sensor electronics while the bottom section holds the batteries. The two halves connect with a custom adapter that uses O-rings to form water tight seals. The sensing half uses a custom machined faceplate for optical measurements. It includes a fused silica glass window for the fluorescence/absorbance measurement, a port for the absorbance lamp fiber, and a valve for vacuum testing. The sensing area is protected by a copper mesh to help reduce fouling and protect the optical area from floating debris. The entire housing is pressure tested to 3 m of water, however all the seals are rated to far greater depths.

3.3.8 Instrument Measurement Procedure

The instrument operation is automatically controlled by the microcontroller firmware in combination with a user-defined configuration file. Applying power or resetting the microcontroller always begins the process of acquiring a measurement from the beginning. The measurement procedure consists of three phases: initialization of the instrument, data acquisition, and sleep.

The initialization procedure consists of the following major steps:

1. Measure the voltage of the main 48 V battery pack and the 3.7 V idle battery.
2. Switch power over to the 48V battery pack. This also automatically begins recharging the 3.7V idle battery.
3. Establish communication with the microSD card.
4. Establish communication with the RTC and store the current date and time.
5. Read the configuration file from the microSD card and save the measurement parameters.
6. Establish communication with the USB4000 spectrometer and set scan parameters used for all measurements.

If at any point during the initialization an error is encountered, the microcontroller attempts to alert the user via three status LEDs. Depending on the severity of the error, the microcontroller will either attempt a restart or will load default parameters.

Once the microcontroller completes initialization, it begins acquiring the measurement data. A single measurement is comprised of a number of fluorescence scans with different

excitation sources, transmittance scans at two different gains, and a reflectance scan. The microcontroller loops through the following procedure to collect each scan:

1. Set the spectrometer to the correct integration time. The integration time can be thought of as the gain control, where longer integration time is equivalent to higher gain.
2. Turn on a fluorescence excitation LED or the wideband absorbance lamp, and let the source warm up.
3. Trigger the spectrometer to take a scan.
4. Immediately write the streaming data transmitted from the spectrometer to the microSD card.
5. Turn off the LED or lamp.

The microcontroller also records dark scans (i.e. no LED or lamp turned on) for each integration time. The dark scans provide baseline and noise values used for offline processing of the spectrum information. If at any point during scanning an error occurs, the microcontroller attempts to troubleshoot the problem, and if necessary restarts the instrument. Errors are noted in a log file on the microSD card.

When the microcontroller finishes collecting the measurement, it proceeds to put the instrument into a low power mode with the following steps:

1. Finish writing and close any open files.
2. Set the alarm on the RTC for when the instrument should wake up for its next measurement.
3. Switch power from main 48 V battery to 3.7 V idle battery.
4. Enter sleep mode.

When the RTC alarm time is reached, the microcontroller wakes up and restarts itself to begin the instrument initialization.

The instrument's only user control comes through the configuration file. In this file, the user defines all important instrument parameters including the integration times for all measurements, the measurement frequency (i.e. how long the instrument sleeps between measurements), and spectrometer settings.

3.4 Methods

Three methods were used to test the performance of the instrument. River samples were collected and analyzed in the laboratory with the instrument and with a benchtop fluorometer and spectrophotometer; the instrument was deployed in the Ambawang River in Indonesia; and a computer model was developed to simulate absorbance and fluorescence with this instrument's non-standard geometry.

3.4.1 Laboratory Testing With River Water

Water was collected from Ambawang River near Pontianak Indonesia on 1/27/2014 and analyzed in the laboratory. In an attempt to quantify the instrument's response as a function of DOC and turbidity, two sets of serial dilutions were performed with the goal of measuring a range of turbidity/concentration pairs. To reduce only the turbidity, sub-volumes of the sample volume were removed, filtered through 0.7 μm glass fiber filters, and returned to the sample volume. To simultaneously reduce DOC and turbidity, sub-volumes of the sample volume were removed and replaced with tap water. (The tap water contained approximately 3 mg DOC / l, and the dilution calculations were corrected for this.)

At several dilution levels, samples were removed and preserved for further analysis. Dr. Gandois' lab measured samples for total organic carbon (TOC) via catalytic oxidation (Shimadzu TOC 5000 A). (Those samples were filtered and prepared in such a way that the only carbon measured was in the dissolved form. Therefore in this case DOC equals TOC measured.) At MIT, the river sample's absorbance was measured with a spectrophotometer (Beckman DU 640), and its fluorescence excitation emission matrix was measured with a benchtop fluorometer (Perkin Elmer LS 50 B).

3.4.2 River Deployment

The instrument was deployed on two occasions in the Ambawang River (0° 3'34.07"S, 109°28'25.48"E – see Figure 3.7). The location was approximately 100 m downstream from the convergence of two smaller rivers. The first deployment spanned 13 days (February 1-14, 2014) and the second deployment spanned 41 days (February 16 to March 29th, 2014), and recorded measurements every 20 minutes. The instrument was secured to a jetty that extended

approximately 10 meters into the river, as close as possible to the river bottom (~ 0.5 m). A water level logger was deployed simultaneously at the site to record river depth.

On February 2nd, the day after the initial deployment, river water samples were collected between 9:30 and 14:30 every hour. Samples were collected in a bucket from the surface of the river. They were filtered through 0.7 μm glass fiber filters and preserved, and analyzed for TOC in Dr. Gandois' lab two weeks later.

3.4.3 Optical Absorbance/Fluorescence Simulation

In highly absorbing and fluorescing media, standard correction methods for inner filtering and other effects cannot be used. Additionally, with the instrument's 0-degree excitation/detection geometry and significant offset between excitation LED collection optical fiber, the effective fluorescence pathlength is a non-linear function of absorbance (i.e. CDOM concentration). Given these multiple variables, it is challenging to explicitly solve the radiative transport equations (RTE) that govern photon interactions arising from absorbance, scattering, and fluorescence. Researchers in many disciplines have turned to Monte Carlo simulation in this scenario [11]. To understand both the instrument magnitude and wavelength response as a function of water CDOM concentration, a model was developed in MATLAB to simulate photon travel from excitation source to the detector.

To reduce computing time and enable faster sensitivity analysis, the model is divided into two parts: photon propagation and photon detection. The propagation section models photons leaving the LED, being absorbed and fluoresced, and moving through the system. The output from this simulation is a list of photons that could potentially be detected by the spectrophotometer – i.e. the photons that cross back into the instrument. The propagation code is dependent on the LED characteristics (e.g. beam width) and the water characteristics (e.g. concentration of DOC). The detection portion of the code uses the output of the propagation code to check which photons are actually detected by the spectrometer. This half of the simulation requires only the detector parameters (e.g. fiber acceptance angle, fiber size). Performing the two halves of the simulation separately allows for computation optimizations at the cost of large intermediary data files.

3.4.3.1 Photon Propagation Procedure

The propagation simulation follows a series of steps to propagate a photon across several boundaries and through the absorbing and fluorescing water media. The procedure has been adapted from Prahl [11] to include fluorescence.

1. The photon is launched from the LED at a randomly chosen elevation and azimuth. The angles are selected from a cumulative distribution function corresponding to the LED's viewing angle.
2. The photon is moved to the first boundary: air-glass. At each boundary crossing, the simulation checks for several conditions.
    a. The photon is reflected at the boundary if its incidence angle is greater than critical angle for the two respective boundary media. (Only applicable when indices of refraction $n_t < n_i$.)
    b. At any boundary, there is some probability that the photon will be reflected. This probability is given by the Fresnel reflection coefficient, which is calculated from the incidence and transmission angles.
3. If the photon is not reflected, it travels through the glass window with a new altitude angle calculated from Snell's law.
4. The photon is moved to the second boundary: glass-water. The same system of checks described in step 2 occurs.
5. If the photon is not internally reflected, it now is in the water. A new altitude angle for the photon is calculated using Snell's law.
6. The photon is moved a step size, s in cm, from its current boundary location. The step size is chosen randomly by

$$s = \frac{-\ln r}{\mu_a}$$

where r is a uniform random variable between 0 and 1, and μ_a is the wavelength specific absorption coefficient (cm^{-1}). The step size is the distance the photon travels before being absorbed.

7. A new photon with a new wavelength is randomly selected from a fluorescence wavelength probability distribution. The simulation uses an excitation-emission matrix of

the water solution to generate cumulative distribution functions for all excitation wavelengths.

8. The photon's new direction is randomly selected. Since fluorescence is isotropic, all possible directions are weighted equally.
9. The photon is moved (see Step 6).
10. The simulation checks if during the Step 9 photon propagation it crossed the water-glass boundary. If it did not, Steps 7-9 are repeated until the photon either crosses the boundary or is absorbed three times. After the third absorption event, the photon is lost.
11. If the photon crosses back into the glass, the simulation performs the same checks as in Step 2. The only difference is that if the photon is reflected, it remains in the water and continues to be absorbed and fluoresced (i.e. repeat steps 6-9). Photons not reflected are assigned a new transmission angle from Snell's law.
12. Photons that enter the glass are propagated to the glass-air boundary (See Step 2).
13. If the photons pass through the glass-air boundary into the air, the simulation stores the photon information. This includes the photon's location at the boundary, the photon's propagation direction (including adjusting for the change in angle across the glass-air boundary), the photon's wavelength, and the number of times the photon was absorbed (either 1 or 2).

3.4.3.2 Photon Detection Procedure

Using the output of the photon propagation simulation, the detection code calculates which photons are observed by the spectrometer. The detection code uses the optical fiber diameter, location (x, y, z), and acceptance angle to calculate if photons are captured. Photons that intersect the air-fiber boundary at the fiber location and have an incidence angle less than the fiber acceptance angle are considered detected by the spectrometer. Although photons can also be reflected off the fiber, this is not a function of photon wavelength and so was ignored for the sake of faster simulation run times. The saved results include the photons' wavelengths and number of absorption events so that primary and secondary fluorescence can be compared.

3.4.3.3 Simulation Parameters

Numerous simulation parameters can be adjusted to test their impact on the fluorescence measurements. These parameters include: the LED viewing angle, the distance between the LED

and the light collection fiber, the distance between the collection fiber and the glass window, the collection fiber diameter, and the collection fiber acceptance angle. The simulation is run multiple times with these parameters incremented across a range of potential values.

The characteristics of the water/DOM mixture can also be controlled. In all cases the simulation uses the absorbance spectrum and fluorescence excitation emission matrix (EEM) of the river water sample measured in the lab. Both the absorbance and fluorescence spectra have a resolution of 1 nm. The excitation resolution in the EEM is 10 nm (i.e. measurements were taken with the excitation equal to 360nm, 370nm, 380mm... up to 550 nm). Fluorescence spectra for excitation wavelengths between measurements are linearly interpolated from the two nearest measurements.

To simulate different concentrations of DOC, the absorption spectrum is multiplied by the ratio of the simulated concentration to the baseline river concentration. For example, to simulate a DOM concentration 20% greater than the actual river water, each element of the absorbance spectrum is multiplied by 1.2. Since only the relative shapes of the fluorescence spectra are used in the simulation, no changes are made to the EEM.

3.5 Results

3.5.1 Simulation

Selected results for the photon propagation simulations are shown in Figure 3.8 and Figure 3.9. Most notably, the simulation predicts a negative and nonlinear relationship between DOM concentration and detected fluorescence photons. It also shows there is a mix of primary and secondary photons detected, and the ratio of primary to secondary photons decreases as DOM concentration increases. The simulated spectrum from primary fluorescence is red shifted by several nm from the input spectrum. This is expected due to preferential absorbance of the fluorescence signal at lower wavelengths. The secondary fluorescence spectrum is even further red shifted and centered at approximately 525nm. The amount of secondary fluorescence is significantly less than primary fluorescence due to the quantum yield of only 5%. Tertiary fluorescence is neglected as its emission decreases by the square of the quantum yield.

Several relationships between other instrument attributes and detected photons are also apparent. As expected, the number of photons detected is linearly proportional to the fiber area.

The fiber acceptance angle also plays a significant role in photon capture, with an apparent second order polynomial relationship. This result is expected because the volume delineating the viewable fluorescence locations is an approximate cone, and therefore is proportional to the square of the cone radius. The cone radius is defined by the fiber acceptance angle. Lastly, the number of photons detected is positively correlated with the distance between the fiber and the glass window, but the effect is minimal. All of these results confirm expected relationships between the instrument design parameters and observable fluorescence.

3.5.2 River Water Dilution

Selected results for the instrument test are presented. Figure 3.10 shows the discrete excitation-emission spectra of the water sample resulting from measurements with the instrument. The fluorescence response was largest with the 375nm and 395nm excitation, although also visible with the 365nm and 405nm excitation. The fluorescence peaks were independent from excitation wavelength and located around 495nm. For comparison, Figure 3.11 shows the discrete excitation-emission spectra for the river sample measured using the benchtop fluorometer. The fluorescence peaks are located approximately 90nm longer than excitation. The absorbance spectrum for the river water, as measured on the lab spectrophotometer, is shown in Figure 3.12.

Figure 3.13 and Figure 3.14 show the fluorescence response to 375nm excitation for the two dilution tests. Both tests show an increase in fluorescence with decreasing DOM concentration and decreasing turbidity. Figure 3.15 and Figure 3.16 further demonstrate the relationships between fluorescence, DOC, and turbidity. For samples where the DOC concentration was measured by the TOC analyzer, that concentration is used. For samples that were not analyzed for TOC, an estimate is interpolated from the nearest analyzed samples and the known volume of dilution water. The reported turbidity is as a percent of the initial turbidity, and this was solely estimated based on the amount of filtered sample and dilution volume. As expected for these DOC concentrations, in all cases there is an inverse relationship between fluorescence and both DOC and turbidity.

Transmittance measurements were unsuccessful for the dilution tests. The data often failed to stabilize over the course of a measurement, consistently decreasing with time. It was also found that very slight changes to the transmittance fiber optic location yielded large changes

in signal. Therefore transmittance measurements obtained by the instrument are not used or presented in any of the findings, and all absorbance results come from laboratory measurements instead.

3.5.3 River Deployment

The river deployments were to test both the hardware's performance in the field and the sensor's data capture capabilities.

3.5.3.1 Hardware Performance

The instrument was successfully deployed and retrieved on both field campaigns. Most importantly, there was no evidence of leaking for either deployment. The sensor correctly triggered every 20 minutes to capture data, and there were no logged errors during data capture or missing values in any of the data files. Battery usage was monitored and exceeded the design goal of 30 days of operation (see Figure 3.17 for voltage drop over time.) During the first deployment, there was no visible biofouling or sediment accumulation on the window. However on the second deployment, the entire instrument became covered in a layer of silt after approximately two weeks. It is unclear what caused the difference, except that on the second deployment there may have been times when the water level was low enough to expose the instrument to the air. During these events, any water remaining on the instrument would evaporate leaving behind solids. Alternatively there appeared to be a period of larger tidal swings leading up to optical window becoming obscured, so there may have been greater levels of suspended solids mobilization and then settling.

3.5.3.2 Field Data

Selected field data are shown in Figure 3.18 through Figure 3.20. In the first deployment, fluorescence signals are visible for the duration of the experiment with both the 375nm and 395nm excitation sources. Some fluorescence is apparent with the 365nm excitation, although only barely greater than background noise. No fluorescence is visible with either the 405nm or 430nm excitation.

In the second deployment, similar fluorescence signals were initially observed, but the instrument eventually underwent changes that impact the measurements. At some point the optical window became obscured with a layer of sediment. The data suggest that this occurred

between 3/4/2014 and 3/7/2014, following a period of high tidal variability and increasing tidal differentials.

Results comparing the DOC in collected water samples from Feb. 2nd to instrument measurements are shown in Figure 3.20. The change in DOC concentrations was not large enough to differentiate using the fluorescence data.

3.6 Discussion

The results from the laboratory experiments, field deployment, and computer simulation provide important findings regarding the in situ study of high-DOM water. The instrument results highlight some of the difficulties in measuring natural waters with high levels of DOM. The following sections discuss the most notable features of these results.

3.6.1 Field Data Interpretation

Both field deployments yield results that indicate there may be significant short-term (hourly) temporal variability in river DOM, turbidity, or both. It is clear that changes in fluorescence are correlated with the tidally driven river stage, although the relationship is not necessarily direct or always apparent. Typically the fluorescence is at its maximum shortly after maximum river stage, and is at its minimum at low tide. During the first deployment, the average integrated DOM fluorescence is approximately 10^5 counts, and the change in fluorescence counts over a single tidal period ranges between approximately $5*10^4$ and 10^5 counts. These results indicate that the river during high tide has lower DOM and/or turbidity levels than at low tide. Additionally the fluorescence appears to lag the tidal signal by approximately 2 hours. These observations are consistent with backflow of river water that has had a longer time to undergo processes that consume DOM, or infiltration and dilution by low DOM seawater.

The results from the second deployment also suggest a tidal effect on fluorescence. Unfortunately the collection of particles on the instrument limit the amount of relevant data to the first third of the deployment. The instrument did capture much larger swings in fluorescence for several days (a change over $5*10^5$ counts), however this may have been influenced by the partial obstruction of the optical window. Alternatively, the events which caused these large changes in fluorescence (e.g. periods of high suspended solids) may have been responsible for the instrument becoming covered in sediments.

3.6.2 Inverse Fluorescence Response

Instrument observation of DOM fluorescence intensity is a nonlinear function with two different regimes. For low concentrations there is a positive relationship between concentration and fluorescence, however at some high level of DOM this relationship inverts. For this instrument and the DOM concentrations found in the Ambawang and similar peatland rivers, fluorescence response is always inversely related to concentration. This conclusion is expected given the large DOM absorbance coefficients and long light pathlengths associated with the instrument geometry. The simulation results provide additional evidence for this phenomenon in the range of DOM concentrations of interest with our instrument's geometry.

3.6.3 Absorbance Measurements

The alignment between the instrument's absorbance light fiber optic and the detector fiber optic did not remain constant. On short time scales, the tip of the light fiber optic was too flexible and susceptible to minor forces and vibrations. On longer time scales (e.g. the deployment), it appeared that the alignment gradually, and permanently, shifted. The result is unusable absorbance data. Given that analysis of the instrument data relies significantly on the absorbance data, the resulting fluorescence data interpretation is less precise than desired and more qualitative than quantitative.

3.6.4 Fluorescence Peak Shift

A striking difference between our instrument and laboratory measurements is the shape and peak of the resulting fluorescence spectrum. DOM fluorescence peaks are generally approximately 90 nm greater than the excitation wavelength when excited in the UV range. The river water samples measured with a laboratory fluorometer yield spectra with the expected shape and peak. However the spectra generated with the peat instrument show no fluorescence until ~450nm and a peak at ~495nm. The laboratory fluorometer spectra agree with previous studies of peatland pore water [8].

The Monte Carlo simulation was largely developed to determine the effect of the excitation-detector geometry on potential wavelength shifts. While the simulation results show a primary fluorescence peak red-shift and the presence of higher wavelength secondary fluorescence, these results do not explain the narrower, shifted spectrum measured with the

instrument. Wavelength dependent sensitivity of the USB4000 spectrometer appears to explain the remaining amount of observed wavelength shift.

3.6.5 Calibrating For Concentration and Turbidity

Developing a calibration curve for the instrument proved difficult. Results show that potentially both DOM concentration and turbidity effect the fluorescence response. Separating the two variables is not possible with the current data and a lack of a mathematical model for their interaction. In 0, for the first dilution the slope of the response with only turbidity changing is statistically significant from the data with both turbidity and concentration changing. However for the second dilution, the slope for the changing turbidity only data is not significantly different from the initial slope. Overall, in the range of DOM values of interest, there is some interaction between DOM fluorescence and turbidity that cause an increase in signal with decreases in either or both of the variables. Without simultaneous absorbance data, it is difficult to predict whether the change in fluorescence is from changes to turbidity or DOM.

3.6.6 Estimating Changes in DOC

Using the collected measurements, it is possible to make an estimate of changes in DOC in the river. Doing so requires making several broad assumptions but can bound the possible changes in DOC. To begin, the calibration data can be fit to a three dimensional curve of the form

$$F = a * C + b * T + c$$

where F is the number of fluorescence counts integrated across the wavelengths for DOM fluorescence, C is the concentration of DOC in mg / l, and T is the turbidity (in % of the initial river sample used in the calibration). The fit found values of -2609, -2143, and $4.7*10^5$ for a, b, and c, respectively. The R^2 value was 0.93, indicating that solution does not completely model the data. Additionally, there are nonlinear effects that limit the ability to calculate results at concentrations far from those used to fit the model (i.e. ~ 30 mg / l DOC and similar turbidity as in the sample used for calibration).

Even with these limitations, we can attempt to calculate the change in DOC from the change in fluorescence signal. Since the fluorescence is a function of both DOC and turbidity, we must make assumptions about changes in one while solving for the other. There was no

measurement of river turbidity at the deployment site when water samples were obtained, so we solve for that using the DOC value measured in the lab from the water sample collected at the start of the deployment (35.9 mg /l). From this value, we estimate that the turbidity was 117% of the turbidity in the river sample used for calibration in the lab. To calculate the upper bound on change in DOC concentration we assume that turbidity remained constant throughout the deployment. The results are shown in Figure 3.21 and average ~40 mg / l with typical changes of +/- 10 mg / l per tidal cycle. The most extreme results, 10 and 65 mg / l, are most likely due to model errors (e.g. far from the values used to fit the equation where nonlinear terms dominate) or additional river changes besides changes in DOC.

3.7 Conclusion

An instrument for measuring water with high levels of DOM was designed and tested at a river field site in Pontianak, Indonesia. The instrument was deployed on two occasions in the field, and continuously collected fluorescence data at 20 minute intervals for nearly 6 weeks. These field trials validated the pressure housing and electronics design for future long term deployments in remote locations. The battery storage proved more than sufficient for the deployment goal of four weeks. The microcontroller firmware in conjunction with the real time clock flawlessly controlled the instrument operation and logged more than 120 MB of errorless data.

The fluorescence sensing capabilities of the instrument were also demonstrated. Precisely calibrating the instrument was difficult, however a strong inverse relationship between DOM concentration and fluorescence was demonstrated for the range of concentrations found in peatland rivers. During the two field deployments, significant changes in fluorescence were repeatedly observable and correlated with tidally driven changes in river height. Estimates of DOC from this fluorescence data show possible changes of +/- 10 mg DOC / l. This most likely indicates that the hydrologic dynamics effect the DOM concentrations in ways that are not yet fully understood.

Future design iterations can address the few technical issues that limited the instrument on these initial deployments. Most importantly, a new absorbance measurement scheme that ensures constant alignment between the lamp output and the detector should be implemented. The experiment results confirm that the absorbance spectrum is required to correct for effects

from turbidity and inner filtering of fluorescence. Additionally, implementing algorithms in the microcontroller code to adapt how and when measurements are taken can improve the sensor's dynamic range and battery life. For example, drastic changes in river optical properties, like those observed in the two deployments, could cause the instrument to automatically adjust the spectrometer gain to ensure that the detector never saturates. Also, to better capture intermittent events while maximizing battery life, the frequency of measurements could vary as a function of the rate of change of river conditions.

Measuring high DOM waters in situ presents many challenges but is important for the advancement of peatland rainforest research. The natural waters draining from these ecosystems exhibit particularly complicated bio-chemical interactions that are just now being properly investigated. Understanding these tropical peatland systems, and particularly the effect of massive deforestation, is of great importance for determining the role of these large carbon repositories in global climate change.

3.8 Acknowledgements

The author would like to thank the following organizations and individuals. Funding for this project came from the Singapore MIT Alliance for Research and Technology (SMART). The project design and implementation was performed in conjunction with Prof. Charles Harvey, Dr. Laure Gandois, Dr. Alex Cobb and Alison Hoyt. Dr. Chee-Loon Ng aided with instrument design and testing. The field work and logistics were made possible by Prof. Gusti Anshari of Tanjungpura University and his students, in particular Muhammad Nuriman.

3.9 References

[1] S. E. Page, J. O. Rieley, and C. J. Banks, "Global and regional importance of the tropical peatland carbon pool," *Glob. Chang. Biol.*, vol. 17, no. 2, pp. 798–818, Feb. 2011.

[2] J. Miettinen, C. Shi, and S. C. Liew, "Deforestation rates in insular Southeast Asia between 2000 and 2010," *Glob. Chang. Biol.*, vol. 17, no. 7, pp. 2261–2270, Jul. 2011.

[3] L. Gandois, a. R. Cobb, I. C. Hei, L. B. L. Lim, K. A. Salim, and C. F. Harvey, "Impact of deforestation on solid and dissolved organic matter characteristics of tropical peat forests: implications for carbon release," *Biogeochemistry*, no. Hooijer 2006, Oct. 2012.

[4] D. M. McKnight, E. W. Boyer, P. K. Westerhoff, P. T. Doran, T. Kulbe, and D. T. Andersen, "Spectrofluorometric characterization of dissolved organic matter for indication of precursor organic material and aromaticity," *Limnol. Oceanogr.*, vol. 46, no. 1, pp. 38–48, 2001.

[5] A. Cobb, "Personal Communication," 2013.

[6] J. Kalff, *Limnology : inland water ecosystems*. Upper Saddle River, NJ: Prentice Hall, 2002.

[7] T. D. Gauthier, E. C. Sham, W. F. Guerln, W. R. Seltz, and C. L. Grant, "Fluorescence Quenching Method for Determining Equilibrium Constants for Polycyclic Aromatic Hydrocarbons Binding to Dissolved Humic Materialst," *Environ. Sci. Technol.*, vol. 20, no. 11, pp. 1162–1166, 1986.

[8] L. Gandois, a. R. Cobb, I. C. Hei, L. B. L. Lim, K. A. Salim, and C. F. Harvey, "Impact of deforestation on solid and dissolved organic matter characteristics of tropical peat forests: implications for carbon release," *Biogeochemistry*, vol. 114, no. 1–3, pp. 183–199, Oct. 2012.

[9] K. Johnson and L. Coletti, "In situ ultraviolet spectrophotometry for high resolution and long-term monitoring of nitrate, bromide and bisulfide in the ocean," *Deep Sea Res. Part I Oceanogr. Res. Pap.*, vol. 49, no. 7, pp. 1291–1305, Jul. 2002.

[10] C.-L. Ng, S. Senft-Grupp, and H. F. Hemond, "A multi-platform optical sensor for in situ sensing of water chemistry," *Limnol. Oceanogr. Methods*, vol. 10, pp. 978–990, 2012.

[11] S. A. Prahl, M. Keijzer, S. L. Jacques, and A. J. Welch, "A Monte Carlo Model of Light Propagation in Tissue," *SPIE Inst. Ser.*, vol. IS 5, pp. 102–111, 1989.

3.10 Figures

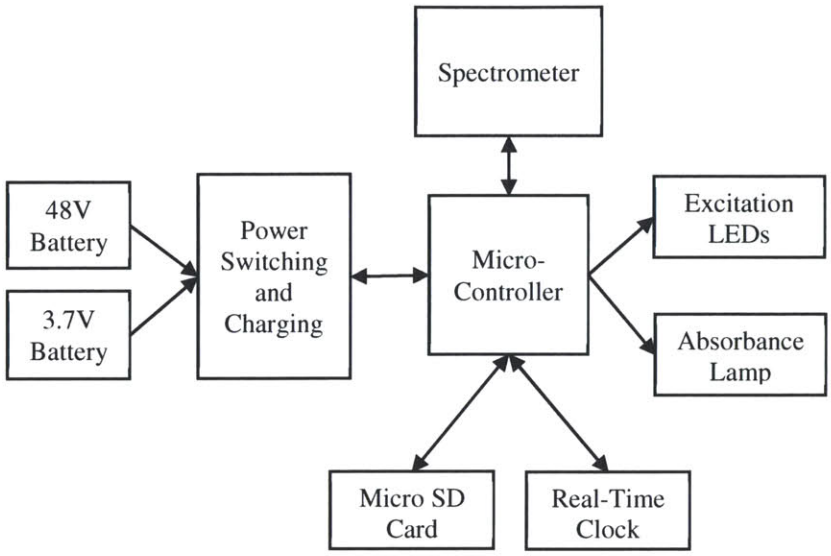

Figure 3.1 System Overview.

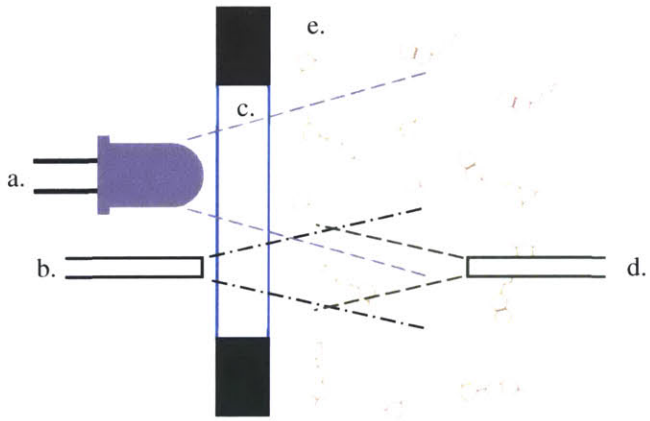

Figure 3.2 Optical Component Orientation. Instrument optical component layout consisting of a) a fluorescence excitation LED; b) light collection fiber optic cable connected to spectrometer; c) fused silica optical window; d) fiber optic cable connected to wide spectrum lamp for fluorescence; and e) the high DOC concentration water. Dashed lines indicate the cones of light created by a and d, and the cone of acceptance for b. Since a and b are in the same plane looking out the same direction, they are considered to be at 0 degrees orientation.

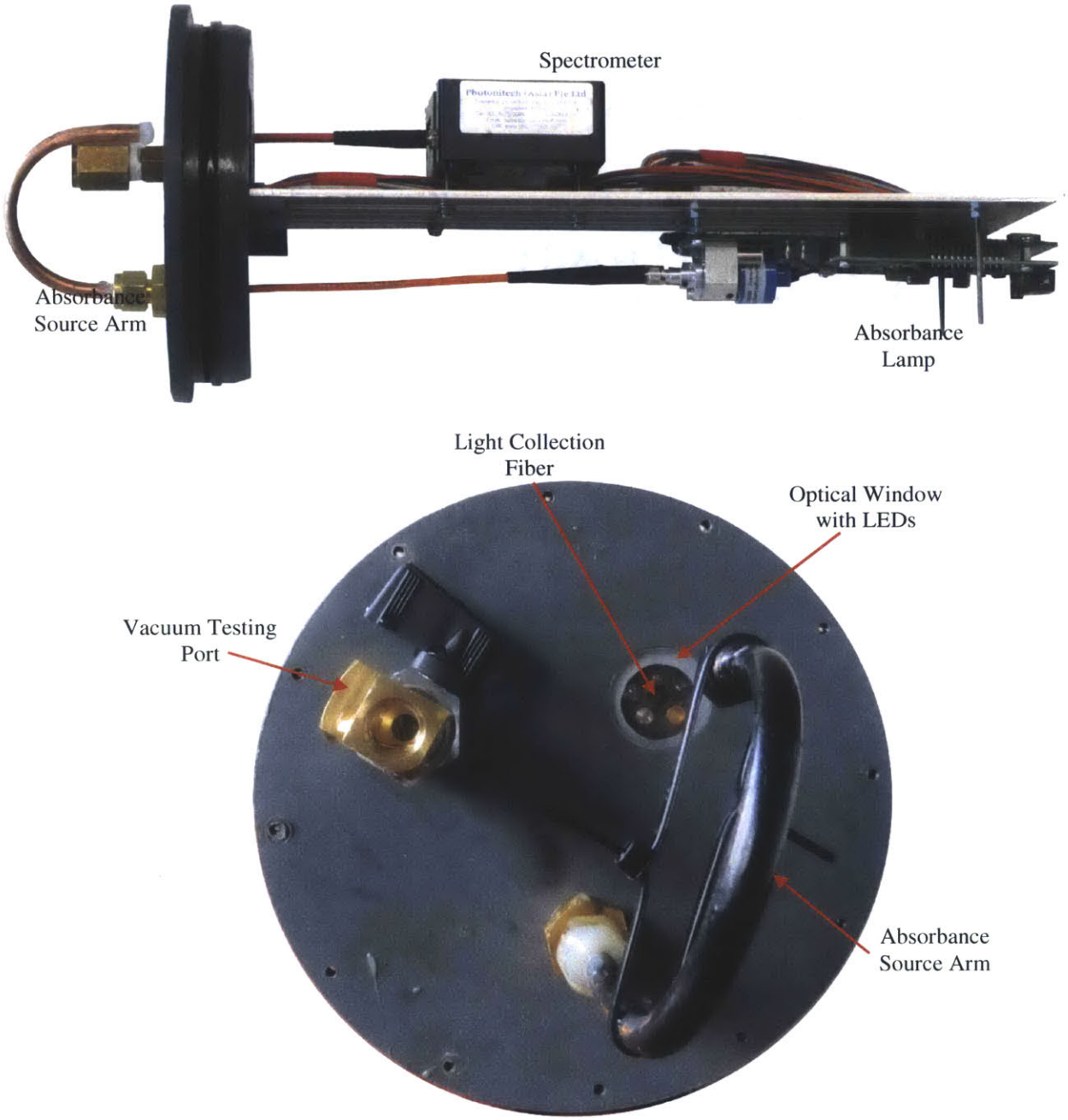

Figure 3.3 Instrument Configuration and Optics. Top: Side view of the initial prototype of the instrument optical components. Bottom: Front view of the instrument face for the final deployed instrument. The absorbance source arm was modified and painted black to reduce its reflectiveness.

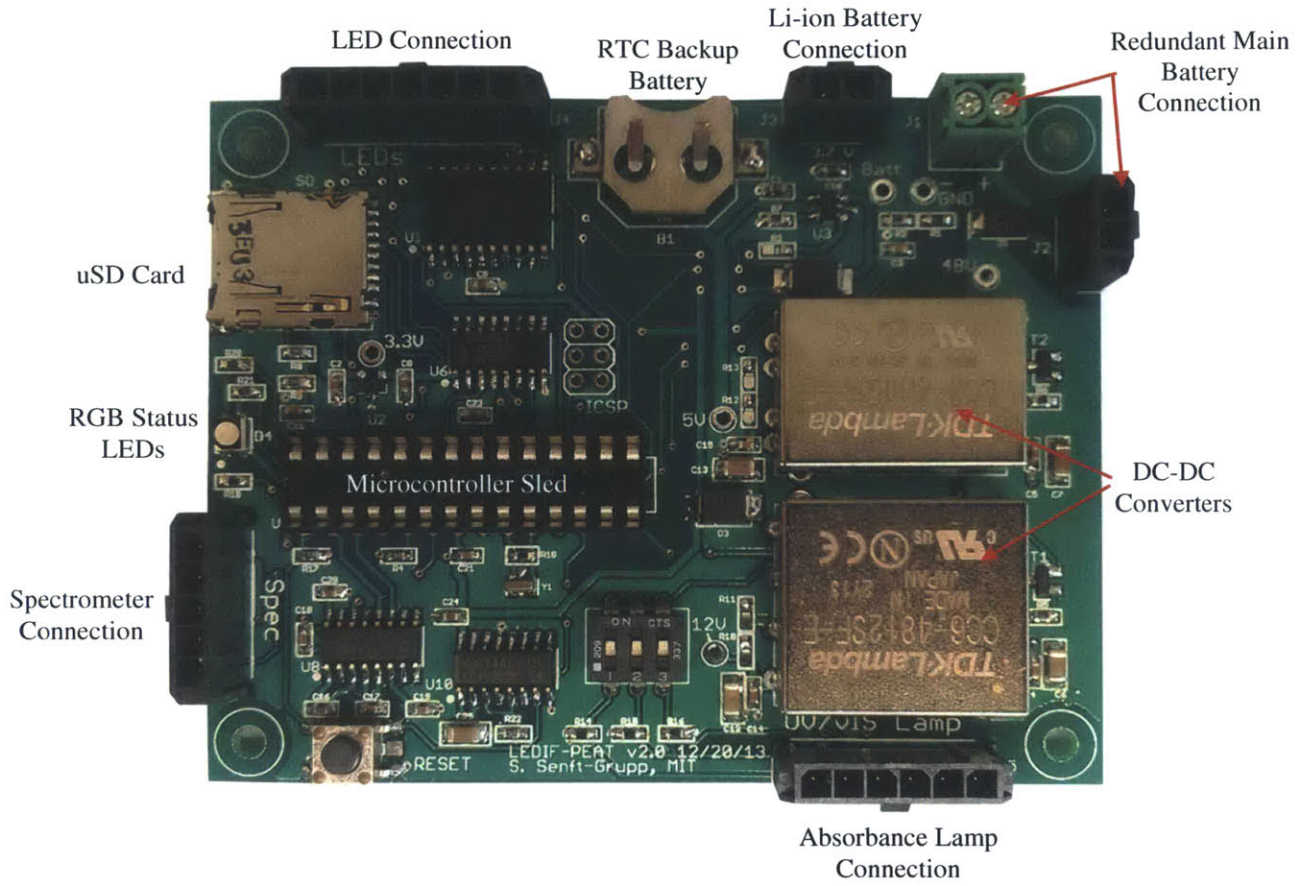

Figure 3.4 Control Circuit Board.

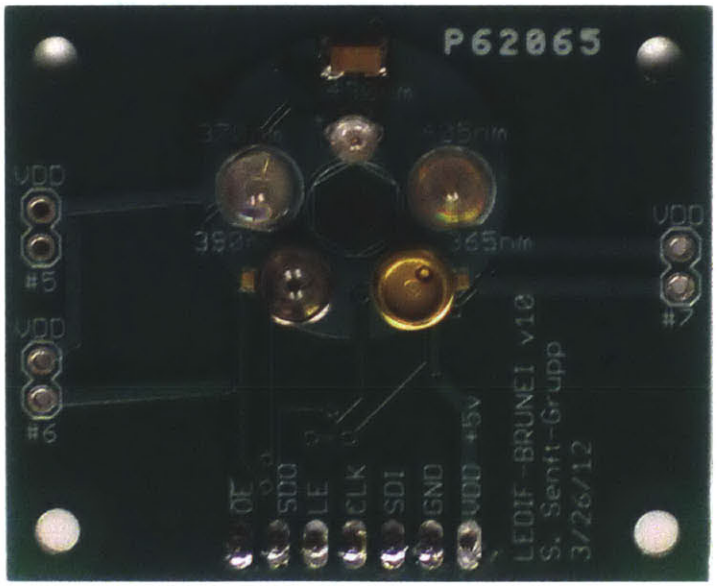

Figure 3.5 LED Circuit Board. The PCB is populated with five excitation LEDs and has an opening for the collection fiber optic. The LED controller IC and wire connector are located on the back of the PCB.

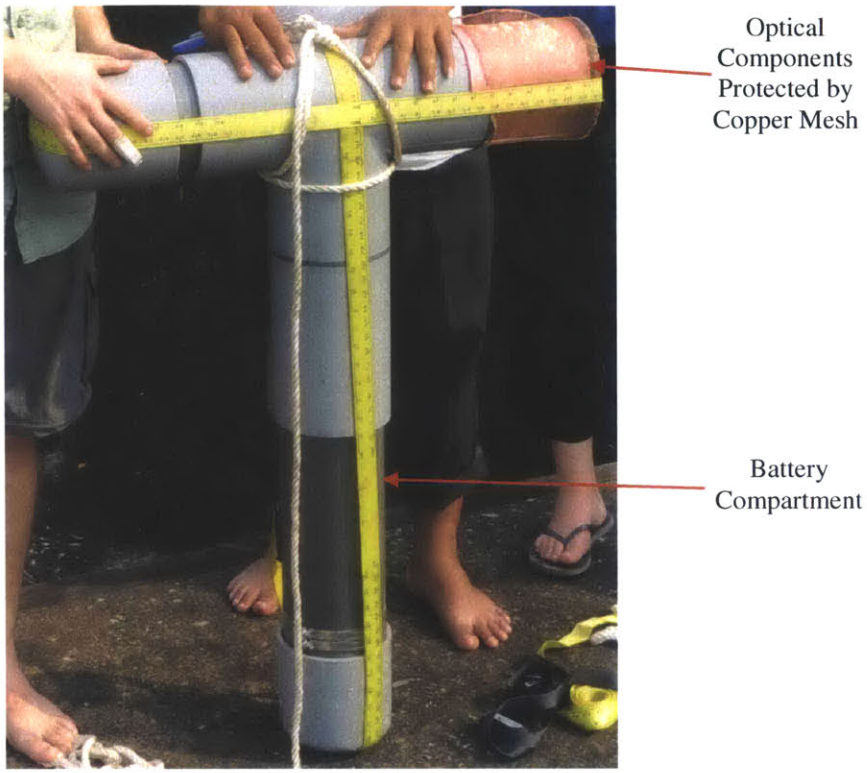

Figure 3.6 Instrument Housing. The instrument, shown prior to deployment, is held together with ratcheting straps.

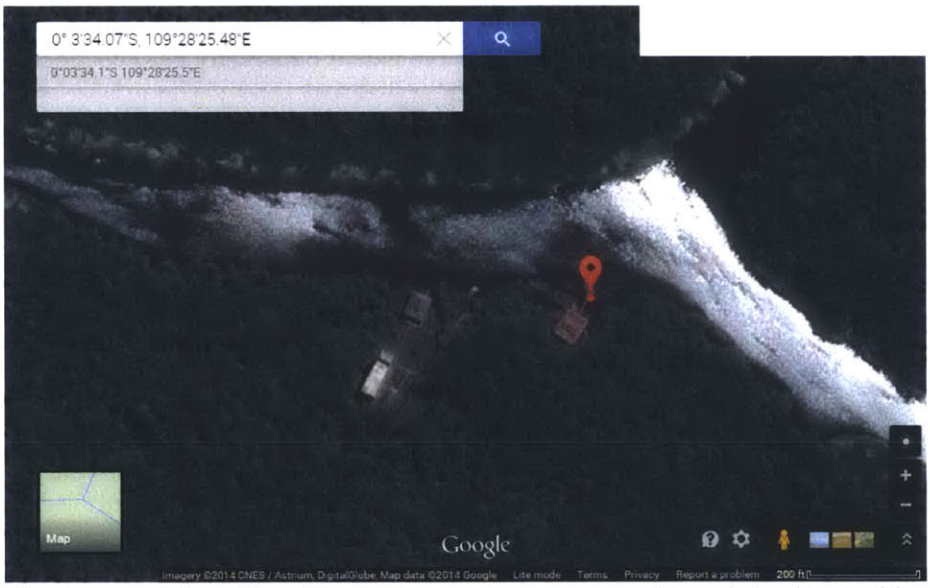

Figure 3.7 Deployment Location. The instrument was secured to a jetty located in front of the red building, downstream from the river convergence. River flow is from right to left

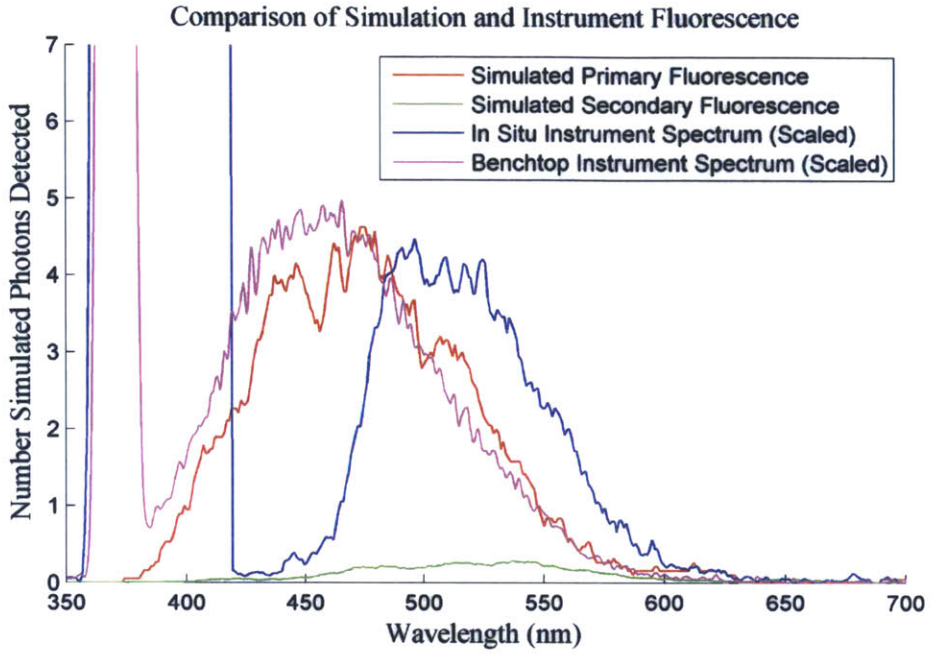

Figure 3.8 Comparison of Simulation, Instrument, and Lab Fluorescence Spectra. The instrument spectra have been scaled to the simulation data to better illustrate shape and wavelength range.

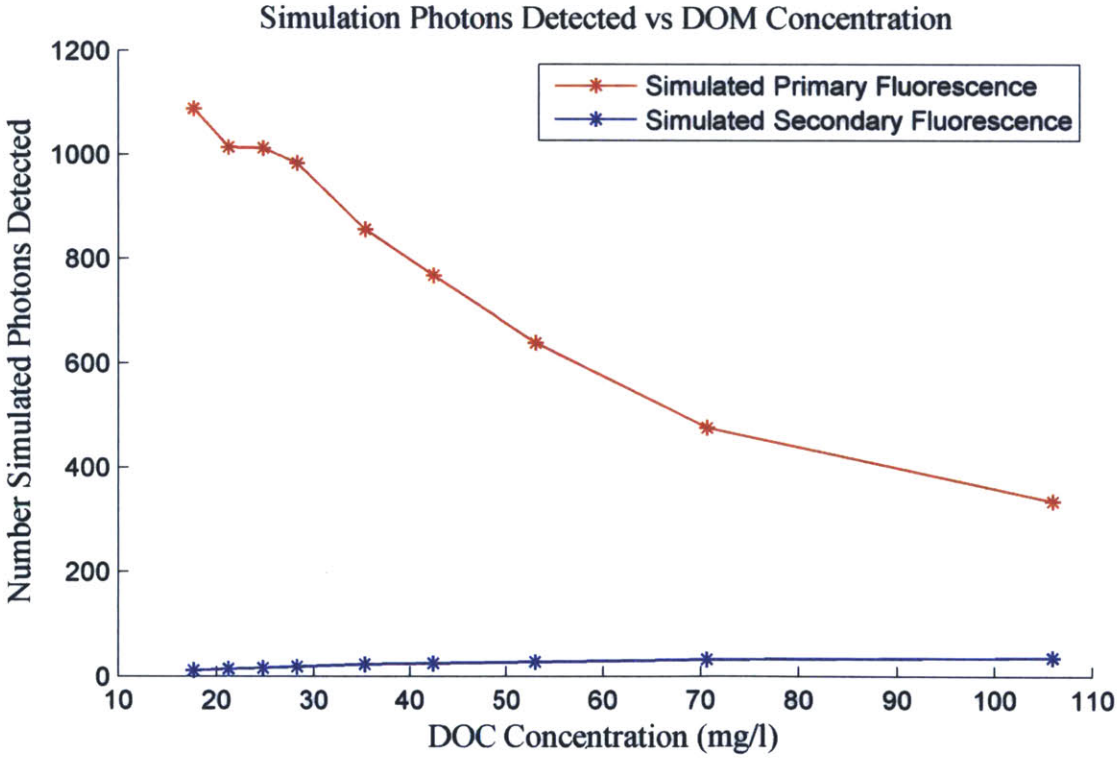

Figure 3.9 Simulation Results for Increasing DOM Concentrations.

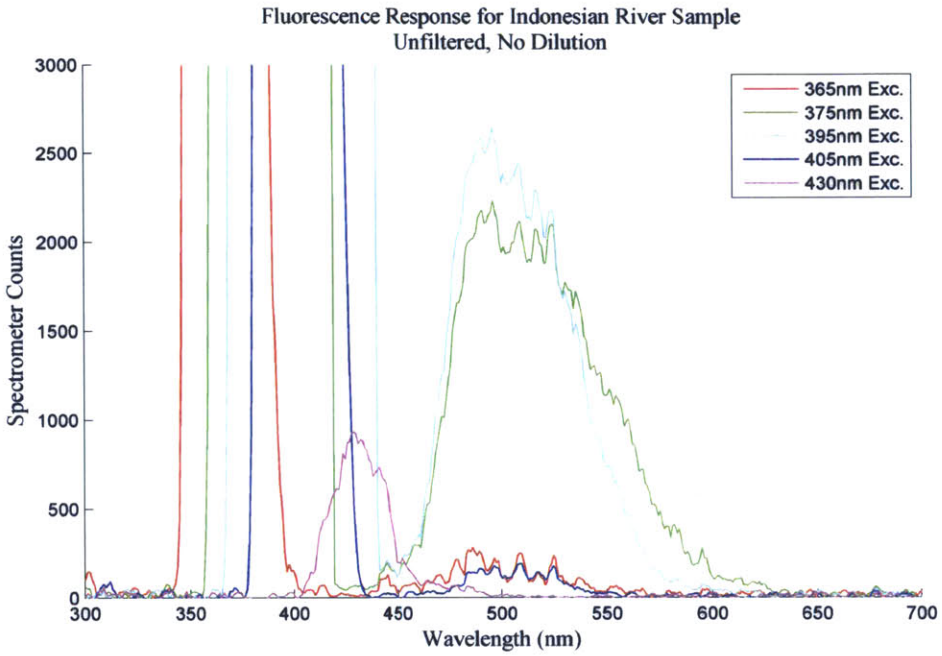

Figure 3.10 River Fluorescence Measured with Instrument. Each line represents the fluorescence with a different excitation wavelength.

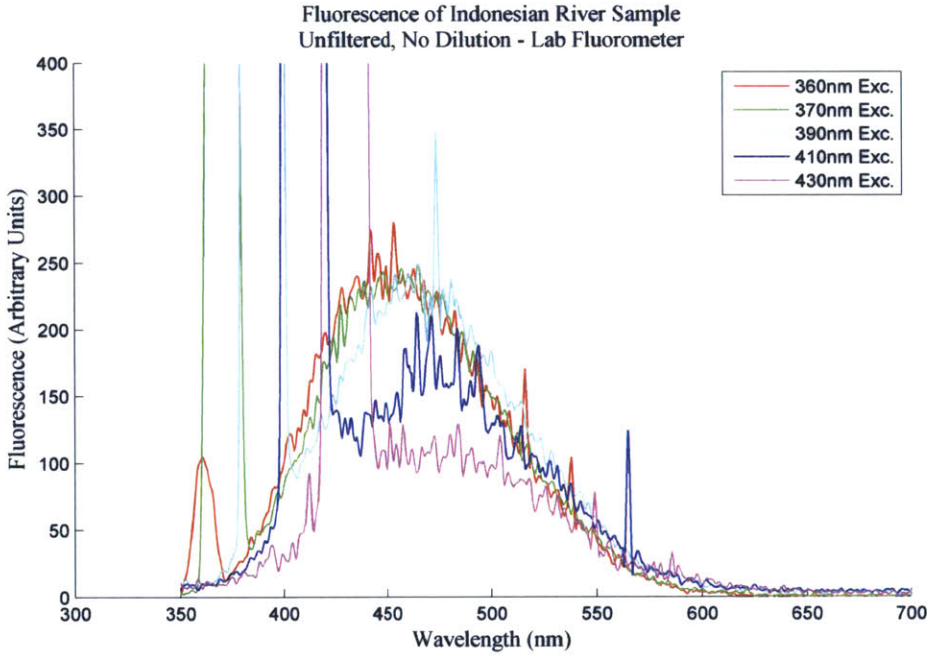

Figure 3.11 River Fluorescence Measured with Lab Fluorometer.

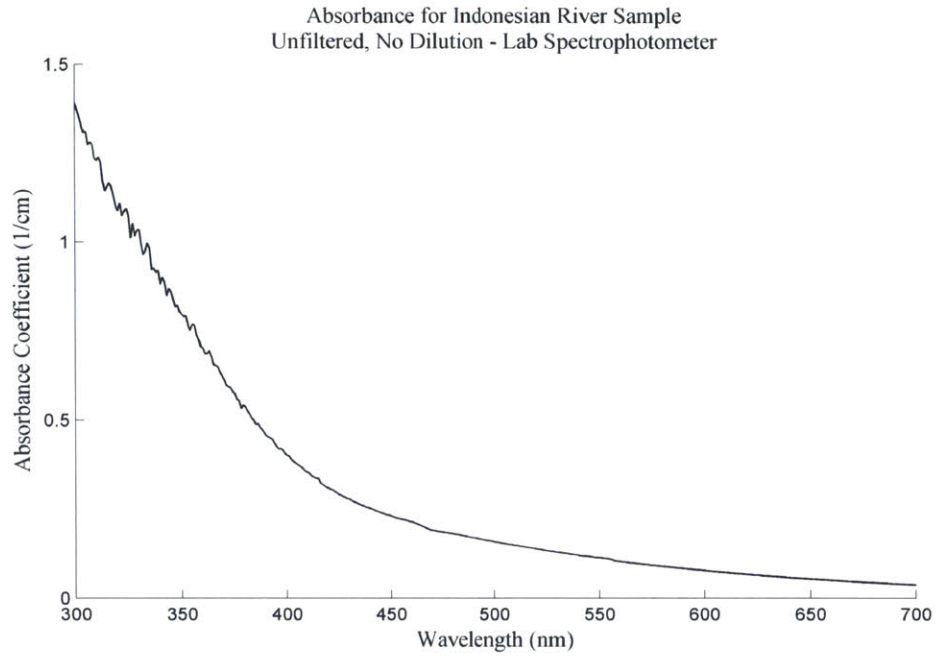

Figure 3.12 River Absorbance Spectrum Measured with Lab Spectrophotometer.

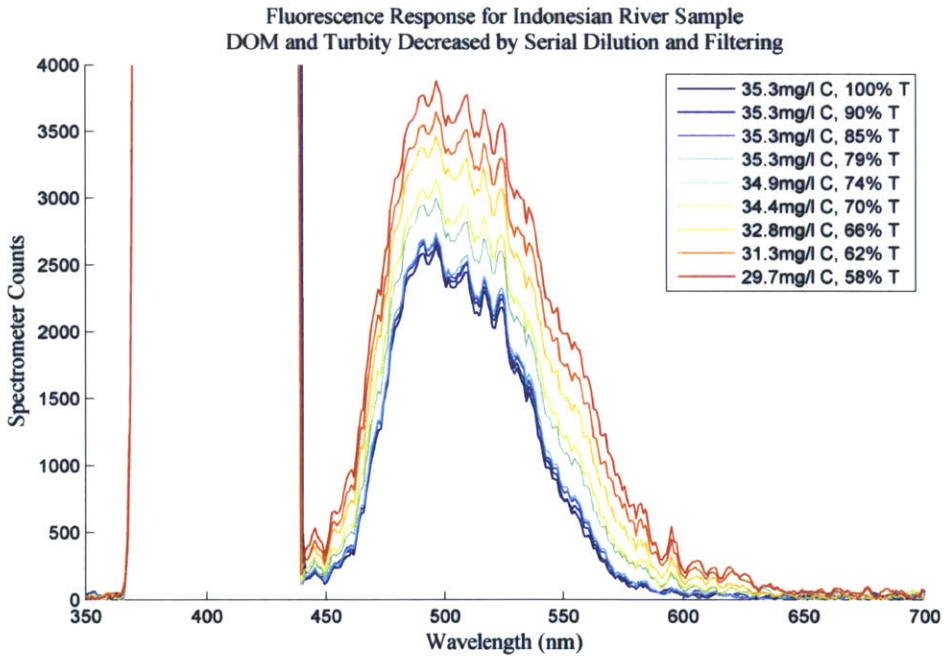

Figure 3.13 River Dilution Fluorescence Test #1. This figure shows the results of the first river water dilution test with excitation at 375nm. Each line represents a different DOM concentration and turbidity. The turbidity values shown in the legend represent the percent turbidity relative to the initial sample. Lower DOM and lower turbidity are correlated with greater fluorescence.

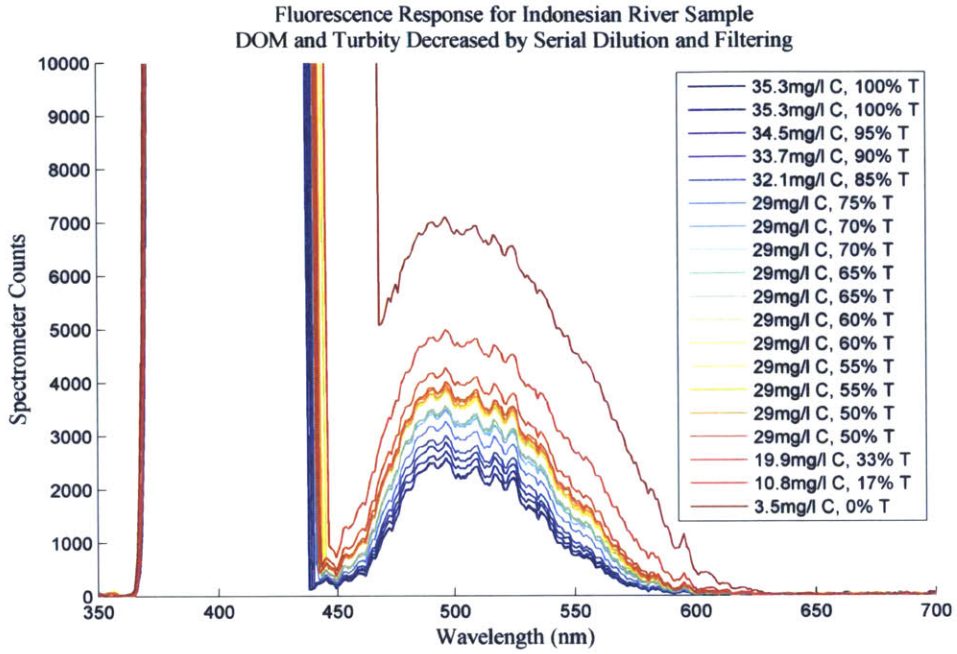

Figure 3.14 River Dilution Fluorescence Test #2. This figure shows the results of the second river water dilution test with excitation at 375nm.

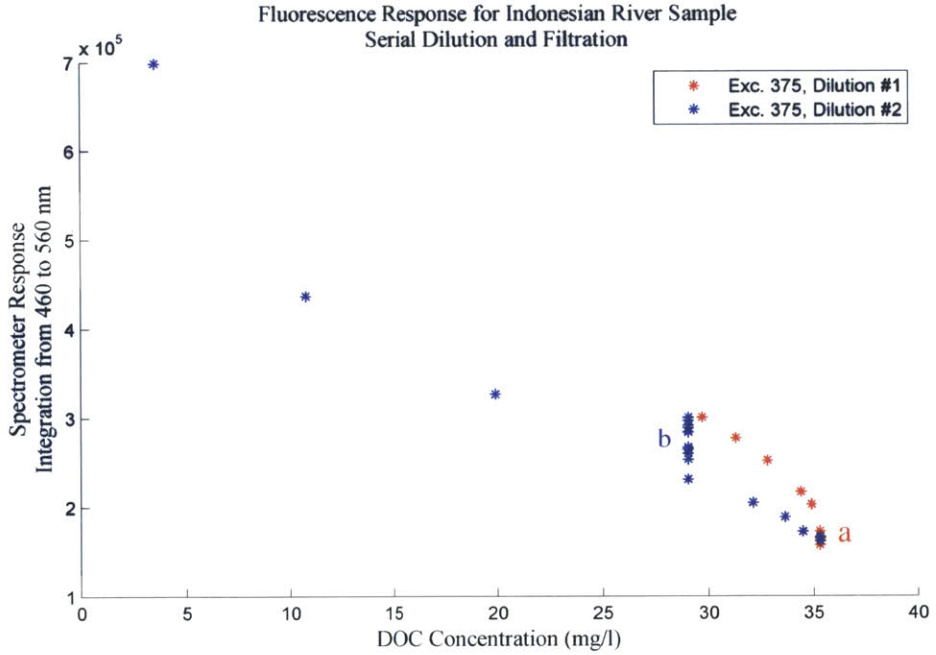

Figure 3.15 Fluorescence Response as Function of DOM. This figure shows the cumulative measured fluorescence for the dilution tests as a function of DOC. In the regions marked a and b, the change in fluorescence is due to changing turbidity.

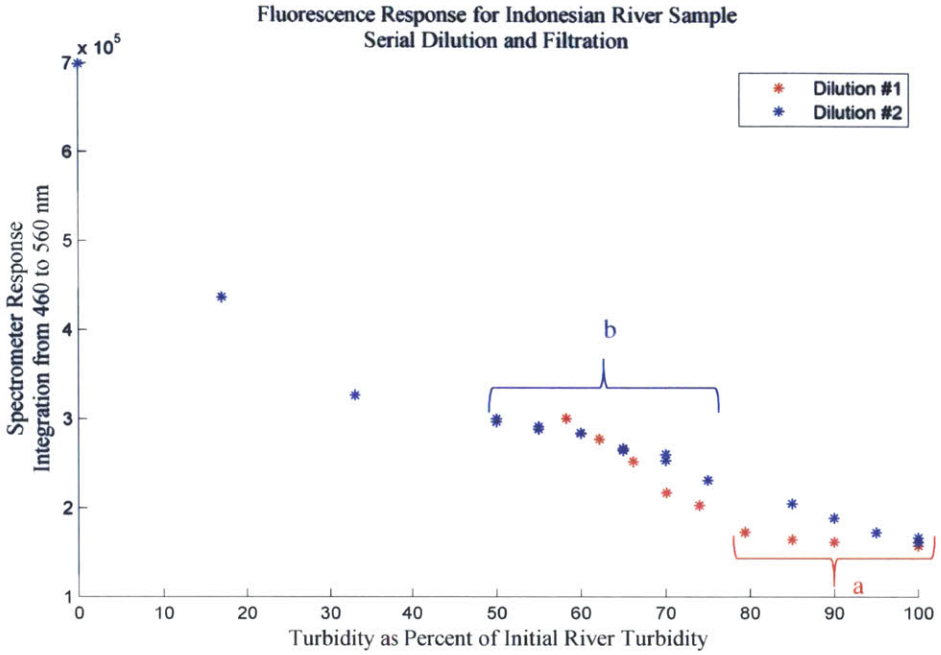

Figure 3.16 Fluorescence Response as Function of Turbidity. This figure shows the cumulative measured fluorescence for the dilution tests as a function of turbidity. In the regions marked a and b, turbidity is changing but DOM concentration is constant.

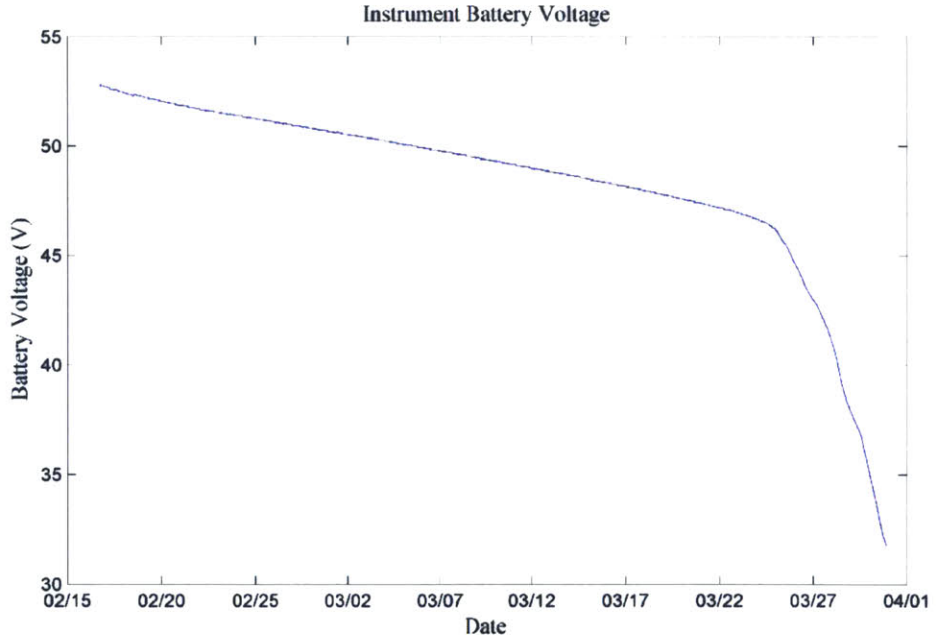

Figure 3.17 Instrument Battery Voltage. The battery exceeded its specified lifetime of four weeks. Even with the eventual significant decrease in voltage the instrument was able to keep operating down to 32 V.

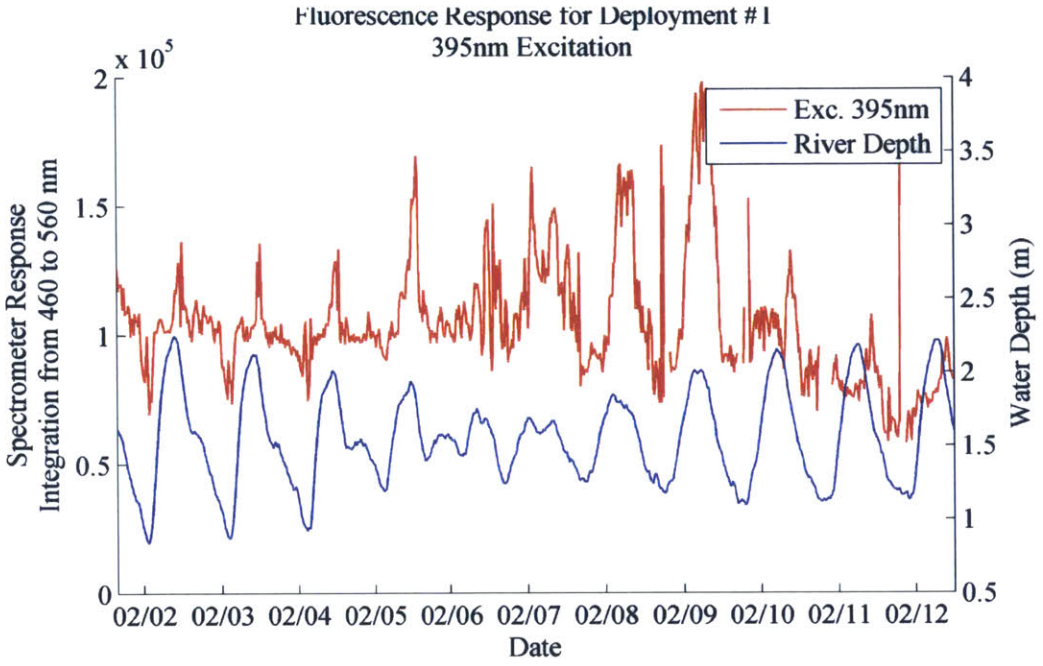

Figure 3.18 River Deployment #1. Fluorescence peak values for two excitations are plotted along with river depth. Higher fluorescence indicates lower DOM and/or turbidity.

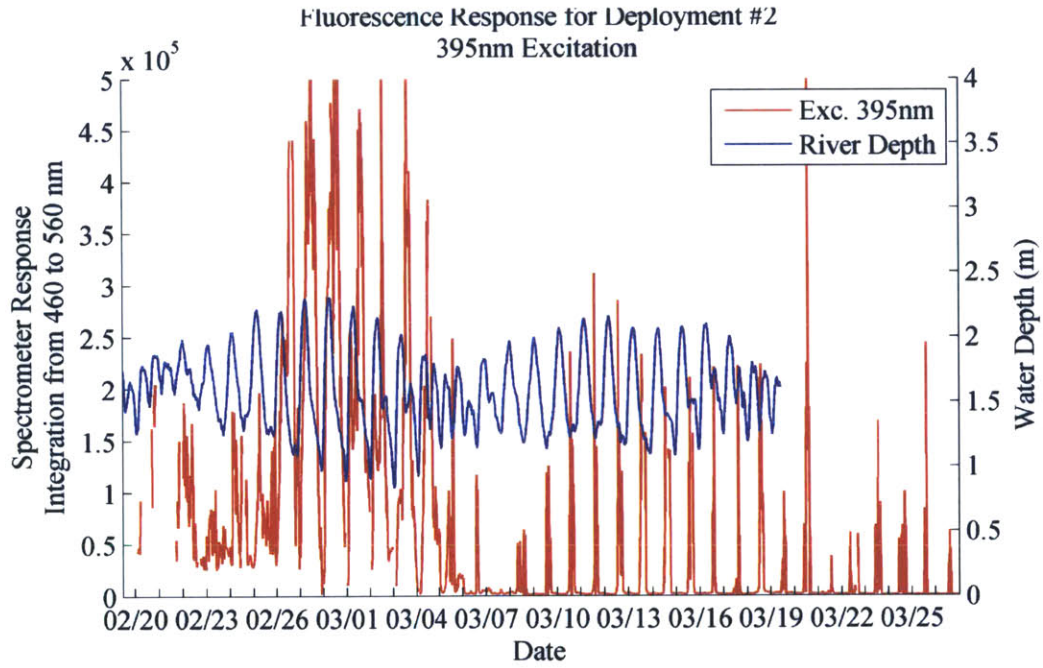

Figure 3.19 River Deployment #2. Fluorescence peak values for two excitations are plotted along with river depth. Higher fluorescence indicates lower DOM and/or turbidity. The instrument experienced conditions around 2/27 that impaired its measurement ability for the remainder of the deployment by covering the optical window in silt.

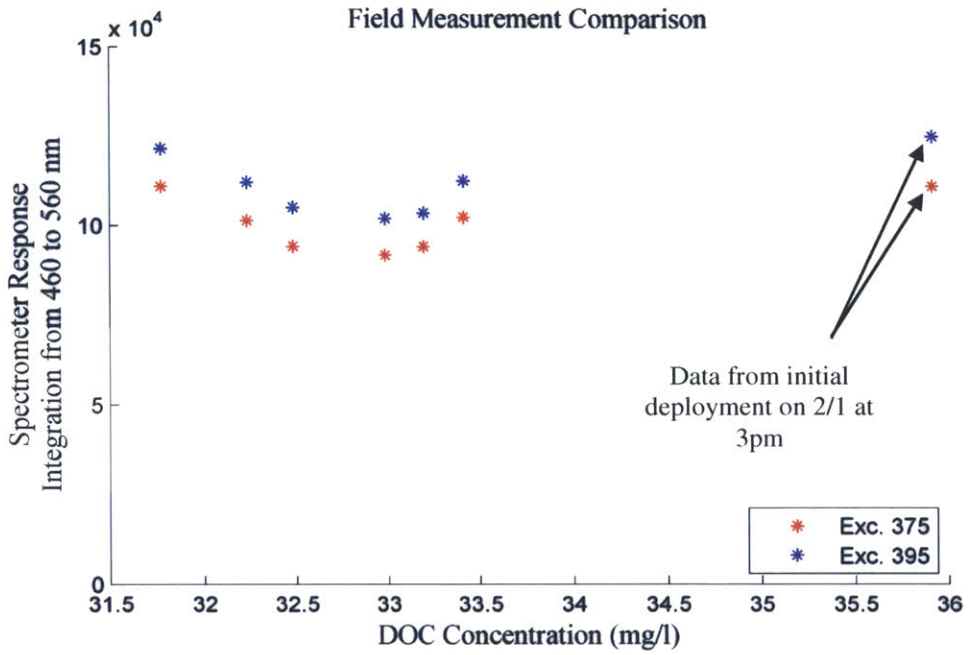

Figure 3.20 Comparison between TOC Analyzer and Instrument. The samples were gathered over a 6 hour period on February 2nd.

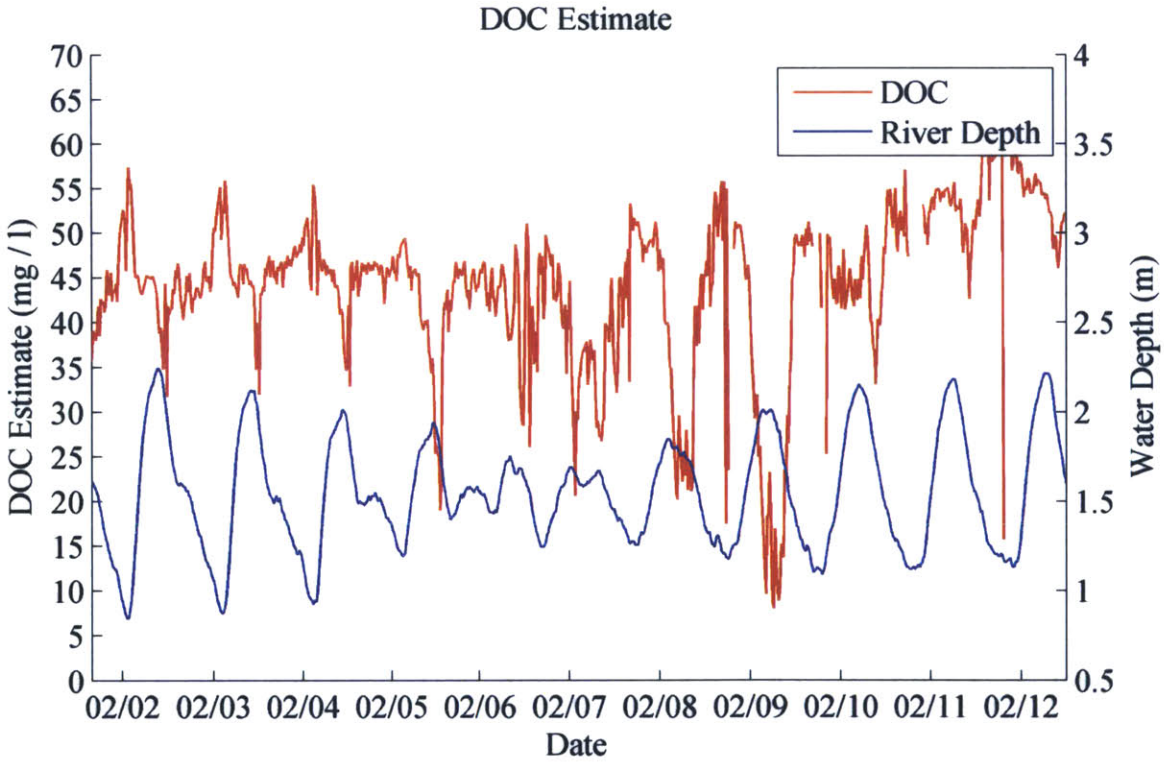

Figure 3.21 Estimates of DOC concentrations assuming constant turbidity.

Chapter 4

Gigahertz Data Acquisition System for Embedded Sensors

Abstract

New field deployable, laboratory grade instruments often require high speed (e.g. GHz) data acquisition capabilities, however no commercial options meet the size, power, or usability requirements for embedded sensors. We have developed a compact, low power, inexpensive data acquisition circuit board capable of acquiring data at a resolution of 8 bits and rate of 1 gigasample per second (GSPS). The board includes several features, including signal amplification, a fast trigger capture circuit, and simple USB-serial communication. The board's field programmable gate array (FPGA) stores up to 40 thousand data values and provides flexibility in real-time processing and data reduction that allows future users the ability to implement the best solution for their instrument. The analog input specifications have been tailored to connect directly to a photomultiplier tube (PMT).

4.1 Introduction

A significant research effort, especially in the environmental sciences, is devoted to developing new field deployable, laboratory grade sensors. These sensors range from physical to chemical, aquatic to atmospheric, taking advantage of a wide range of physical phenomena to measure the environment. In order for these instruments to be deployable in the field, they must be significantly smaller, lower power, and less expensive than their laboratory counterparts. They also must operate autonomously and without the support of typical laboratory equipment such as computers, oscilloscopes, or traditional data acquisition systems. For several types of instruments currently under development that rely on high speed data acquisition, such as fluorescence lifetime (see Chapter 5), time-gated Raman spectroscopy [1], or time-of-flight mass

spectrometry (TOF-MS)[2], there does not exist an off-the-shelf data acquisition system which meets the requirements to miniaturize these instruments for field use.

Development of high speed data acquisition systems has been recently accelerating. Faster analog-to-digital converters have led to the development of numerous boards for applications such as software defined radio, radar instruments [3], and radio astronomy [4], [5]. However none of the published designs are suitable for use in small field sensors. Typically the designs are too large and/or too expensive to meet the needs of environmental instruments.

The research aim was to develop a design that is easily usable by sensor researchers and ready for field instrument deployments. Figure 4.1 depicts the board in a typical instrument. To meet the research goal, there were several important design specifications. The first and most important was size. Many aquatic chemistry instruments are deployed on autonomous underwater vehicles (AUV's) with a circular payload diameter less than 20 cm, so the board's smaller dimension had to be significantly less than that. (Previous experience [6] shows that any object with a second dimension greater than 10 cm becomes difficult to package.) The second most important constraint was cost. In addition to component cost, the board needed to be inexpensively printed and assembled in low quantities. This requirement guided many of the design decisions regarding part selection and board fabrication. For performance, the minimum acceptable data conversion rate was 1 sample/ns. There was no specific constraint on the input voltage since it was assumed that that any gain, attenuation, or filtering could be performed prior to the board connection, however the input must accept both positive and negative signals. (Ultimately the design uses an analog-to-digital converter (ADC) with an adjustable full scale range between 595 mV and 805 mV.) Lastly, there also needed to be an easy method to connect to the board for control and data transfer, such as a USB or serial port. This paper presents our final design that meets these requirements and enables inexpensive data acquisition at rates of 1 gigasamples per second (GSPS) in a small form factor.

4.2 Data Acquisition System Description

This section describes the design of a high speed data acquisition system for embedded field instruments. The board consists of several modules: a 1 GHz analog ADC, a field programmable gate array (FPGA), a high speed trigger input, a USB to UART (Universal Asynchronous Receiver/Transmitter) converter, and a power supply system to provide the

required voltages. The analog signal to be digitized enters the board through a 50 Ω impedance SMA coaxial cable connector. The voltage must be between +/- 72 mV. It is fed through the board's analog front end circuitry which amplifies the signal by a fixed 13.7 dB and shifts the signal to satisfy the ADC's input common mode voltage of 1.26 V. The ADC converts the signal to an 8-bit digital representation and transfers that data to the FPGA for storage. The FPGA acts as both the storage for the data and as the controller for the board. It receives ASCII commands over USB to control the board's settings and data collection behavior, and transmits the collected data over USB to an external host (e.g. embedded computer). To aid with data capture, there is a second analog input that connects to dedicated, programmable hardware for identifying short trigger signals. The output from this circuit is transmitted to the FPGA and can be used for precisely timed data collection. Lastly, a single 5 V power input is efficiently regulated to six distinct rails and distributed to the various circuit components. Figure 4.2 provides a schematic system overview and Figure 4.3 shows a picture of the assembled circuit board. A complete schematic and layout is also provided. The following sub-sections discuss each module in further detail.

4.2.1 Analog-to-Digital Conversion

A high speed ADC is the core of the design. The circuit uses a Texas Instruments IC (TI ADC08D500) [7] from their line of 8-bit high speed ADCs to capture the input signal. The IC incorporates two ADCs, each operating at 500 MHz, which can be operated out of phase from each other to act as a single ADC operating at 1 GHz. The ADC provides a 1:4 time demultiplexer that reduces the data clock to 250 MHz and allows the output signals to be captured by low cost FPGAs running at moderate speeds. Along with cost and performance, this ADC was chosen because it exists in several speed grades, from 1 to 3 GSPS. By providing multiple speed options in the same package and pinout, future versions of the system can test higher data capture rates and other users of the device can choose the appropriate performance device for their application.

The ADC requires a differential input with a fixed common mode voltage. Since many signals of interest do not meet these conditions, we implemented TI's recommended solution. The single ended analog input is buffered by a differential driver (TI LMH6555) [8] which automatically adjusts the output common mode voltage based on a reference provided by the

ADC. Much of the ADC and analog front end design was aided by the TI reference design for its high speed ADCs [9].

To clock the ADC, we used a Silicon Labs factory programmed chip (SI530) [10]. The ADC noise value is strongly dependent on the system clock input jitter. Silicon Labs provides a series of pin compatible, clock sources that range over the potential frequency required by this and faster ADCs, and have very low phase jitter (0.25 ps) and period jitter (2 ps RMS). Although this chip does not provide the ability to program the clock frequency in system, it greatly simplifies design and provides lower clock jitter than many multi-chip clock reference designs.

The ADC provides an on-chip temperature diode to monitor when a new calibration sequence should be initiated. The circuit uses a TI TMP421 [11] to record the ADC and ambient temperature with +/- 1 C resolution.

4.2.2 Data Capture and Storage

An FPGA is used to capture and store the high speed digital signals. FPGAs are typically used for high speed data applications due to their large number of inputs, high speed parallel data processing capability, and design flexibility. We chose the Xilinx Spartan-6 (XC6SLX9) FPGA for several reasons: it is inexpensive, it comes in a pin package (i.e. not ball grid array) that simplifies layout and reduces assembly costs, and it has adequate processing power and internal storage for many data capture applications. The introductory Xilinx development environment is also free, easy to use, and well supported by an active developer community.

The FPGA is used to receive the 32 LVDS ADC data signals, control the ADC behavior through a combination of 1-bit signals and a serial data bus, interface with peripheral ICs over an I2C data bus, provide a serial interface for circuit control and data transfer, and handle power sequencing.

4.2.3 High Speed Trigger

For applications that rely on collecting data from a precise start point, a fast trigger system is incorporated. The trigger circuit consists of a programmable reference level and a latch-enabled comparator. Figure 4.5 provides a complete trigger schematic. A latch-enabled comparator works in two modes. With the latch off, it performs as a standard comparator: when input A is greater than input B, the output is high, and vice versa. If at any point the latch pin is

turned on, the output is locked at its current state and the inputs no longer drive the output. This latch functionality can be leveraged in cases where the input trigger signal is potentially shorter than the clock period of the IC servicing the trigger request (i.e. the FPGA). As an example, laser trigger pulses in optical measurement systems can be on the order of picoseconds, much shorter than even a fast FPGA operating at several hundred megahertz.

Positive feedback from the output to the latch is used to extend the time the output stays high. For comparators with single ended outputs, this effect can be achieved with an RC timing circuit [12]. However the fastest comparators typically use a specialized differential signaling method at the output (e.g. LVDS), and an RC circuit would decrease response time and lead to improperly terminated transmission lines. The comparator in our design (ADCMP553) uses LV-PECL differential signals for the output and for the latch. The output signals connect to the FGPA, through proper PECL termination, and are also fed back through a resistor network to the latch pins, enabling the latch whenever the output goes high (i.e. the system receives a trigger signal). However there also needs to be a way reset the comparator latch. For this, the latch signals are also connected through a resistor network to pins on the FPGA, referred to as the trigger reset pins. During normal operation when the comparator is waiting for a trigger signal, the trigger reset pins are set as high impedance inputs. When the comparator receives a trigger signal, the output goes high and the latch is enabled. Once the FPGA acknowledges the comparator output, it changes the trigger reset pins to outputs for one clock cycle and turns the latch off. The resistor network is present to maintain the voltages on the latch pins close to the levels specified for LVPECL, although in the worst case scenario it is calculated that they may exceed for less than one clock cycle (4 ns) the maximum and minimum recommended voltages by 0.5 V and 1.2 V, respectively.

The comparator reference voltage is generated from a programmable digital to analog converter (DAC). The 10-bit DAC operates at 3.3V, providing a reference resolution of approximately 3 mv. The host controller can program the reference voltage at any time by sending the appropriate ASCII commands to the FPGA.

4.2.4 Power Management System

The circuit's power consists of six distinct power rails. Three supplies at 1.2V, 1.8V, and 3.3V power the FPGA and other digital logic chips. The other three supplies provide voltages of

1.9V, 2.5V, and 3.3V to power the ADC, the analog front end, and the ADC clock. All six rails are initially generated by a high efficiency DC-DC converter (LTC3374) [13] that accepts an input voltage between 3.6 and 5.5V. The schematic and board layout for this IC was copied and modified from the provided test design [14]. For the three supplies feeding the analog components, the DC-DC converter generates intermediate voltages of 2.3V, 2.8V, and 3.6V that are further reduced by low dropout (LDO) linear regulators. The regulators produce power signals with very low ripple and fast response times to abrupt power changes, requirements for the high performance analog portion of the circuit.

Power is enabled by one of two methods: a physical toggle switch or a digital strobe input. Both signals are inputs to a push button power controller that controls the initial power sequencing and monitors for subsequent power loss or turn-off signals. The turn off signal allows for proper power down sequencing to protect the ADC chip.

4.2.5 External Communication

The circuit board provides a USB-UART converter and four general purpose input/outputs for communication with peripherals. The USB-UART bridge is achieved with a Future Technology Devices (FTDI) FT230X. This chip was chosen due to the wide availability of FTDI drivers, including on embedded Linux based systems. The four I/O pins connect directly to the FPGA, however three of these are also connected to status LEDs.

4.2.6 Printed Circuit Board

The printed circuit board (PCB) is designed for inexpensive manufacture in low quantities. It uses a standard 4-layer stack up (Figure 4.4) with calculated trace widths for the specific required impedances of high speed signals, and does not require impedance control from the manufacturer. The minimum trace width and spacing is 5 mil, and the minimum hole width and spacing is 12 mil.

4.3 Circuit Operation

The following sections describe the typical operation flow of the circuit.

4.3.1 Power On and Initialization of FPGA

Upon sensing a valid input voltage (from either the toggle switch or the external supply being activated) or by receiving a strobe signal on the pushbutton input pin, the circuit board initiates the power on sequence. Rails of 1.2V, 1.8V, and 3.3V, which power the FPGA, programmable read-only memory (PROM), and USB-UART, are enabled sequentially. When all three voltages reach minimum levels for the FPGA and PROM, those two chips communicate to program the FPGA with the PROM's stored firmware. Once programming is complete, the FPGA waits for commands over the UART before continuing.

4.3.2 Power On and Initialization of ADC

The ADC is activated by a command over the UART. When the command is received, the 1.9V ADC supply voltage is enabled. After 10 milliseconds, the 2.5V and 3.3V, which power the analog input amplifier and 500 MHz clock, supplies are enabled. This sequence ensures that the ADC never experiences a voltage on its analog input or clock pins before it is powered. The FPGA then waits until it locks on the clock signal received from the ADC. This wait time is a combination of the time for the clock IC to stabilize, for the ADC to lock onto the clock input, and for the FPGA to lock onto the ADC clock output, and is approximately 20 ms.

Once the clock signal is locked, the FPGA begins serial communication with the ADC to program its 8 control registers. The control registers provide access to settings such as single or dual data rate, data clock phase, and dual edge sampling. After programming the registers, the ADC calibration sequence is begun. When the calibration is complete, the ADC begins sampling a single input at 1 GSPS and transmitting the resulting data to the FPGA.

4.3.3 Data Acquisition

Given the flexibility of an FPGA, there are many ways to collect and process the data coming from the ADC. The following are descriptions of the simplest schemes, although other implemented options are discussed later.

4.3.3.1 Data Acquisition Start

There are multiple ways to signal to the board that it should begin storing data. The simplest is to send it a "Start" command over the UART. Immediately after the board receives this command it collects a set of data.

Typically a more useful method is to use an external input trigger signal to start data collection. (See section 4.2.3 for a discussion of the trigger). There are two trigger modes: one-shot and automatic continuous. When the trigger is placed in one-shot mode using an ASCII command, the circuit waits for a trigger signal to start collecting data. When it is done collecting one set of data, the board must receive another command to re-arm the trigger to collect additional sets of data. In automatic continuous mode, the board automatically re-arms the trigger once a set of data has been collected and processed, and continues to do so until it receives an ASCII command to stop re-arming the trigger.

The last method is to trigger from a feature in the data stream. The only implemented example of this method is to trigger if the input signal exceeds a threshold. However it is possible to program other features such as pulses, pulse trains, etc. as the trigger condition. As with the external trigger, this can be configured in a one-shot or continuous triggering mode.

4.3.3.2 Data Acquisition

Once the desired data acquisition start condition is met, the board collects a set of data. The term "set of data" is used here as an arbitrary definition since the FPGA can be programmed myriad ways to collect, process, and reduce data as defined by the user's needs. However two of the simplest schemes have been implemented and are described here.

The first option is to use the board as intermediate storage between the signal and the host controller. In this case, the user controls the number of points or, put another way, the length of time, to collect data after the start condition is met. The data is immediately stored in a first-in first-out (FIFO) 32-bit wide buffer clocked from the ADC data clock. In this configuration, the maximum FIFO size on this FPGA is ~40 kilobytes, i.e. data can be collected for 40 microseconds after the trigger. As soon as the FIFO contains any data, the FPGA begins transmitting the values over the UART to the host controller. The FPGA continues to write data to the storage FIFO until it has stored the number of values specified by the user, after which it disables writing to the FIFO until the entire FIFO data content is transmitted to the host computer over the USB-UART connection. At this point the system is ready to be triggered again to repeat the process. Figure 4.6 shows the flowchart of this scheme.

Another simple but useful data acquisition scheme is to sum multiple sets of data before transmitting to the host controller. This method is useful when the rate of raw data collection (trigger rate x data set length) exceeds the continuous throughput possible over the UART. The

user programmatically sets the number of data sets to sum together before transmitting the results to the host controller. For the code currently implemented, this can be a value between 1 and 256. In order to collect data continuously, additional FIFO stages are required to buffer the incoming data and to store the summed results that are ready to transmit. These additional buffers, along with the fact that 2 bytes of data are now required for each data point, reduces the maximum data set length to one fifth of the total available FPGA memory.

To sum the data there are three FIFO buffer stages. The first stage uses a FIFO with independent write and read clocks, and different input and output data widths. The write clock is the 250 MHz data clock and the read clock is the system clock (typically 100 MHz). The data input bus is 32-bits wide and the output bus is 8 bits wide, so the output data is serialized into the proper time order. The second FIFO stage performs the continuous summation of the data. Whenever there is data in the first FIFO, the second FIFO write enable and read enable signals are simultaneously asserted, the new data is summed with the old value, and the result is then re-written to the second FIFO. There are short pipeline buffers to ensure that the new and old data are properly aligned, and logic to control the edge cases of the first and last sets of data to be stored. A counter keeps track of the number of data sets summed together. When this counter reaches the user specified value, the output data from the second FIFO is written to a third FIFO. The third FIFO communicates with the UART to transfer the data over the USB-UART. Figure 4.7 shows the flowchart of this scheme.

4.3.4 Additional System Features

The system has several other features that are also controlled over the UART with ASCII commands. These commands can be received at any time and take effect on the next data collection cycle. These settings include the following: 1) placing the ADC in half speed mode to reduce power consumption; 2) reading the ADC and ambient temperatures; 3) requesting an ADC calibration; 4) placing the system in low power sleep mode.

4.4 Test methods

Two PCBs were printed and populated for performance testing. The circuit was powered from a 5V supply and current monitored with an ammeter. All test analog input signals were generated using an RF signal generator (Marconi Instruments 2022D) with an amplitude of 50

mV (143mV peak-to-peak). The signal amplitude represents approximately 98% of the full scale range of the ADC. The RF signal ranged between 109 kHz and 499 MHz with specific values chosen to enable coherent sampling by the ADC. Table 5-1 shows the specific frequencies selected. The FPGA was programmed to collect 32,768 sequential data points which were then transmitted to a computer and saved for analysis.

At each frequency the signal to noise (SNR), signal to noise and distortion (SINAD), total harmonic distortion (THD), spurious free dynamic range (SFDR), and effective number of bits (ENOB), and gain were calculated in MATLAB using built-in and custom code [14]. Additionally the data were passed through a Fourier transform (FFT) to produce a frequency power spectrum with a resolution of 30,518 kHz.

4.5 Results

4.5.1 Analog-to-Digital Conversion

The results from the data acquisition circuit testing demonstrate the board's performance over a range of frequencies (Figure 4.8 through Figure 4.13). Complete spectra from select frequencies are shown in Figure 4.14 through Figure 4.22. As expected, there is a general trend of decreasing performance with increasing signal frequency, but overall the values are within several dB to the values specified in the ADC datasheet. Over its complete frequency range, the board is able to gather data with approximately 6.5 effective number of bits, one half bit below the datasheet-specified 7.0 bits. Additionally the system gain changes by less than 5% over the entire frequency range.

In each of the collected spectra there is a clear signal at 250 MHz. This signal corresponds to a small difference between the two internal ADCs when converting values. In certain applications this can be compensated for by sampling the ADCs with no input and then subtracting the average background value for each ADC from the signal.

Additionally, unlike in most ADC testing setups, there was no filtering of the input signal. Harmonic signals, particularly the second harmonic, were observed to exist on the test signal using a high speed oscilloscope. Therefore the results presented here may understate the true performance of the board.

4.5.2 Power Consumption

The power was measured with the board in four different modes: active, ADC off, all analog off, and power down. Each mode trades off power consumption reduction with the time required to resume active data collection mode (referred to as transition time). In active mode, with the ADC and FPGA converting and storing data at the highest rate possible, the board consumes 700 mA at 5.07 V for a total power of 3.55 W. Putting the ADC chip in low power mode reduces the power consumption to 2.0 W, and requires a transition time of 500 ns. In the third mode, with all of the analog components powered down, the circuit consumes 0.78 W. In this mode, the ADC, 500 MHz clock, and input amplifier are all turned off, however the trigger circuit is still active and accounts for approximately 40% of this power consumption. Transition time from this mode to active data collection is approximately 20 ms and is due largely to the power up time of the 500 MHz clock. The final mode, power down, disables all power supplies with only the push button controller active and listening for a digital input strobe signal. This mode's power consumption is 62 uW and the transition time to data collection is approximately 2.5 s, due mostly to the initial FPGA programming.

4.5.3 Design and Cost

The board was designed with the goals to minimize size and cost. Table 4-2 provides a detailed cost breakdown. The final board dimensions are 6.35 cm wide by 11.43 cm long by 1.27 cm thick. (This thickness includes optional programming header.) Total cost for parts, board, and assembly is approximately $500 for a single board.

4.6 Discussion

4.6.1 Applications

This board has been designed as a generic data acquisition system, although its immediate intended application is as part of a new laser induced fluorescence (LIF) field instrument to measure certain aspects of natural water chemistry (see Chapter 5). The instrument uses a flow cell, q-switch laser, monochromator, and photomultiplier tube (PMT). By measuring the wavelength-specific exponential decay of observed fluorescence, it is intended to estimate the water concentration of various chemicals of interest such as polycyclic aromatic

hydrocarbons (PAHs) (e.g. pyrene). The instrument is small enough to be deployed on *in situ* oceanography platforms including autonomous underwater vehicles (AUVs) and buoys. Figure 4.23 shows the results of fluorescence lifetime data of an aqueous solution containing pyrene measured with this circuit board in the laboratory. Two exponential decays are apparent: one lifetime of ~2 ns that is attributable to background compounds in the water, and a second lifetime of ~130 ns that is attributable to the pyrene.

4.6.2 FPGA and Digital Signal Processing

The current FPGA code provides the simplest data acquisition operation but leaves significant resources available for further development. In designing this board for ease of use, we traded off high speed data transport with a simple serial UART interface. To compensate for these relatively low data rates, we suggest implementing digital signal processing and data reduction methods on board the FPGA. The specific solution depends on the application but can include averaging multiple data acquisitions to reduce random noise, performing line fitting and transmitting the resulting fit parameters, or measuring the frequency composition of the signal and reporting peak values. The ubiquity of FPGAs has led to ample design resources for implementing the logic for these types of signal processing algorithms.

4.6.3 Future Work

Several additional suggestions are made for future evolution of this board. The first is to further reduce the overall board size. On the current version, a significant portion of the total board area is used to route the high speed low voltage differential signals (LVDSs) between the ADC and the FPGA. This routing was done to keep the data lines at similar lengths, and ensure that the signals arrive at the FPGA at the same time. (Note: The signals were divided into three groups corresponding to three distinct clock regions of the FPGA, but within each group all the signal wires are the same length.) However the FPGA has dedicated delay lines on each of its inputs that are supposed to be used to accomplish a similar effect without the need to take up board space. On the first board version this feature was neglected in order to simplify FPGA design and timing, but later versions could take advantage of these advanced features. Also now that all the device sub-circuits have been verified, certain board debugging features can be removed to reduce the total space required.

Another future hardware revision is to investigate the board's performance with faster ADCs. In theory, no changes to the PCB should be necessary to use the other ADCs in TI's ADC08 series. Some significant changes are required, however, to the FPGA code to handle faster data rates. These include using dedicated dual data rate input buffers and operating certain portions of the chip at higher clock speeds.

4.7 Conclusion

We have developed a data acquisition board capable of capturing an input signal at a rate of 1 GSPS with 8-bit resolution. The board can be manufactured for $500, making it one of the least expensive options for researchers who need to capture high speed signals. The circuit's small size and moderately low power consumption allow it to be used in a wide variety of emerging field instruments. The on-board FPGA provides flexibility in real-time processing and data reduction, allowing future users the ability to implement the best solution for their instrument.

4.8 Acknowledgements

The authors would like to thank the following organizations and individuals. Funding for this project came from the Singapore MIT Alliance for Research and Technology (SMART) and MIT Sea Grant. Texas Instruments, Silicon Labs, and Linear Technology provided samples of their ICs. Contributors eteam00 and gszakacs on the Xilinx forums gave invaluable advice, encouragement, and entertainment.

4.9 References

[1] J. V Sinfield, O. Colic, D. Fagerman, and C. Monwuba, "A low cost time-resolved Raman spectroscopic sensing system enabling fluorescence rejection.," *Appl. Spectrosc.*, vol. 64, no. 2, pp. 201–10, Mar. 2010.

[2] M. J. Manard, "A design for a compact time-of-flight mass spectrometer.," *Rev. Sci. Instrum.*, vol. 83, no. 10, p. 105111, Oct. 2012.

[3] V. T. Vijayendra, "Design and Testing of a Prototype High Speed Data Acquisition System for NASA," University of Massachusetts Amherst, 2011.

[4] J. M. Ford, R. M. Prestage, and M. Bloss, "Experiences with the design and construction of wideband spectral line and pulsar instrumentation with CASPER hardware and software: the digital backend system," *Proc. SPIE 9152, Softw. Cyberinfrastructure Astron. III*, vol. 915218, p. 915218.

[5] H. Jiang, H. Liu, K. Guzzino, D. Kubo, C. Li, R. Chang, and M. Chen, "A 5 Giga Samples Per Second 8-Bit Analog to Digital Printed Circuit Board for Radio Astronomy," *Publ. Astron. Soc. Pacific*, vol. 126, no. 942, pp. 761–768, 2014.

[6] C.-L. Ng, S. Senft-Grupp, and H. F. Hemond, "A multi-platform optical sensor for in situ sensing of water chemistry," *Limnol. Oceanogr. Methods*, vol. 10, pp. 978–990, 2012.

[7] Texas Instruments, "High Performance, Low Power, Dual 8-Bit, 500 MSPS A/D Converter," ADC08D500 datasheet, May 2005, [Revised Apr 2013].

[8] Texas Instruments, "Low Distortion 1.2 GHz Differential Driver," LMH6555 datasheet, Nov. 2006, [Revised Mar. 2013].

[9] Texas Instruments, "Big Gig Reference Platform," 2005.

[10] Silicon Labs, "Crystal Oscillator (XO) (10 MHz to 1.4 GHz)," Si530/531 datasheet, Revision D.

[11] Texas Instruments, "±1°C Remote and Local Temperature Sensor," TMP421 datasheet, Jul. 2007, [Revised May 2012].

[12] C.-W. Pei, "Planet Analog - Articles - Fast, simple one-shot pulse stretcher detects nanosecond events," *Planet Analog*, 2006. [Online]. Available: http://www.planetanalog.com/document.asp?doc_id=527407. [Accessed: 09-Feb-2013].

[13] Linear Technology, "8-Channel Parallelable 1A Buck DC/DCs," LTC3374 datasheet, 2013.

[14] L. Yongping, "Sine Wave Spectrum Analysis Function." 2013.

[15] Advanced Assembly, personal communication, 2013.

4.10 Figures and Tables

Table 4.1 Test Frequencies

Target Frequency	Coherent Frequency
100 kHz	91.6 kHz
1 MHz	946 kHz
10 MHz	9.6741 MHz
50 MHz	49.957 MHz
75 MHz	74.677 MHz
90 MHz	89.691 MHz
100 MHz	99.823 MHz
110 MHz	109.65 MHz
120 MHz	119.96 MHz
140 MHz	139.86 MHz
160 MHz	159.82 MHz
175 MHz	174.47 MHz
200 MHz	199.98 MHz
250 MHz	249.97 MHz
350 MHz	349.95 MHz
425 Mhz	424.84 MHz
500 MHz	499.91 MHz

Table 4.2 Total Board Costs

Item	Cost	Notes
ADC	$178	[1]
FPGA	$17	[1]
ADC Clock	$25	[1]
Power Ics	$30	[1]
Other Components	$84	[1]
PCB	$70	[2] Minimum 5 boards
Assembly	$100	[2] Minimum 1 board
Total	**$504**	

[1] Prices estimates from Digikey on 11/29/14.
[2] Actual costs from Advanced Assembly.

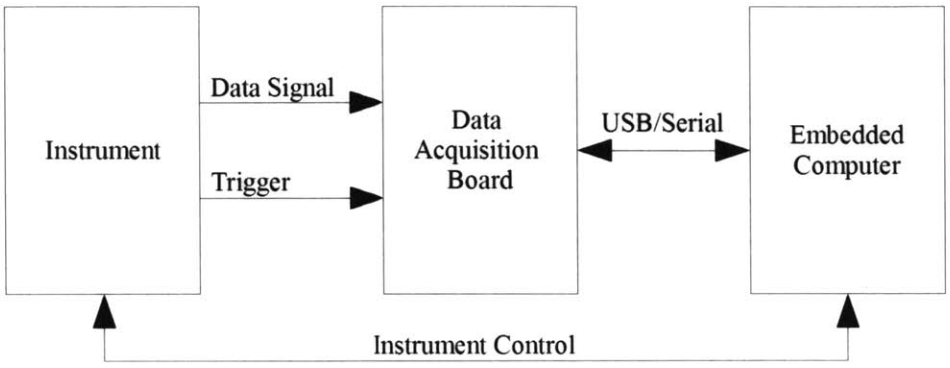

Figure 4.1 Data acquisition board as part of an instrument.

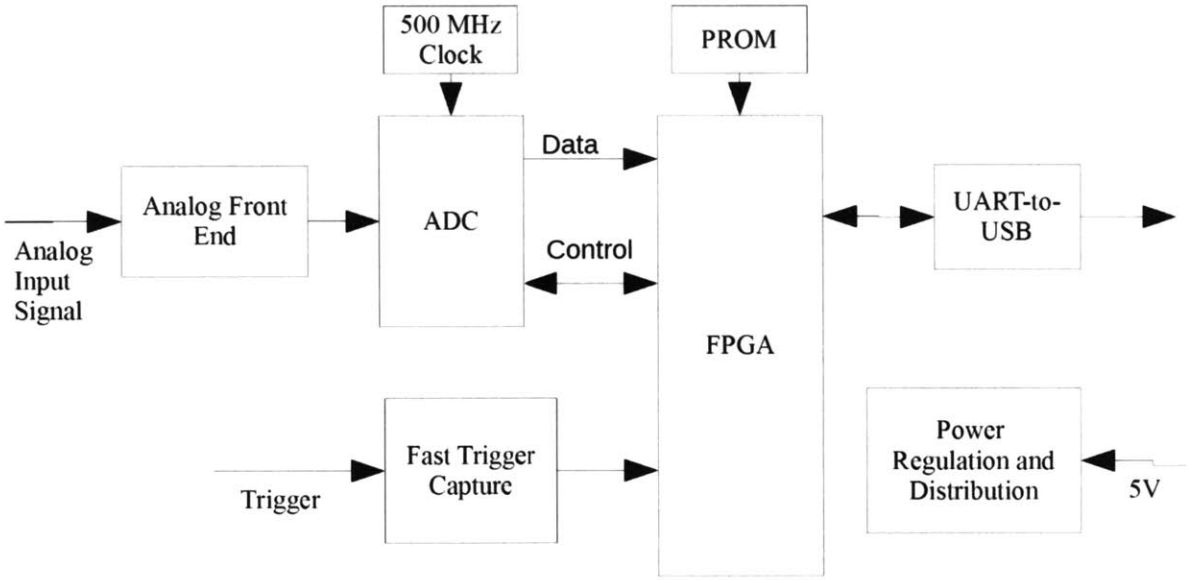

Figure 4.2 Data acquisition circuit sub-system diagram.

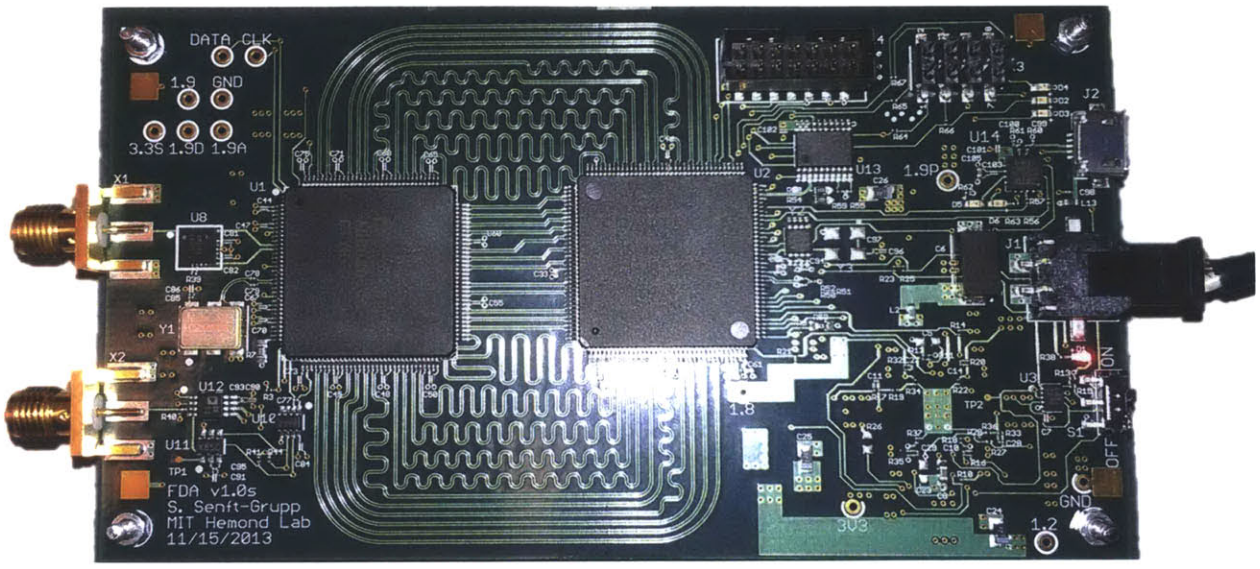

Figure 4.3 Photo of populated circuit board.

Layer	Stack up	Processed Thickness	Description
			Liquid PhotoImageable Mask
1		1.900	Copper Foil
		3.600	PrePreg 2113
		3.600	PrePreg 2113
2		1.400	
		39.000	FR4 Core
3		1.400	
		3.600	PrePreg 2113
		3.600	PrePreg 2113
4		1.900	Copper Foil
			Liquid PhotoImageable Mask

60.0000

Figure 4.4 PCB 4 Layer Stack Up. The 4-layer board stack up is standard and available through most PCB printing companies [15]. Units are mil (thousands of an inch).

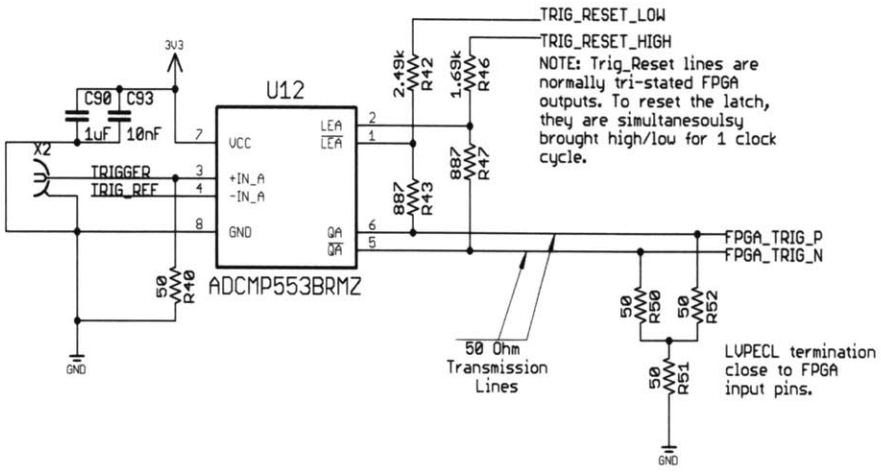

Figure 4.5 Trigger Circuit Schematic

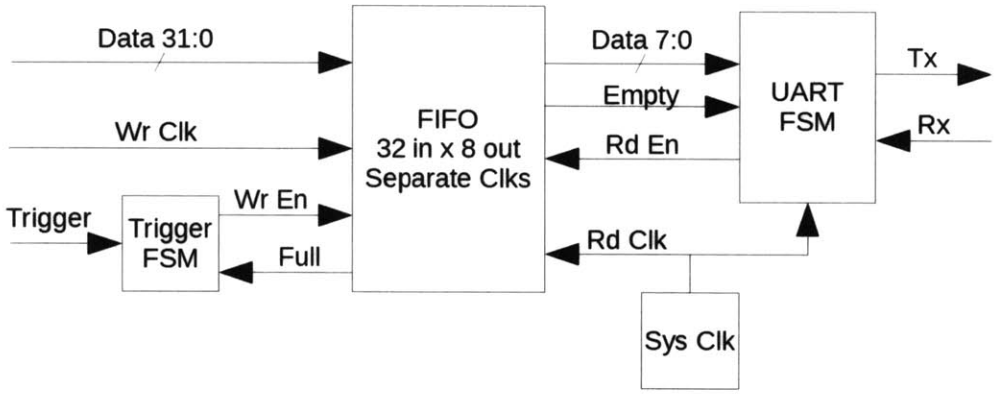

Figure 4.6 Simplified diagram of FPGA for basic data acquisition. The trigger signal feeds a state machine that asserts the Write Enable signal of the FIFO until it is full. The UART state machine controls the Read Enable signal and asserts this whenever it is ready to send the next byte of data and the FIFO is not empty. The FIFO is automatically generated by the Xilinx ISE and handles cross clock domain logic and asymmetrical data write and read widths. Additionally the user can programmatically set the FIFO Full threshold with ASCII commands (not shown).

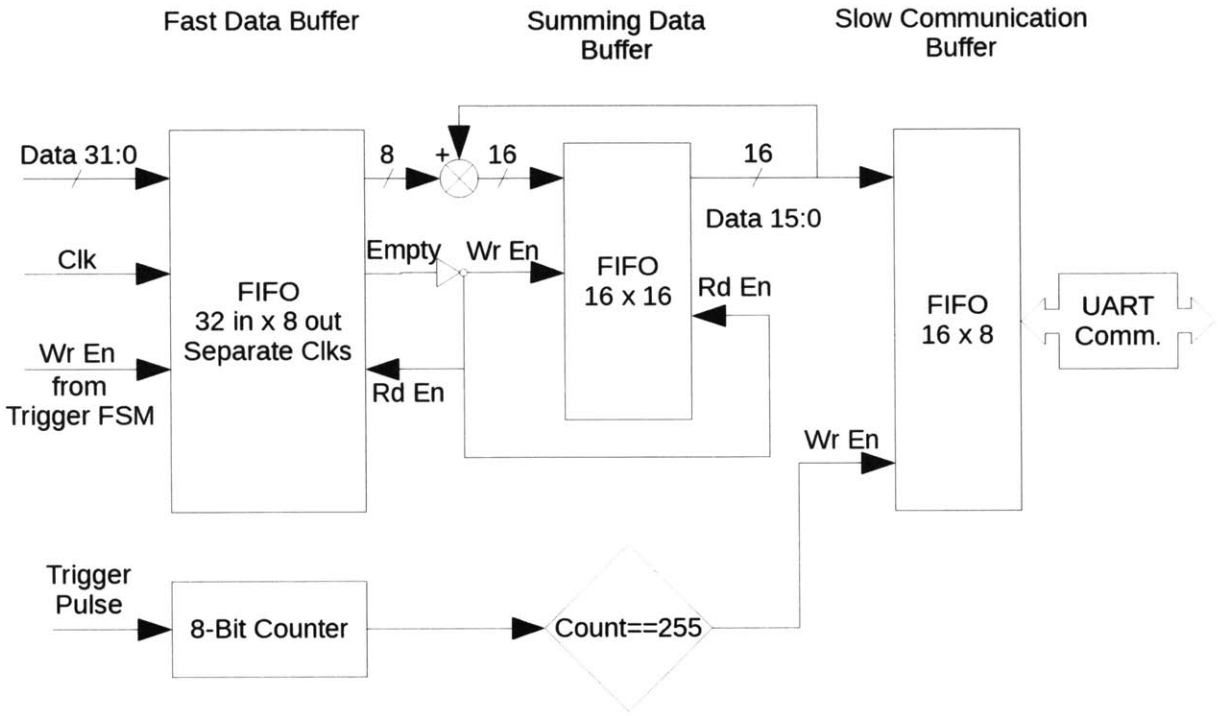

Figure 4.7 Simplified diagram of FPGA for summing of multiple data sets.

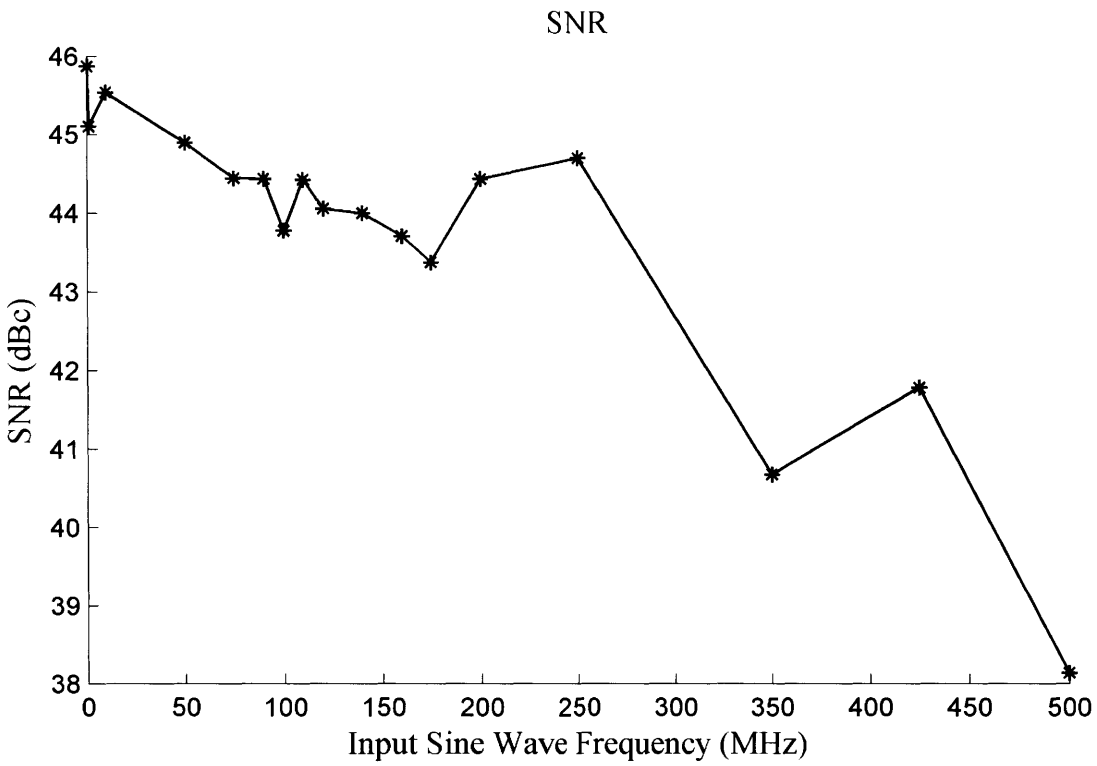

Figure 4.8 Signal to Noise Ratio.

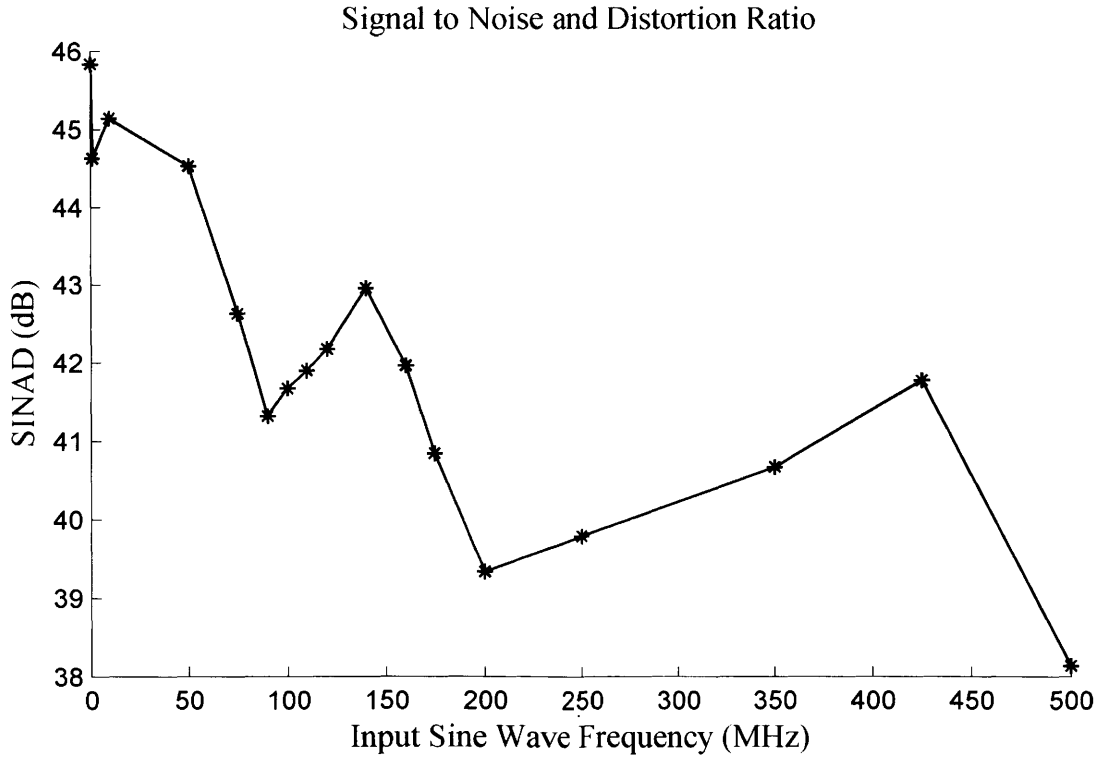

Figure 4.9 Signal to Noise and Distortion Ratio.

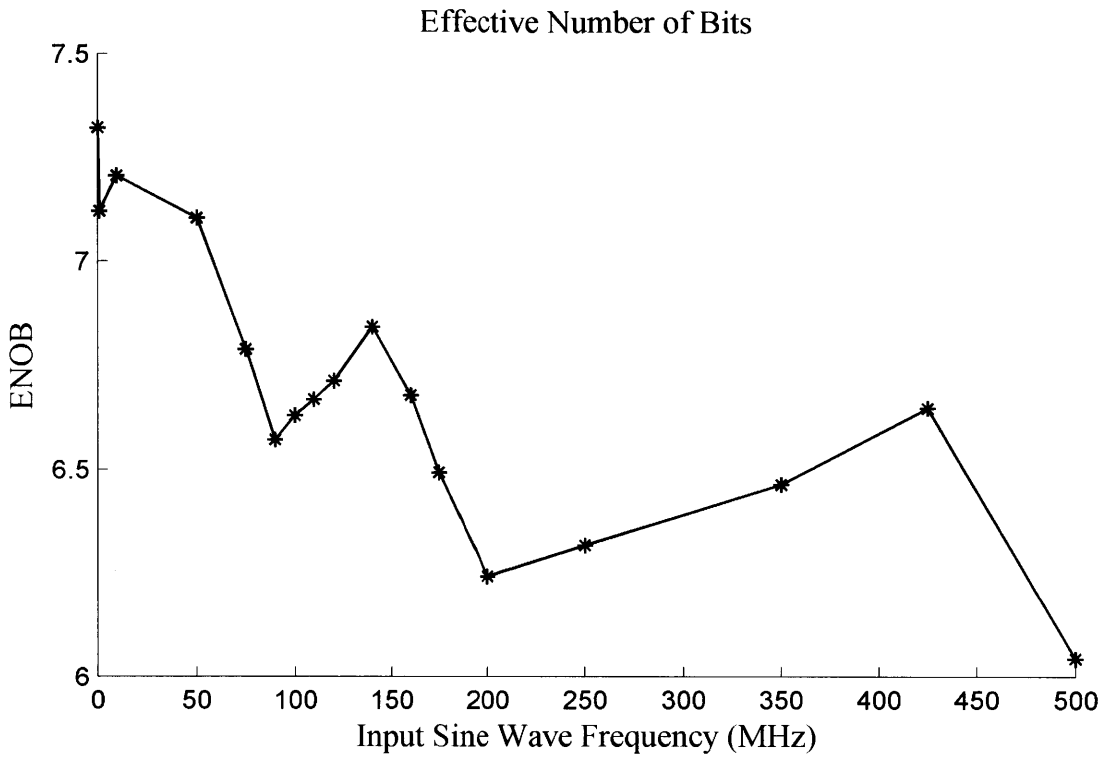

Figure 4.10 Effective Number of Bits. The ADC chip ENOB is 7.0 at 250 MHz. The measured values show a slight degradation presumed to arise from the additional circuitry.

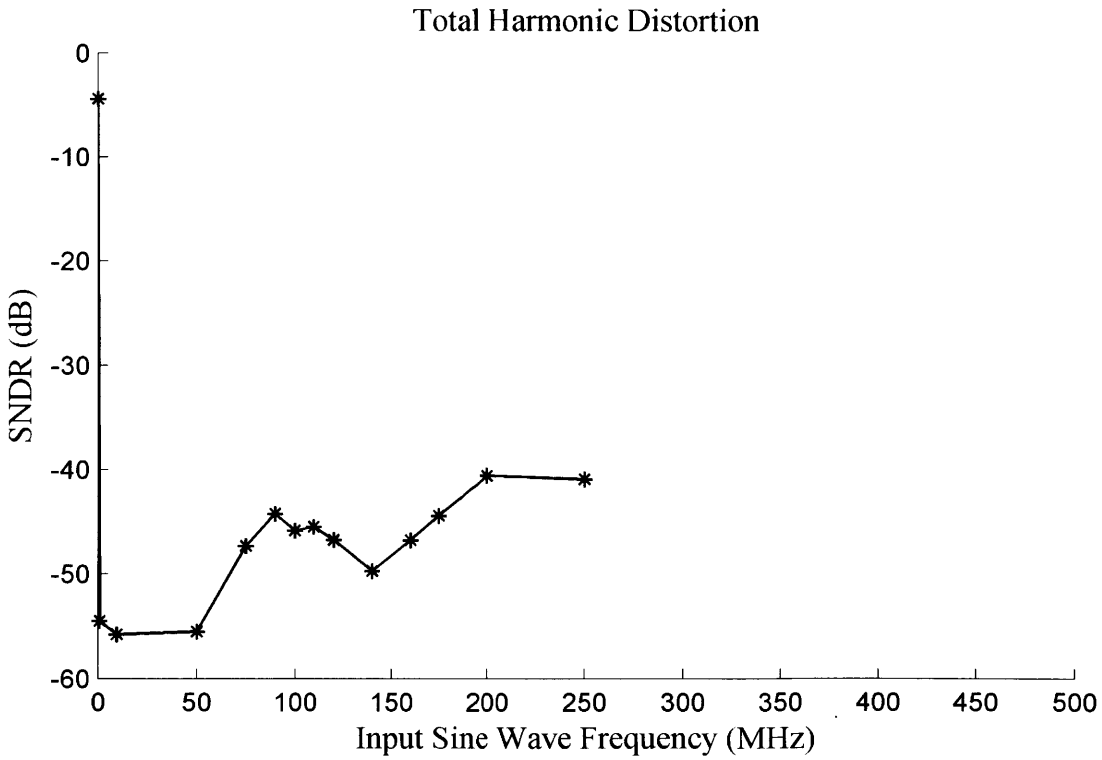

Figure 4.11 Total Harmonic Distortion.

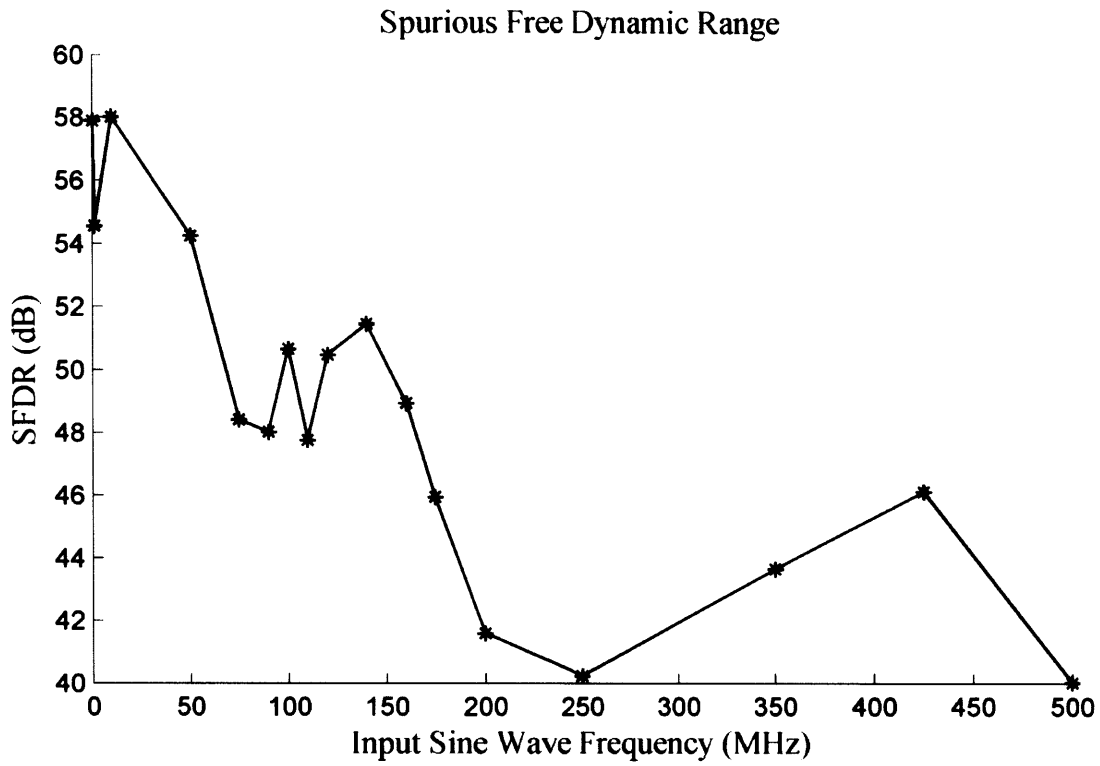

Figure 4.12 Spurious-Free Dynamic Range

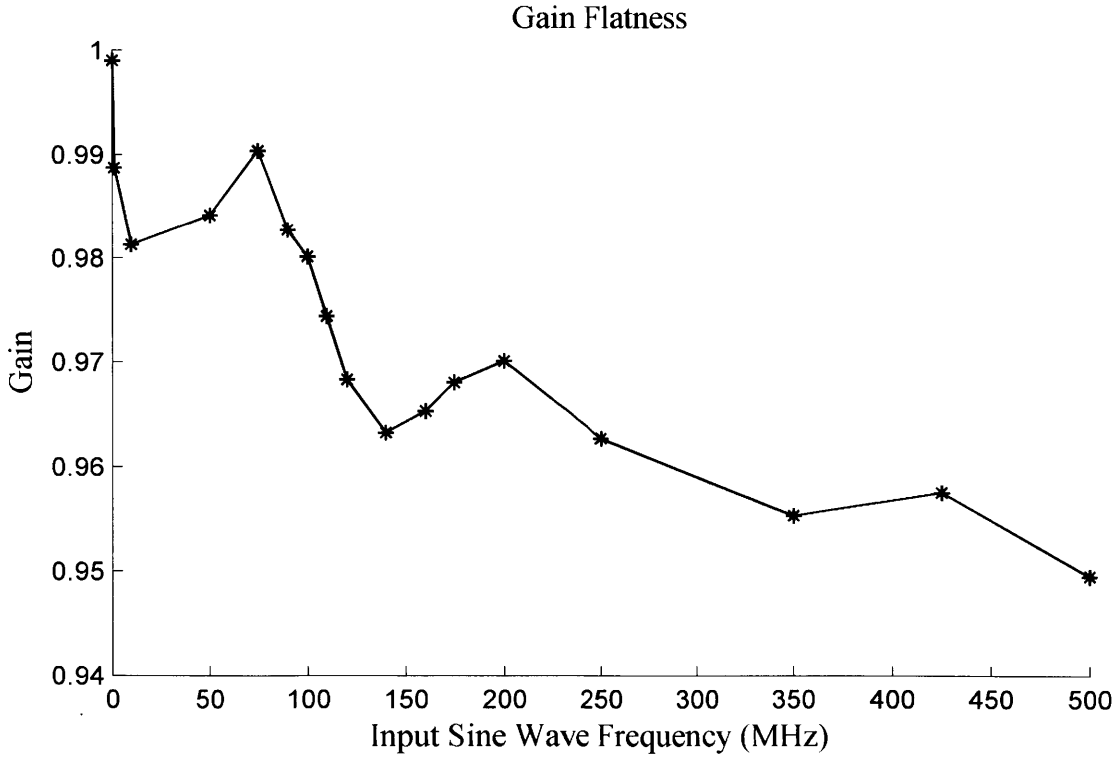

Figure 4.13 Gain Flatness.

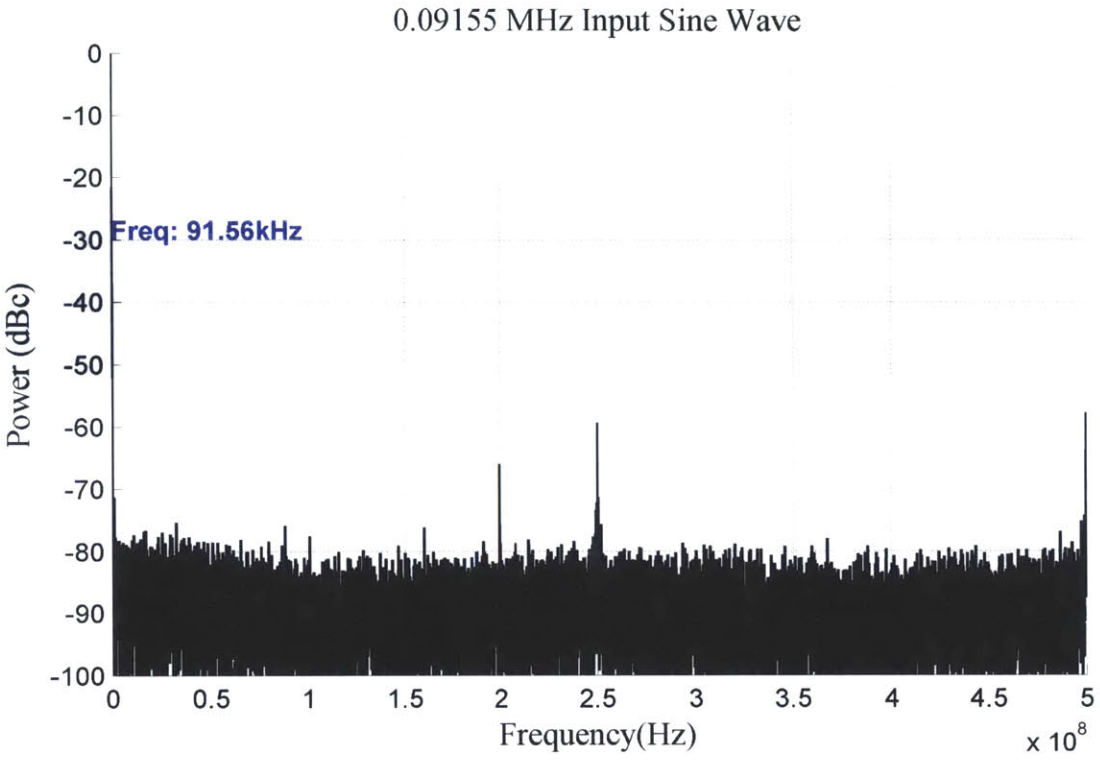

Figure 4.14 91.55 kHz Sine Wave Input.

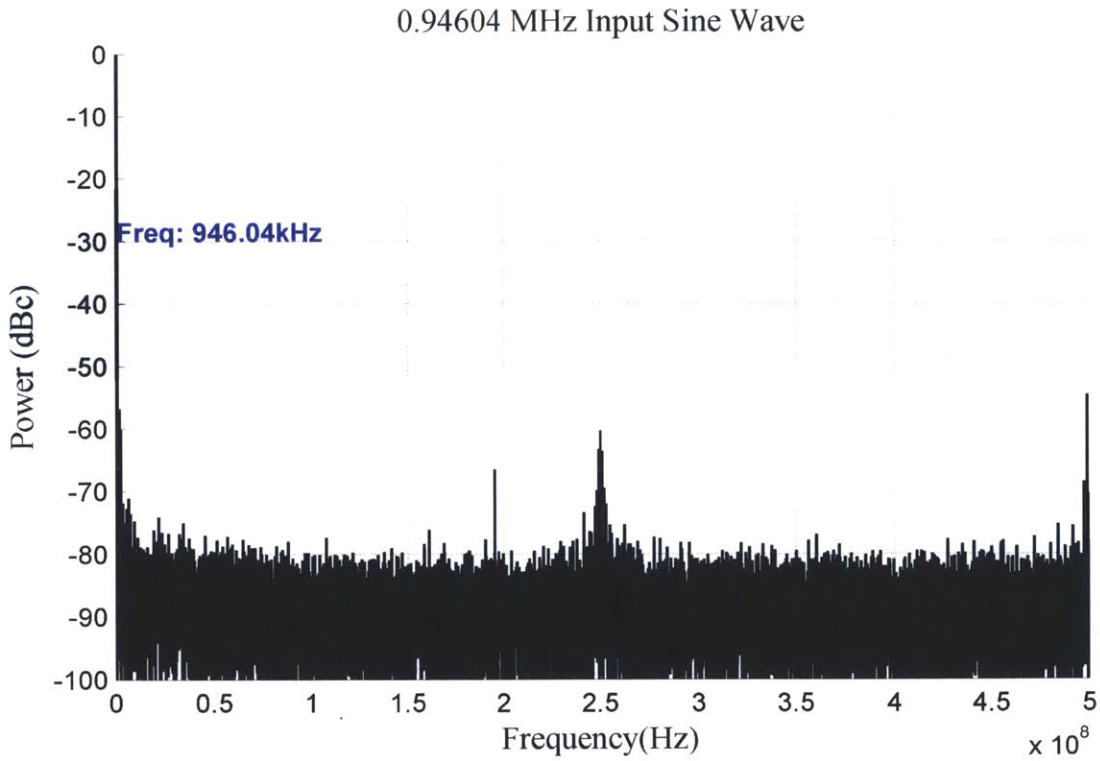

Figure 4.15 946.04 kHz Sine Wave Input.

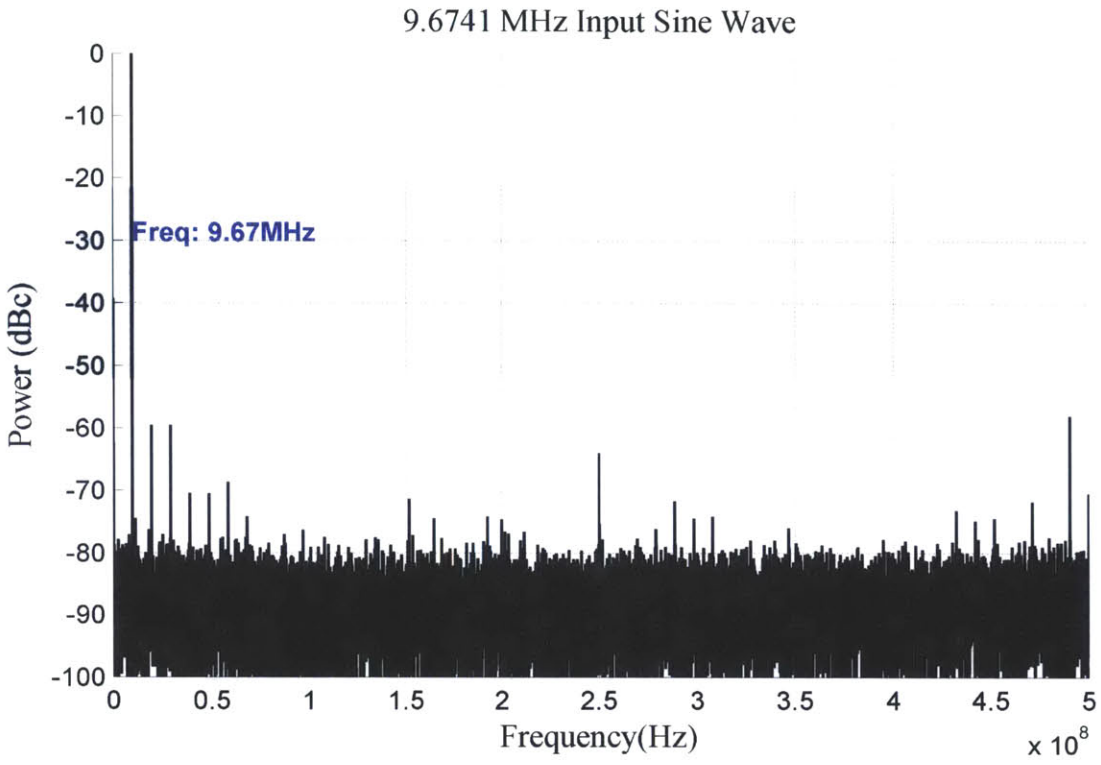

Figure 4.16 9.6741 Mhz Sine Wave Input

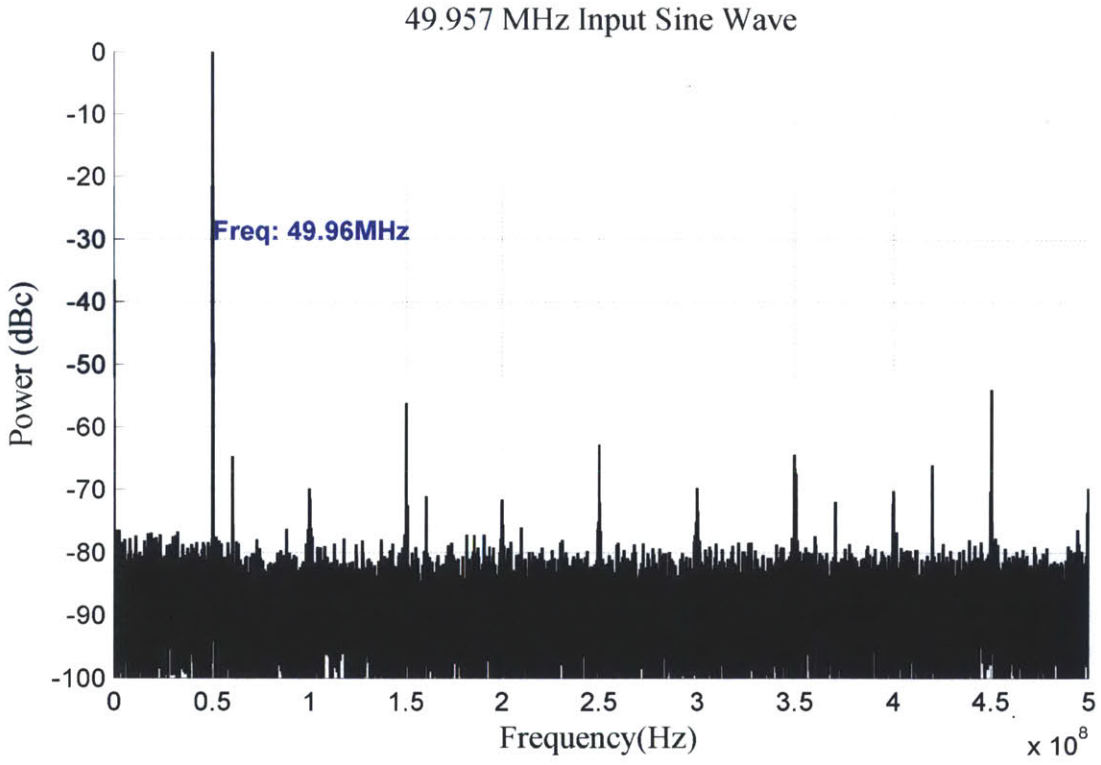

Figure 4.17 49.957 MHz Sine Wave Input.

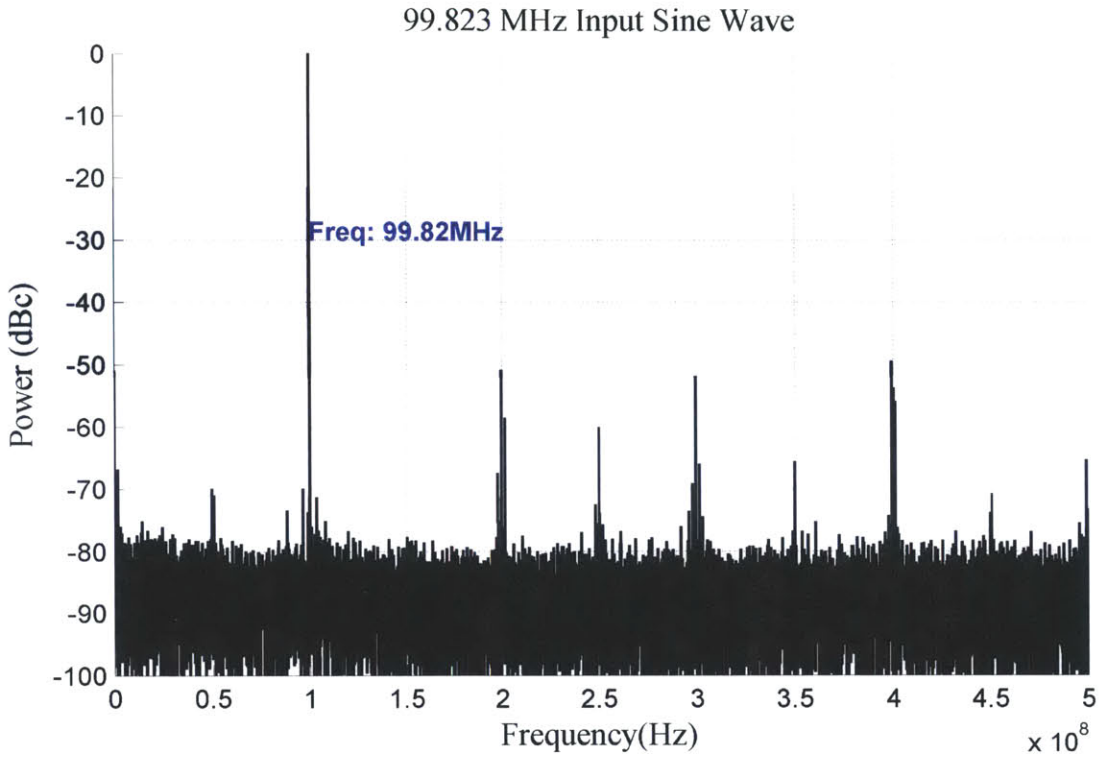

Figure 4.18 99.823 MHz Sine Wave Input

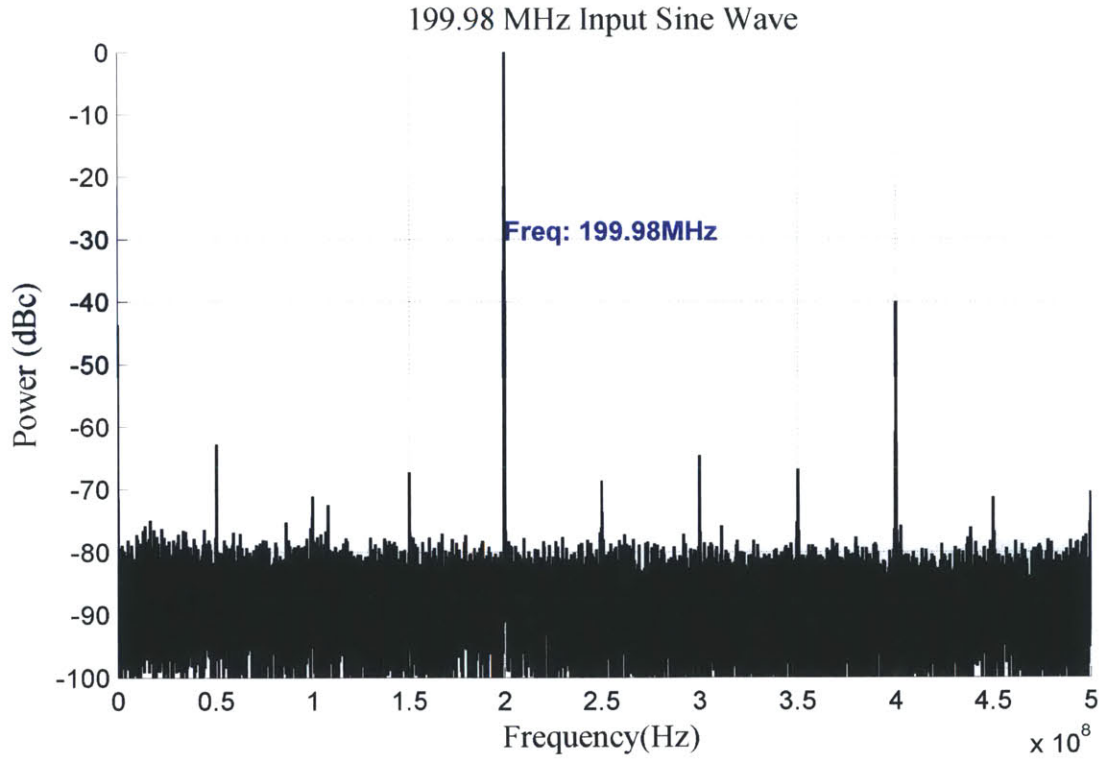

Figure 4.19 199.90 MHz Sine Wave Input.

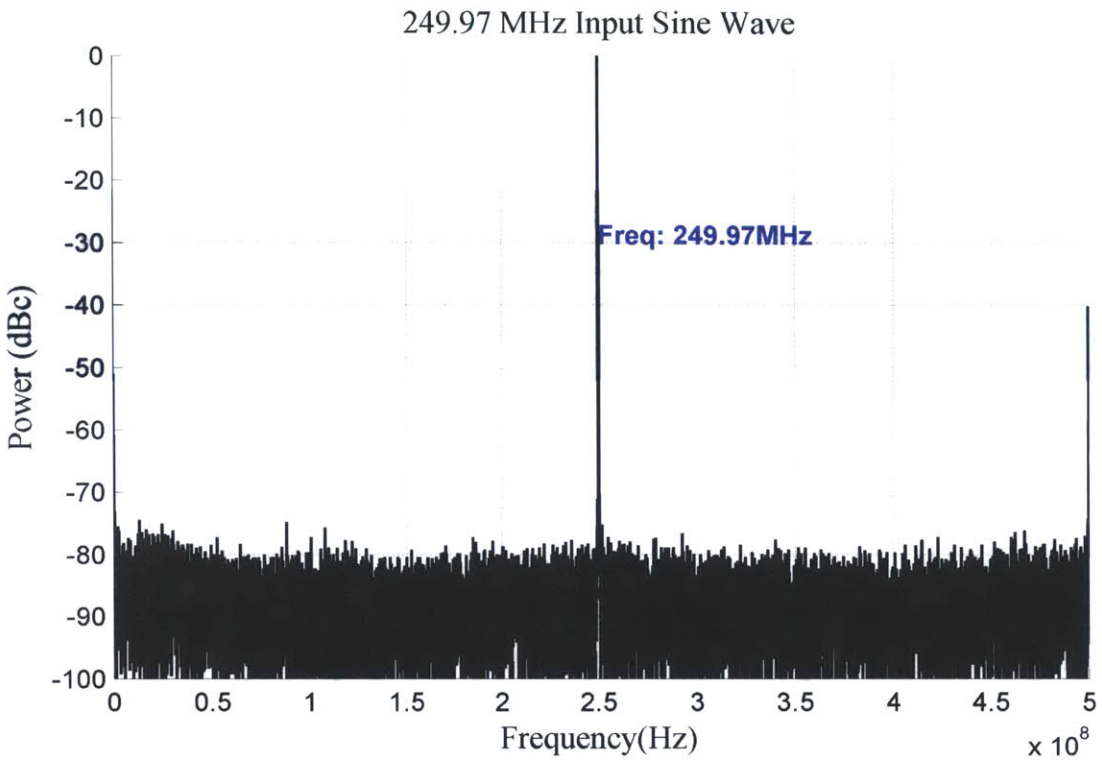

Figure 4.20 249.97 Sine Wave Input.

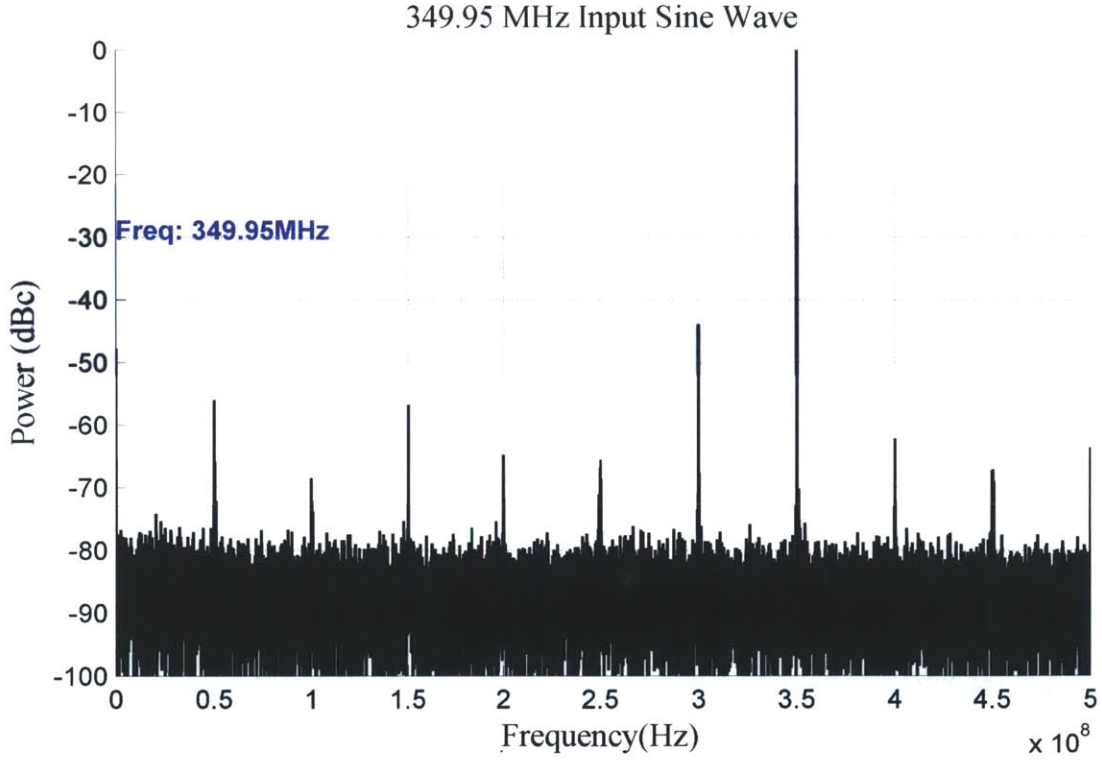

Figure 4.21 349.95 MHz Sine Wave Input.

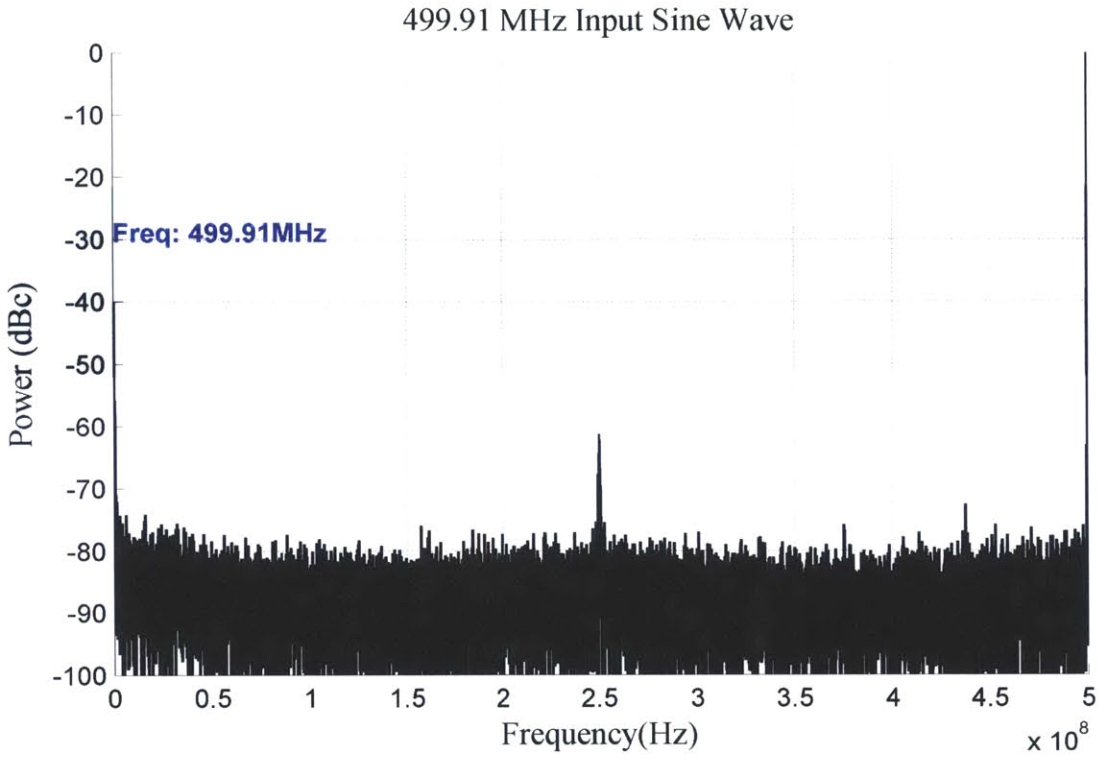

Figure 4.22 499.91 MHz Sine Wave Input

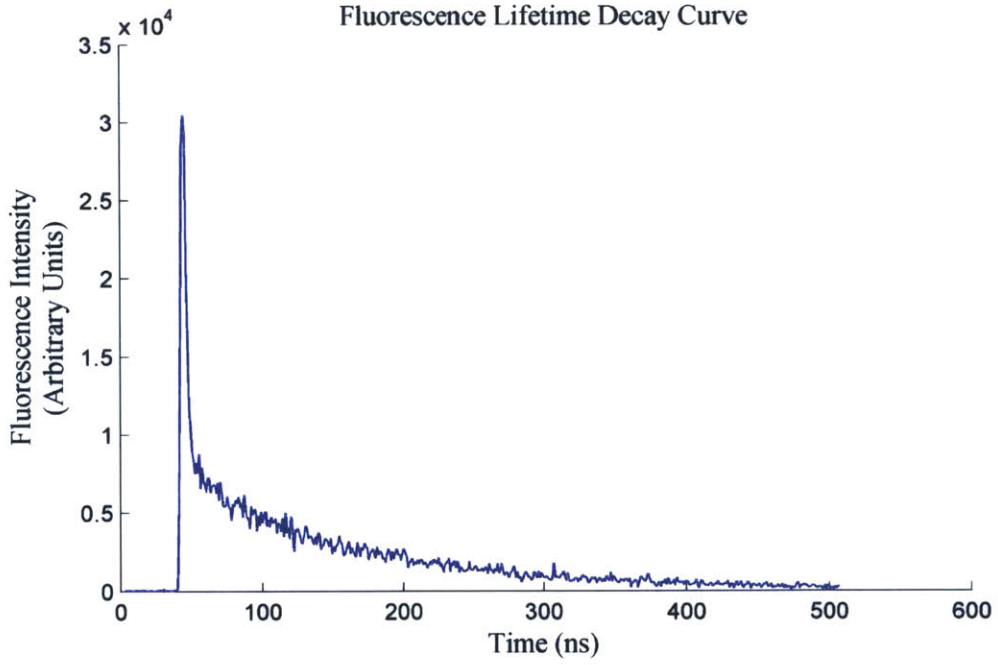

Figure 4.23 Example Fluorescence Lifetime Decay Data. The graph shows the accumulation of 100,000 measurements of fluorescence light intensity from a water sample containing short (~2 ns) and long (~130 ns) lived fluorophores. The visible delay of 44 ns between the trigger and fluorescence is due to a combination of system delay and ADC pipelining.

Chapter 5

A Compact Fluorescence Lifetime Instrument for In Situ Investigation of PAHs

Abstract

A fluorescence lifetime instrument for in situ investigation of natural waters is described. The instrument utilizes a pulsed laser at 266 nm to excite water samples, a monochromator and photomultiplier tube (PMT) for wavelength tunable photon detection, and a custom high speed data acquisition board for signal storage and data reduction. Signal analysis to separate the individual lifetime components present is described and demonstrated. The instrument is tested with aqueous solutions containing low concentrations of pyrene, a polycyclic aromatic hydrocarbon (PAH) often measured in environmental research. In all experiments, the pyrene signal was discernable even with significant background fluorescence signals present. The instrument has been designed to minimize size and power.

5.1 Introduction

5.1.1 Overview

The Holy Grail for an in situ aquatic chemistry instrument is the combined ability to detect both a wide range of chemical compounds and to do so with a high level of sensitivity. Given the stringent size and power requirements of many in situ applications (e.g. autonomous underwater vehicles (AUVs), buoys), rarely are both achievable. Off the shelf instruments targeted at AUV payload applications are typically only capable of sensing one specific compound (e.g. O_2 sensors), or, when that is not possible, broad groups of compounds (e.g. CDOM, crude oil). Additionally, many chemical-specific sensors often exhibit significant

interference from non-target compounds, which unless simultaneously measured and accounted for can lead to erroneous chemical estimates [1].

The class of instruments that measures the optical properties of chemicals provides a potential solution for sensing a wide range of compounds found in natural waters. These instruments, namely spectrophotometers and fluorometers, measure light absorbed and fluoresced from chemical mixtures, and are ubiquitous in laboratories that study environmental chemistry. Adapting these instruments for use aboard small AUVs is becoming increasingly feasible with advances in electronics, light sources, and light detectors, and is an active research area. This chapter discusses research on a new fluorescence lifetime instrument developed for AUV deployment capable of identifying fluorophores by their lifetimes as well fluorescence wavelength. We have focused on measuring the polycyclic aromatic hydrocarbons (PAHs) pyrene due to its relevance in environmental science and previous work characterizing its fluorescence behavior.

5.1.2 PAHs in the Environment

Polycyclic aromatic hydrocarbons (PAHs) are a class of organic compounds that are ubiquitous throughout the environment. The interest in PAHs comes largely from certain PAHs having carcinogenic effects [2], which has led to the EPA listing sixteen PAHs as priority pollutants. Anthropogenic activity causes PAHs to enter aquatic systems from a variety of sources including from fossil fuels, combustion and fires, and industrial and domestic wastewater [3].

There are two particularly interesting emerging applications for PAH sensing: oil spill mapping and sediment source discovery. In the wake of several large oil spills, such as the BP Gulf Oil incident, there has been increased interest in identifying oil plumes and determining the way in which specific components of oil separate into the water column. Gulf researchers noted that standard oil UV fluorometer readings were widely affected by concentration, weathering, and dispersion, and that it was impossible to reliably interpret these measurements to specific PAH levels [4]. Additionally, PAH toxicity is chemical specific [5], and as crude oil undergoes weathering, specific PAHs dissolve into the water at different rates [6]. The capability to measure specific PAH compounds in situ is therefore necessary for understanding the evolving environmental hazard posed by oil spills.

5.1.3 Fluorescence and Fluorescence Lifetime Theory

Molecular fluorescence is the emission of a photon due to the relaxation of an orbital electron's energy state. First, incoming light is absorbed by the molecule and excites an electron to a higher energy state. The electron eventually returns back to its ground state, releasing energy in the process. In some instances this energy takes the form of a photon i.e. fluorescence. The photon's wavelength is a function of the change in electron energy. Steady state fluorometers report the fluorescence spectrum for a given excitation light source.

Since many compounds exhibit broad fluorescence signals, it is difficult to distinguish between individual compounds whose fluorescence spectra overlap. With only wavelength information, it can be impossible to identify signals from low concentration chemicals of interest when there are large magnitude, broad spectrum compounds in the mixture. In these cases, fluorescence lifetime measurements can aid in spectrum separation.

Fluorescence lifetime instruments report the average time electrons remain in the excited state before fluorescing. The length of time an individual electron stays in the excited state, Δt, is random, but the Δt probability distribution is an exponential decay function. When many measurements of Δt are made, the decay rate of the exponential can be determined, and this value is referred to as the fluorescence lifetime. The lifetime is an additional dimension of information, along with fluorescence wavelength, that can be used to identify chemical components in a mixture.

Lifetime measurements are widely used in a variety of scientific, medical, imaging, and environmental applications [7]. Fluorescence lifetime measurements can be made either in the time or frequency domain, and while the implementation of the two methods is considerably different, they produce theoretically identical outcomes [8]. The research presented here performs measurements in the time domain.

In time domain fluorescence lifetime systems, a light source is pulsed for a short duration and the fluorescence response is measured as a function of time. The light source must be pulsed significantly faster than the lifetime of interest, which for many systems equates to pulses less than 1 ns. The minimum pulse width achievable is dependent on the light source, which historically has been lasers with pulses in the picosecond range. More recently, LEDs have been used, although LED minimum pulse widths are on the order of nanoseconds [9], [10]. Most time domain systems use time-correlated single photon counting (TCSPC) as a way to calculate

lifetimes. In these systems the excitation source is pulsed many thousand times, and the duration from the pulse to the arrival of the first fluoresced photon at the detector is measured. A histogram of results is generated to derive the fluorescence lifetime.

The system presented here uses a modified TCSPC method. Fluorescence intensity is measured at a constant rate of 1 sample / ns for a fixed length of time (~500 ns) after the laser pulse. Real time signal processing identifies the arrival times of all photons that are fluoresced in that sampling window, and the results are used to generate a histogram of photon arrival times. The advantages of this method are that more than one photon arrival can be detected per laser pulse and multiple photons arriving at the same time are weighted greater than single photons.

5.1.4 Pyrene Fluorescence

The fluorescence characteristics of pyrene dissolved in water are well documented. Pyrene absorbs UV light between 220 and 340 nm, with absorbance peaks near 240, 260, 275, 315, and 330 nm [11], [12]. It fluoresces most strongly between 370 and 420 nm, with peaks in decreasing magnitude at 373, 393, and a tail with smaller peak around 415 nm [11], [12]. The quantum yield for pyrene (i.e. the fraction of absorbed light that is fluoresced) is reported as 0.69 [11]. The fluorescence lifetime value for pyrene was measured as 126 and 131 ns in air-saturated water [13], [14] and 129 ns in sea water [15]. In the extreme conditions of O_2 saturated water, degassed water, and N_2 saturated water the lifetimes were 69, 201, and 226 ns, respectively [14]. For the purposes of this research, where variations in O_2 and other background compounds are expected, fluorescence lifetimes in the range of 120 to 140 ns occurring at the wavelengths associated with pyrene were assumed to be pyrene signals.

5.1.5 AUV In Situ Fluorescence Research (LEDIF)

Previously we developed an AUV deployable UV-VIS chemical fluorometer with additional absorbance and light scattering measurement capabilities [16]. The instrument, named LEDIF for LED Induced Fluorescence, senses a wide range of fluorescing compounds and compound families while attached as a payload to a STARFish AUV. The work presented here attempts to advance LEDIF's capabilities by increasing its sensitivity to compounds such as PAHs like pyrene.

5.1.6 Previous In Situ Instruments for the Study of PAHs in Natural Waters

In situ fluorescence lifetime sensing of PAHs in surface waters has been rarely reported in the literature. The most notable work involved the design of a laser induced fluorescence system deployable aboard ships [17]. Rudnick and Chen demonstrated the ability to use lifetime fluorescence to identify the PAH pyrene, among others, in Boston coastal waters. Time gating of the fluorescence lifetime measurements allowed them to observe the relatively long-lived yet low pyrene signal in the presence of the short-lived, high fluorescence signal from dissolved organic matter. Their instrument's pyrene limit of detection was 8 ng / L. Although capable of ship based sensing, their sensor cannot be used aboard AUVs or small moorings due to its power and size requirements [18]. An updated instrument was later used for the investigation of pyrene desorption from sediment, and was found to have a limit of detection of ~1 ng / l [19].The positive outcomes of these studies provided significant motivation for the research presented here.

5.1.7 High Speed Data Acquisition

Data acquisition at the rates required for fluorescence lifetime measurements is a significant challenge. Currently available commercial solutions that convert signals at gigahertz rates do not meet the size, power, and communication requirements for an AUV deployable instrument. Therefore prior to the development of this instrument, research into the design of a small high speed data acquisition board was required. The results from that work are described in detail in Chapter 4.

5.1.8 Research Objective

The objective of this research was to design a fluorescence lifetime instrument capable of deployment on small AUVs. The instrument uses the same flowcell system developed for LEDIF and has similar size and power constraints so as to also be deployable on the STARFish family of AUVs. The previous work by Rudnick and Chen measuring in situ pyrene was used as a target benchmark.

5.2 Fluorescence Lifetime Instrument Design

The following sections provide details on the instrument design, individual components, operation, and signal processing.

5.2.1 Instrument Overview

This section provides a general overview of the instrument along with a description of the signal of interest at each stage. Figure 5.1 provides a visual representation of the system.

The first stage of the instrument is the excitation laser. This laser produces a short pulse of monochromatic light in a narrow beam. The beam of light enters the flowcell through an optical window and intersects the water sample. A photodiode located 180 degrees from the laser detects the light pulse and is used as a trigger signal for the data acquisition system. A fiber optic cable connected to the flowcell at 90 degrees from the laser light collects a combination of reflected laser light, Raman scattered light, and fluoresced photons. The resulting light spectrum contains significant peaks at the laser excitation wavelength (266 nm), the water Raman shift wavelength (291 nm), and the fluorescence wavelengths from all present fluorophores. This light spectrum is filtered via a tunable monochromator, producing approximately monochromatic light at a user specified wavelength.

The next stage of the instrument converts the light into an electrical signal. The energy of a single photon is very small, so it is necessary to amplify the signal while also converting it from optical to electrical energy. A photomultiplier tube (PMT) provides this functionality, with typical gains up to 10^7. The ideal output from PMT is a nearly instantaneous current pulse, however the instrument's PMT produces a pulse several nanoseconds wide with a decaying ringing signal.

The final instrument stage converts the PMT's analog output signal to a digital representation for storage and digital signal processing. The data acquisition stage receives two inputs: the analog signal and the trigger signal from the photodiode. When the trigger signal is received, the data acquisition board starts converting the analog signal to an 8-bit digital value at the rate of 1 conversion per nanosecond. Data are collected and stored for a user defined length of time, ranging from 10s to 1000s of nanoseconds. Some processing of the signal is done in real time on the board to identify photon arrival times and reduce the overall data throughput. The reduced data are sent over USB to a connected desktop computer (in lab) or an embedded

computer (AUV deployment). The final step performed by the computer is fitting lifetime values to the resulting information and attempting to estimate the concentrations of the chemical compounds causing the fluorescence.

5.2.2 Instrument Components

5.2.2.1 Laser

The light source for the instrument is a 266 nm Q-switched laser from Teem Photonics (part number SNU-02P-0C0). Its pulse width (FWHM) is less than 0.5 ns, with a typical pulse energy of 0.55 micro Joules. Pulses occur at approximately 9 kHz. The laser controller is powered with a 12 V source and receives commands over an RS-232 port. The laser consumes 6 W and its dimensions are 180 mm x 55 mm x 35.5 mm.

5.2.2.2 Monochromator

The instrument utilizes a compact monochromator to scan through the emission light (part number Oriel Mini Monochromator 78025). The monochromator can scan between 200 and 800nm using an integrated stepper motor. Light throughput and resolution are a function of changeable entrance and exit slits that can be chosen between 50 and 1000 micrometers. All results presented used 600 micrometer slits. The stepper motor is controlled with a custom motor controller PCB which receives ASCII commands over a USB-serial line. The overall dimensions are 197mm x 59mm x 48mm.

5.2.2.3 Photomultiplier Tube

The instrument's light detector is a compact, high speed PMT (part number Hamamatsu H9305-03.) Between 300 and 500 nm wavelength light, the PMT's sensitivity is approximately 100 mA / W and maximum current gain is approximately 10^6. The gain is variable between 10^3 and 10^6, however for this application involving photon counting the gain is always set to the maximum. The PMT's power electronics are included in the module, allowing it to be powered from a 12 V source. The PMT is mounted directly to the output slit of the monochromator.

5.2.2.4 Trigger Photodiode

The instrument uses a high speed photodiode to detect the timing of the laser pulses. It is attached to the flowcell at 180 degrees from the laser. The detector (Thorlabs DET10A) has a

rise time of 1 ns and is fitted with a wavelength notch filter to match the 266 nm laser. The output from the detector is connected to the trigger input of the data acquisition board.

5.2.2.5 Data Acquisition Board

The data acquisition board is a custom high speed circuit developed for small embedded instruments. (See Chapter 4 for a complete description.) It digitizes an analog input signal at a rate of 1 gigasamples per second with 8 bits of resolution. The board's trigger input is used to start data capture and synchronize data acquisition for multiple events. A field programmable gate array (FPGA) stores and processes the data. Due to the FPGA configurability, custom data processing routines can be implemented to meet the requirements of the given instrument. (See section 5.2.3 for signal processing details.)

The system has several features that make it ideal for a compact embedded instrument. First, at 6.35 cm wide by 11.43 cm long by 1.27 cm thick, it is small enough to easily package in the hull of the STARFish. Second, it consumes only 3.5 W when operating at full speed and has multiple idle power modes to minimize energy consumption when not in use. Its lowest power mode consumes 62 uW and requires less than 3 s startup time to begin data capture.

5.2.2.6 Flowcell

The flowcell is identical to the LEDIF flowcell. It has two threaded connections to allow the sample volume to circulate through the cell. Around the analytical volume there are 6 optical windows used primarily to attach excitation light sources, such as LEDs or the laser. At 90 degrees to these excitation windows is an optical window connected to a fiber optic cable used to collect resulting fluorescence. This window includes a lens to focus the light into the optical cable.

5.2.3 Signal Processing

5.2.3.1 FPGA Signal Processing for Data Reduction

The data acquisition board's limited transmission throughput requires some data processing on board the FPGA. The FPGA serial data connection operates at a clock speed of 2 MHz. Each 8 bit data byte requires 1 start and 2 stop bits, for a total of 11 clock cycles per byte of data. Therefore the actual data throughput is approximately 180 kB of data per second. The trigger repetition rate for data collection and the length of data collection time at each trigger

determines if some data reduction is required to meet the throughput specification. In our instrument's case, the laser repetition rate is approximate 9 kilohertz and the instrument collects data for 512 ns after the trigger at a rate of 1 8-bit datum per ns, yielding 4.6 mB of data per second. Since this data rate exceeds the serial throughput, either the data must be reduced on the FPGA or some data must be discarded. We chose to process the data to minimize the amount of time the sample is exposed to the laser (and therefore minimize photobleaching) and maximize the chemical data collection rate.

The real-time data processing identifies the arrival times of photons, and sums together the photon values for multiple laser pulses. Identifying the photon signal is more complicated than just implementing a threshold detector due to a ringing signal that accompanies each photon(s). To identify a photon (vs. ringing) the signal is compared to a moving threshold limit that is proportional to the value of the last detected photon and inversely proportional to the time since the last detection. The threshold value is calculated as

$$Threshold = V_{t=0} * e^{-kt}$$

where $V_{t=0}$ is the value of the last detected event, t is the time since the event in ns, and k is a coefficient that determines the rate at which the threshold decays. An experimentally determined optimum k value of 0.25 is used. In practice, this algorithm is implemented discreetly using integer math on the FPGA. The results from the threshold processing are then summed together with the previous data. This process is repeated for 256 trigger signals and can be described by

$$D_{t=0\ to\ 512} = \sum_{i=0}^{255} f(d_{i,t})$$

where D is a 512 element array with each index equivalent to 1 ns in time, f is the function to identify photons, d is the digitized data signal, i is the index for the laser pulse, and t is the time since the laser pulse in discrete 1 ns values between 0 and 511 ns. Since each element of D is the sum of 256 8 bit values, they must be stored as 16 bit integers, and therefore the final data rate is approximately 36 kB (initial data rate divided by 256 and multiplied by 2), allowing for continuous data collection.

5.2.3.2 Estimating Pyrene with 2 Exponential Curve Fitting

Once a set of fluorescence data are collected, they are analyzed in MATLAB to determine the fluorescence lifetimes present in the signal. For the current work, where the

samples being measured have only pyrene and background compounds with a fast fluorescence lifetime, the data are fit to a 2 exponential model of the form

$$F(t) = ae^{-bt} + ce^{-dt}; \quad L_1 = b^{-1} \text{ and } L_2 = d^{-1}$$

where F(t) is the observed fluorescence as a function of time, a and c are the amplitudes of the signals, and L_1 and L_2 are the corresponding fluorescence lifetimes in seconds. All parameters are reported with 95% confidence intervals. L_1 and L_2 are compared to the expected pyrene fluorescence lifetime of ~130 +/- 10 ns, and the signal is assumed to be from pyrene if the bounds of the estimate overlap this range. If neither decay rates match, it is assumed pyrene is present below the instrument detection limit and reported as 0.

Since the amplitude coefficient and decay coefficient are linked, the amplitude estimate can be corrected for offsets in the decay coefficient estimate. For an exponential

$$ae^{-bt}$$

the area under the curve is a/b. A fixed concentration of pyrene should produce a fluorescence decay curve with a constant area, or

$$\frac{a_{true}}{b_{true}} = \frac{a_{est}}{b_{est}}.$$

Therefore, if the estimate of the lifetime deviates from the true lifetime, the amplitude estimate will deviate by a proportional amount. Since b_{true} is known for pyrene, a_{est} is corrected by

$$a_{corr} = \frac{a_{est} * b_{true}}{b_{est}}.$$

The final a_{corr} value is used for calculating the pyrene concentration.

A shortcoming of this method is that fitting two exponential curves to the data only works when a majority of the signal intensity is due to two or less exponential decays. As contributions from additional decay curves increase, the fitting parameters become less accurate and the measure of goodness of fit decreases. In practice, with our pyrene and RO water data, this method was found to yield reasonable results for assessing instrument performance. However, analyzing the data with a more general multi-exponential fit algorithm (described in section 5.2.3.3) revealed more than two decay lifetimes present.

5.2.3.3 Multi-Exponential Fitting

Additional signal analysis is performed to extract all lifetimes present. There are many methods to fit a sum of unknown exponentials (see [7] Chapter 4), and for this analysis a

relatively simple nonnegative least-squares approach (NNLS) discussed by Whittall is used [20]. This method solves the linear system of equations

$$y_i = \sum_{j=1}^{M} A_{ij} s_j, \quad i = 1,2,\ldots N$$

where s is an array of j observations. The A matrix is calculated as

$$A_{ij} = e^{-T_i t_j}$$

where T is an array of M possible exponential decay rates (s^{-1}), and t is an array of the times corresponding to observations s. To account for different uncertainty associated with each measurement, s_j and the row A_j are divided by the measurement's standard deviation. The standard deviation was experimentally found to be approximated by

$$\sigma_j = \sqrt{s_j * 50.}$$

The system of equations is solved using a built in MATLAB NNLS function, and reports the amplitude estimates for each decay rate in T.

5.2.4 Instrument Operation Procedure

The following procedure is used to capture fluorescence data. Code developed in MATLAB running on a desktop computer is used to control all aspects of the instrument.

1. Power is applied to the laser, monochromator, data acquisition board, and PMT.
2. The monochromator performs a calibration routine by scanning to its limits.
3. The data acquisition board settings are configured.
4. The laser is turned on and the system waits 10 seconds for it to stabilize.
5. The monochromator is moved to the desired wavelength.
6. The data acquisition system starts recording data on every trigger signal.
7. The data acquisition system sums the results of 256 laser pulses and immediately transmits the data to the computer. The data acquisition system has separate storage and transmitting buffers, so it keeps acquiring and processing new fluorescence data while the previous data is transferred to the computer.
8. When the computer receives a predetermined number of data points, it instructs the data acquisition board to stop storing data. For the data presented in this chapter,

99,840 laser pulses are accumulated for each measurement. Since the laser operates at ~9 kHz, it takes ~11 s to collect this data.

9. If the system is scanning multiple wavelengths, steps 5 through 8 are repeated at each desired wavelength.
10. The computer turns off the laser, data acquisition board, and monochromator.

5.3 Test Method

5.3.1 Instrument Setup

The instrument was set up for testing in the lab (Figure 5.2). Prepared water samples were held in a glass beaker prior to being tested by the instrument. Copper tubing connected the water sample beaker to the flowcell inlet port. The flowcell outlet port was connected via silicone tubing to a peristaltic pump that controlled the sample flowrate through the flowcell. All measurements were acquired with a flowrate of approximately 3 ml / s.

5.3.2 Sample Preparation

Pyrene standards were prepared for testing the instrument. Initial pyrene stock purchased from Ultra Scientific (1000 ug pyrene dissolved in 1ml methanol) was dissolved in RO water to create a 50 ug-pyrene / l aqueous stock. This stock was further diluted in RO water to create test standards of 500, 100, 50, and 10 ng / l. All glassware was cleaned and heated to 450 C for 10 hours prior to use.

5.3.3 Experiments

The fluorescence lifetimes of 10, 50, 100, and 500 ng / l of pyrene in RO water were measured with the instrument. At each concentration, between 8 and 21 independent measurements were taken. For each measurement the excitation source was the 266 nm laser, the emission monochromator was set to 373nm, and the results of 99,840 laser pulses were summed together. The system was flushed with several liters of RO water between each change in concentration and a measurement of RO water taken to confirm no residual pyrene remained in the system. The collected data were processed as described in section 5.2.3.

A second experiment scanning the monochromator across multiple wavelengths was also conducted. This was done twice: first with RO water and second with pyrene at 50 ng / l

concentration. The monochromator was scanned between 325 and 450 nm wavelengths at 5 nm intervals. At each wavelength, a measurement of 99,840 laser pulses was summed together.

5.4 Results and Discussion

The following sections highlight the results of the instrument. Both results from chemical experiments as well as engineering design of the instrument are presented.

5.4.1 Pyrene Quantification

Pyrene was detectable at all tested concentrations. Figure 5.3 shows an example of the collected data. A background signal with a fluorescence lifetime between 1 and 4 ns was present in all measurements. Figure 5.4 shows the results for the three lower concentration, along with associated error estimates, that were obtained by performing the two-exponential fit. Additionally, the same analysis was performed on data collected from the RO trials, and in each case no pyrene was detected. Using the data from the ten replicates of 10 ng / l pyrene concentration and the standard EPA method detection limit (40 CFR 1.136 App B), the 95% upper confidence limit is calculated as ~3 ng / l.

5.4.2 Full Spectrum Scans

Scans of the fluorescence captured the wavelength dependent lifetime values. Results from the full spectra scans are presented in Figure 5.5 through Figure 5.9. In Figure 5.5 there is a clear change in the fluorescence lifetimes present as a function of wavelength for each pyrene sample. Figure 5.6 and Figure 5.7 show the output from the fluorescence lifetime signal processing discussed in 5.2.3.3 for multiple unknown exponentials. For the RO water, there are two trends. First, there are clearly fluorophores present with a range of lifetimes less than 4 ns present that span nearly the whole spectrum between 325 and 450 nm. Second, there appear to also be fluorophores with lifetimes in the range of 10 to 30 ns, although at much lower intensities. These fluorescence emissions are present most strongly below 360 nm and above 435nm. All of this fluorescence is attributed to a combination of residual organics in the RO water and fluorescence of the flowcell itself.

Figure 5.7 shows the same analysis but for the 50 ng / l pyrene experiment. There is an additional set of lifetimes present at ~ 130 ns and between 360 and 420 nm, consistent with

pyrene [12], [17]. Figure 5.8 presents the same data, but with the spectrum as a function wavelength to more clearly see the fluorescence shape at different lifetimes. (Each line represents the average of 5 lifetime decay rates). Finally, Figure 5.9 shows only the fluorescence intensity as a function of wavelength for the fluorescence corresponding to a lifetime of 130 ns. Peaks are present at 375, 395, and 410 nm, which all can be attributed to pyrene fluorescence.

Interestingly, at 385, 400, and 405 nm there is zero signal attributed to 130 ns lifetime, although some is expected. Upon inspection of the multi-exponential analysis of these wavelengths, it appears the fitting routine has identified two exponential decay rates (one faster and one slower) that nearly average out to the expected 130 ns lifetime. This is a common problem encountered when fitting exponentials [20]. Generally, performing multi-exponential fits with no a priori knowledge of expected lifetime values is imprecise and can be susceptible to the values used in generating the A matrix for the regression. For this reason, we found that performing a specialized analysis focused on identifying pyrene (see Section 5.2.3.2) yielded significantly more consistent results.

5.4.3 Power and Size

Instrument components were largely selected to minimize total size. With all parts, except the flowcell, optimally arranged, the total volume is 200 mm L x 85 W mm x 75mm H with an additional small 15 mm x 50 mm section protruding 50 mm out in the H direction. These final dimensions allow it to be packaged inside a vehicle such as the STARFish with a 200 mm internal diameter.

The total power consumption is estimated at less than 10 watts when operating the instrument at full capacity. The laser requires 6 W and the data acquisition board requires 3.5 W when operating with no power saving. For most applications the monochromator is rarely adjusted, and therefore on average draws little power. The PMT and trigger photodiode draw negligible power. The system requires 5 V and 12 V DC power rails. Both power magnitude and type requirements are easily met on most AUVs.

5.5 Conclusion

We have demonstrated a compact fluorescence lifetime instrument for analysis of natural waters. In benchtop experiments, the instrument was able to sense pyrene at ng / l concentrations

in the presence of a strong short-lived background fluorescence signal. This sensitivity is only feasible using fluorescence lifetime techniques.

Future work will include additional benchtop experiments to quantify the ability to sense pyrene in samples of typical lake and ocean water. Natural waters contain colored dissolved organic matter (CDOM) that exhibits broad fluorescence spectra (see Chapter 3 for examples). Identifying pyrene in complicated water mixtures with levels of humic substances between 1-5 mg / l has been demonstrated on other fluorescence lifetime instruments with similar pyrene detection limits (8 ng / L) to ours [17], so positive outcomes are expected.

The instrument's small size and modest power requirements make AUV deployment feasible. Since our previously developed fluorometer has been successfully deployed aboard a STARFish AUV, we will target that vehicle for this instrument as well. No additional electronics or optics are required, however hardware for mounting and aligning the laser to the flow cell is necessary. The current system uses an adjustable X-Z stage to align the laser and maximize light throughput. To the author's knowledge, this will be the first instance of a fluorescence lifetime instrument used aboard an AUV.

In addition to hardware, the software to run the instrument and analyze the data must be ported to C++ for an embedded computer. The instrument's embedded computer on the AUV should be capable of performing all signal processing. The exponential separation algorithm described in 5.2.3.3 and used to generate Figure 5.6 through Figure 5.9 takes approximately 8 ms to run on a laptop with a 2.53 GHz processor. Since a single measurement of 100,000 laser pulses takes approximately 12 seconds, the embedded computer can operate 1,500 times slower than the laptop and still analyze 100% of the data in real time. The MATLAB code will be automatically ported to C++ and compiled for the embedded processor.

The current signal processing focuses on identifying pyrene and simple exponential separation, however future applications will require a more general approach. Much research has been dedicated to the problem of multi-exponential separation, however there are still numerous challenges for the application of mixed environmental samples. To fully leverage the instrument's capabilities, a signal processing scheme that both separates decay rates and matches data to libraries of known fluorescence spectra is required.

5.6 Acknowledgments

Funding for this project came from the Singapore MIT Alliance for Research and Technology (SMART) and MIT Sea Grant.

5.7 References

[1] A. V Mueller and H. F. Hemond, "Extended artificial neural networks: incorporation of a priori chemical knowledge enables use of ion selective electrodes for in-situ measurement of ions at environmentally relevant levels.," *Talanta*, vol. 117, pp. 112–8, Dec. 2013.

[2] A. Luch, Ed., *The Carcinogenic Effects of Polycyclic Aromatic Hydrocarbons*. Hackensack, NJ; London: Imperial College Press, 2005.

[3] J. M. Neff, *Polycyclic Aromatic Hydrocarbons in the Aquatic Environment: Sources, Fates, and Biological Effects*. London: Applied Science Publishers, 1979.

[4] P. Coble, R. Conmy, A. M. Wood, K. Lee, P. Kenkay, and Z. Li, "Fluorescence detection and characteristics of oil during the Deepwater Horizon oil spill," in *Geophysical Research Abstracts*, 2011.

[5] I. C. T. Nisbet and P. K. LaGoy, "Toxic equivalency factors (TEFs) for polycyclic aromatic hydrocarbons (PAHs)," *Regul. Toxicol. Pharmacol.*, vol. 16, no. 3, pp. 290–300, Dec. 1992.

[6] D. M. Di Toro, J. a McGrath, and W. a Stubblefield, "Predicting the toxicity of neat and weathered crude oil: toxic potential and the toxicity of saturated mixtures.," *Environ. Toxicol. Chem.*, vol. 26, no. 1, pp. 24–36, Jan. 2007.

[7] J. R. Lakowicz, *Principles of Fluorescence Spectroscopy*, 3rd ed. New York: Springer, 2006.

[8] C. M. McGraw, G. Khalil, and J. B. Callis, "Comparison of Time and Frequency Domain Methods for Luminescence Lifetime Measurements," *J. Phys. Chem. C*, vol. 112, no. 21, pp. 8079–8084, May 2008.

[9] M. Wahl, "Application of sub-ns pulsed LEDs in fluorescence lifetime spectroscopy," *Proc. SPIE*, vol. 4648, pp. 171–178, 2002.

[10] W. O'Hagan, M. McKenna, D. Sherrington, O. Rolinski, and D. Birch, "MHz LED source for nanosecond fluorescence sensing," *Meas. Sci. Technol.*, vol. 13, p. 84, 2002.

[11] F. P. Schwarz and S. P. Wasik, "Fluorescence Measurements of Benzene, Naphthalene, Anthracene, Pyrene, Fluoranthene, and Benzo[e]pyrene in Water," *Anal. Chem.*, vol. 48, no. 3, pp. 524–528, 1976.

[12] A. Nakajima, "Fluorescence spectra of anthracene and pyrene in water and in aqueous surfactant solution," *J. Lumin.*, vol. 15, no. 3, pp. 277–282, Sep. 1977.

[13] R. R. Hautala, N. E. Schore, and N. J. Turro, "A Novel Fluorescent Probe. Time-Correlated Fluorescence to Explore the Properties of Micelle-Forming Detergent," *J. Am. Chem. Soc.*, vol. 95, no. 17, pp. 5508–5514, 1973.

[14] M. W. Geiger and N. J. Turro, "Pyrene Fluorescence Lifetime As a Probe for Oxygen Penetration of Micelles," *Photochem. Photobiol.*, vol. 22, no. 6, pp. 273–276, Dec. 1975.

[15] S. M. Inman, P. Thibado, G. a. Theriault, and S. H. Lieberman, "Development of a pulsed-laser, fiber-optic-based fluorimeter: determination of fluorescence decay times of polycyclic aromatic hydrocarbons in sea water," *Anal. Chim. Acta*, vol. 239, pp. 45–51, Jan. 1990.

[16] C.-L. Ng, S. Senft-Grupp, and H. F. Hemond, "A multi-platform optical sensor for in situ sensing of water chemistry," *Limnol. Oceanogr. Methods*, vol. 10, pp. 978–990, 2012.

[17] S. Rudnick and R. Chen, "Laser-induced fluorescence of pyrene and other polycyclic aromatic hydrocarbons (PAH) in seawater," *Talanta*, vol. 47, no. 4, pp. 907–919, 1998.

[18] R. Chen, "A laser-based fiber-optic fluorometer for in situ sea water measurements," in *Chemical Sensors in Oceanography*, M. S. Varney, Ed. Taylor & Francis, 2000.

[19] D. T. F. Kuo, R. G. Adams, S. M. Rudnick, R. F. Chen, and P. M. Gschwend, "Investigating Desorption of Native Pyrene from Sediment on Minute- to Month-Timescales by Time-Gated Fluorescence Spectroscopy," *Environ. Sci. Technol.*, vol. 41, no. 22, pp. 7752–7758, Nov. 2007.

[20] K. P. Whittall and A. L. MacKay, "Quantitative interpretation of NMR relaxation data," *J. Magn. Reson.*, vol. 84, no. 1, pp. 134–152, Aug. 1989.

5.8 Figures

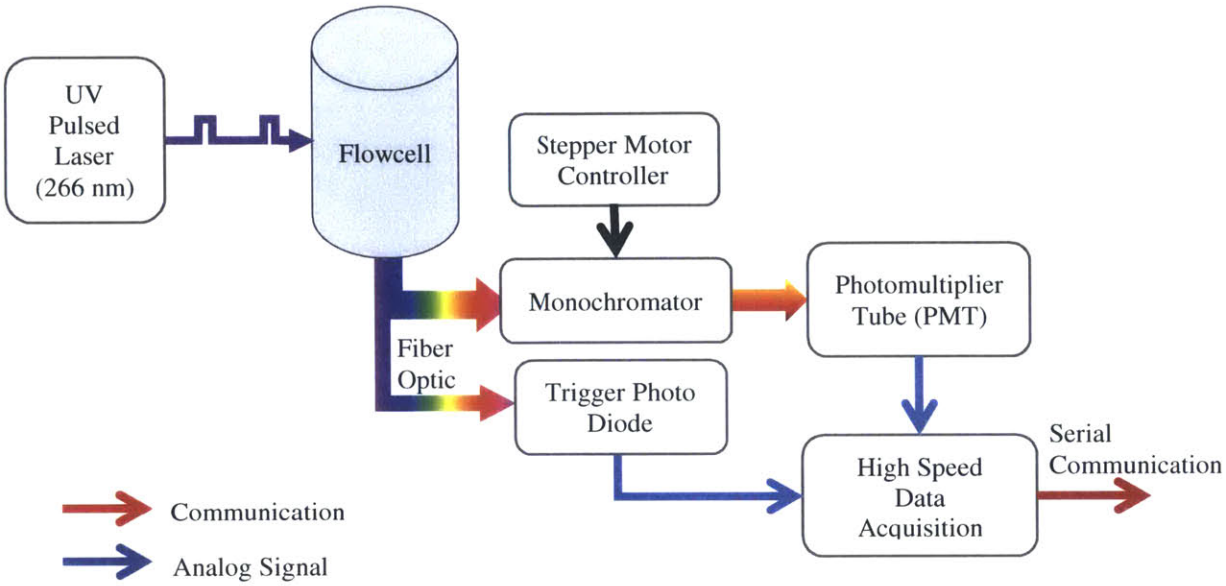

Figure 5.1 System Schematic.

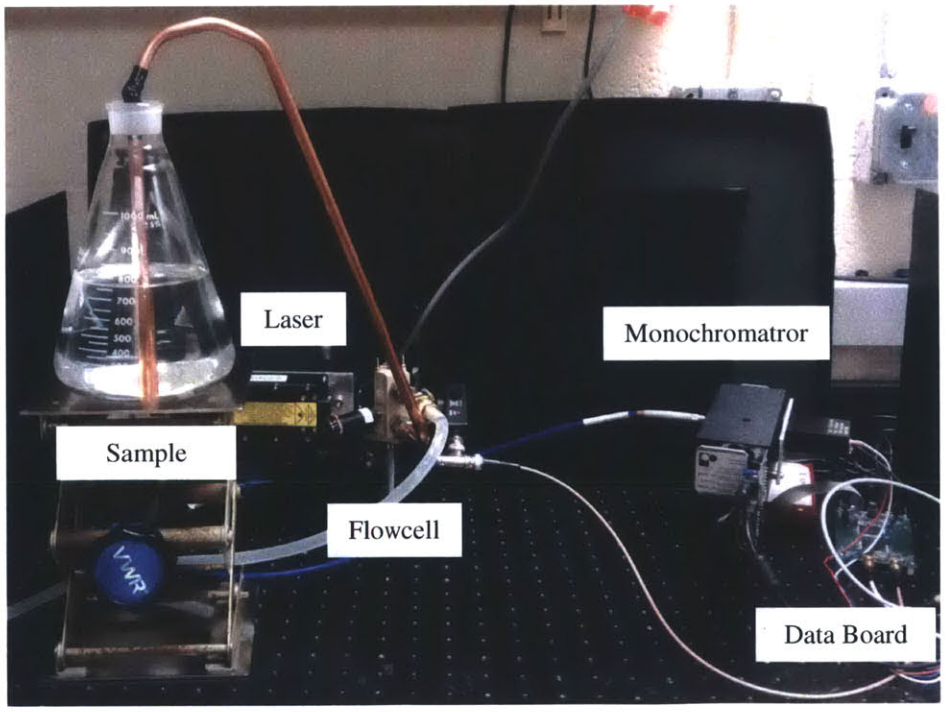

Figure 5.2 Picture of Lab Setup.

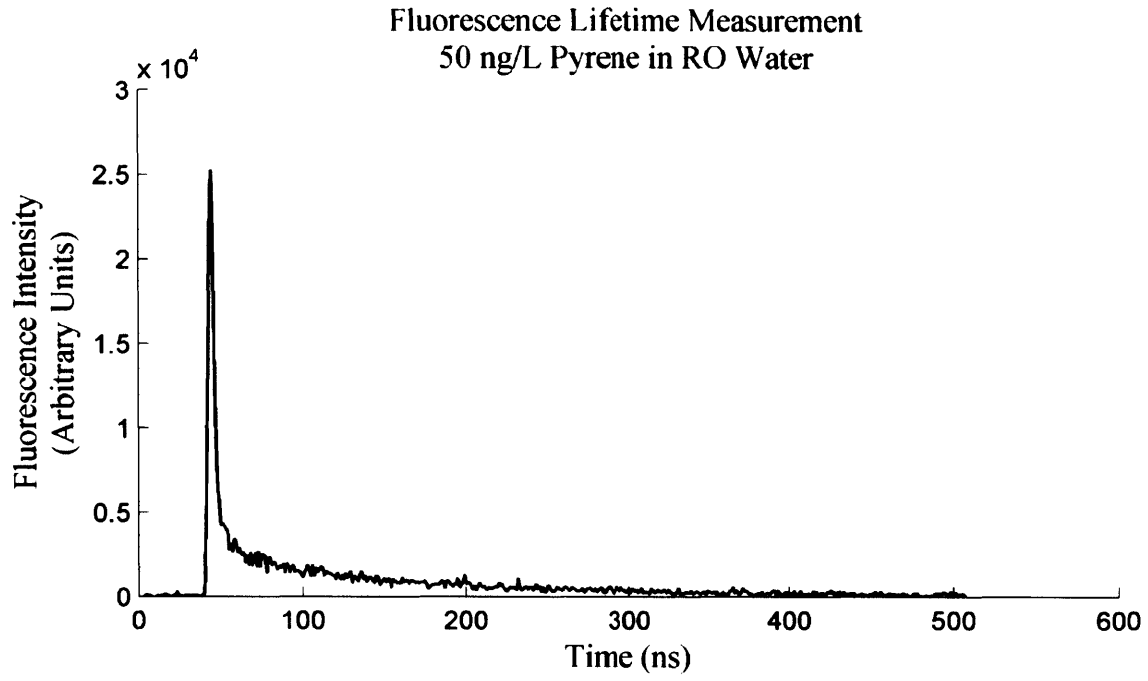

Figure 5.3 Example Fluorescence Lifetime Data. An initial fast decaying background signal is present at early times, but later the signal is dominated by pyrene.

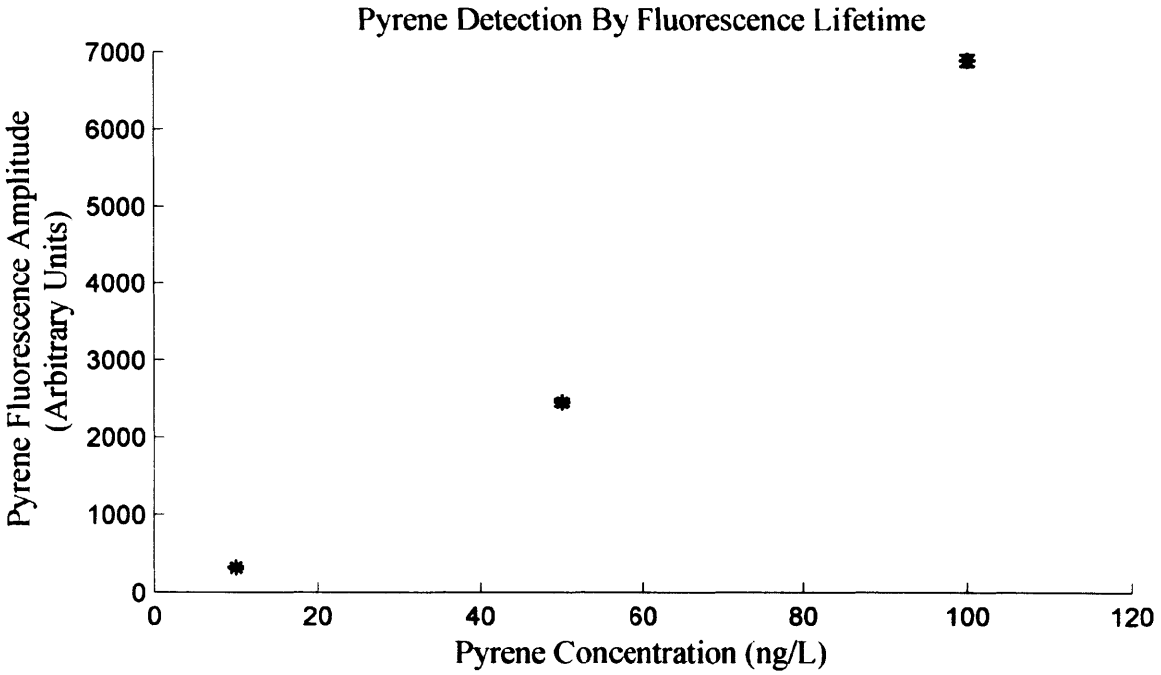

Figure 5.4 Pyrene Results. Error bars are 1 standard deviation of replicate measurements.

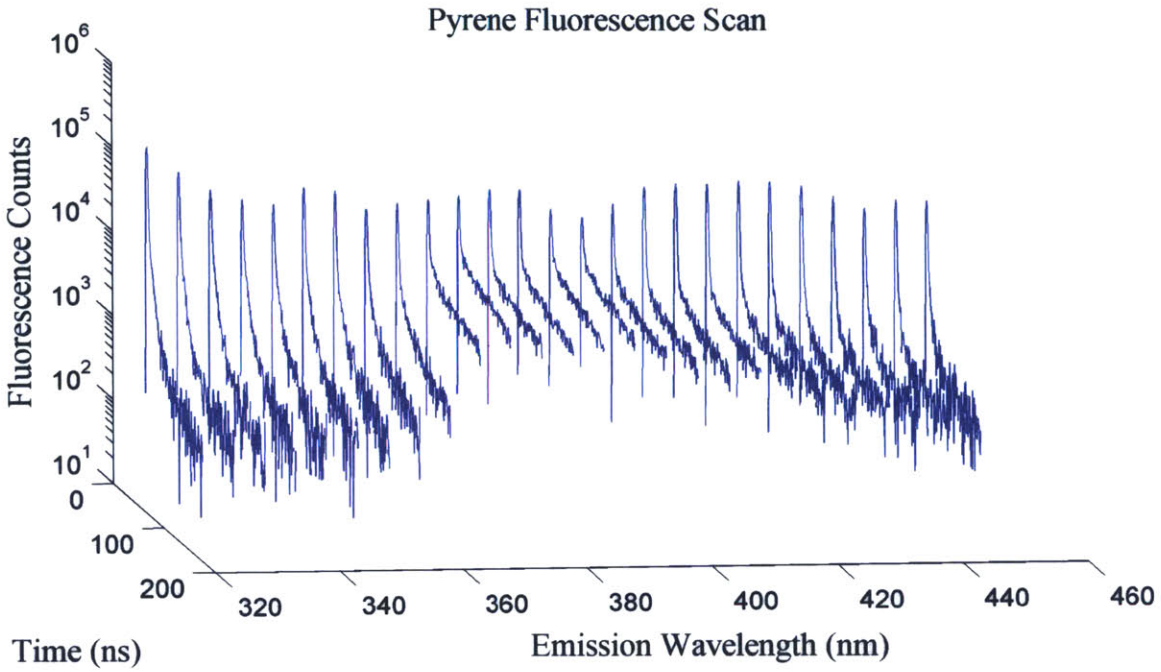

Figure 5.5 Pyrene Scan Raw Data. This plot shows the first 150 ns of collected data from a scan between 325 and 450 nm of a solution of 50 ng / l pyrene in RO water. An increase in longer lifetimes is clearly visible in the wavelength range between 370 and 420.

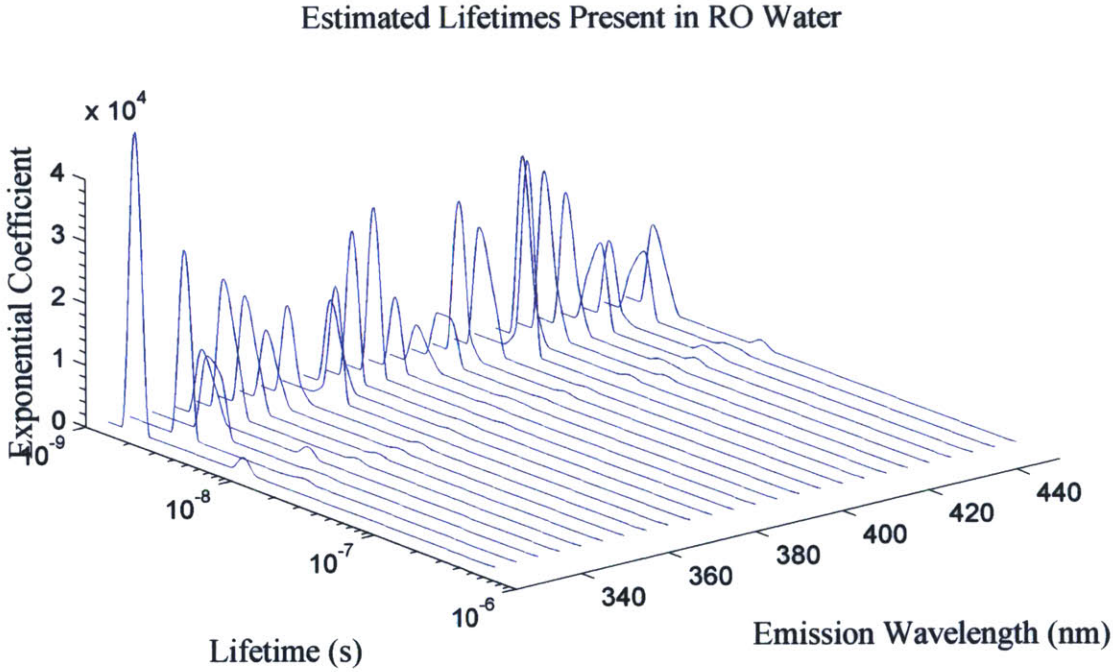

Figure 5.6 Fluorescence Lifetime Estimates for Scan of RO Water. The majority of fluorescence has a lifetime between 1 and 4 ns. Fluorescence at ~20 ns is also visible. The fluorescence is attributed to the flowcell and background substances in the RO water.

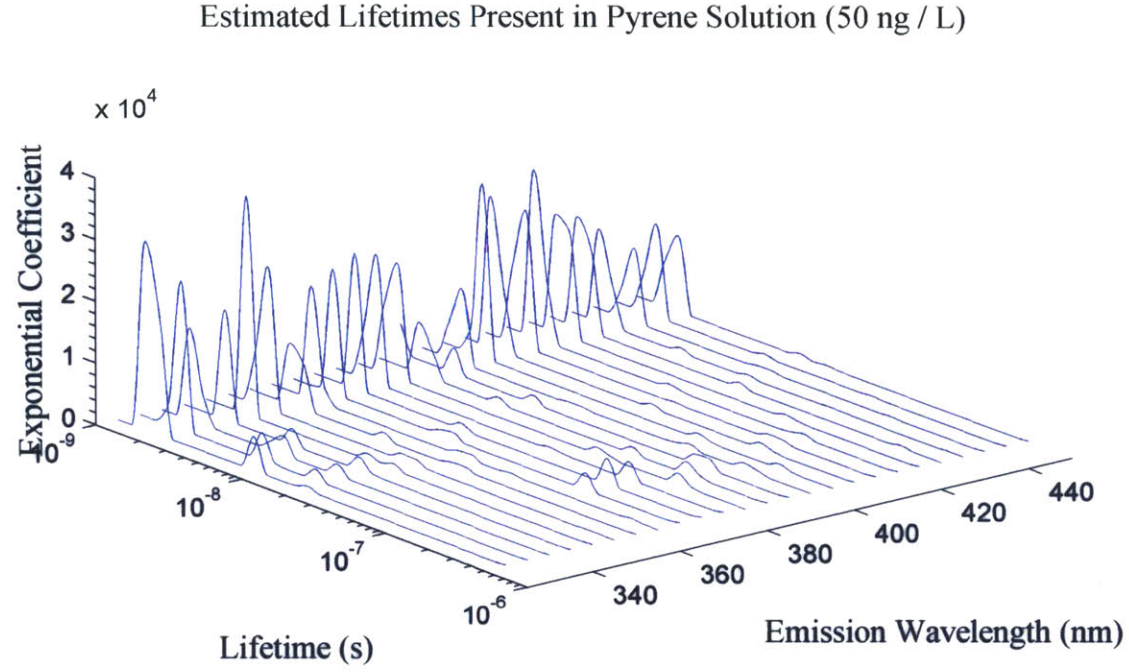

Figure 5.7 Fluorescence Lifetime Estimates for Scan of 50 ng / l Pyrene Solution. Fluorescence with lifetimes around 130 ns and between 360 and 420 nm is now visible and attributed to the pyrene.

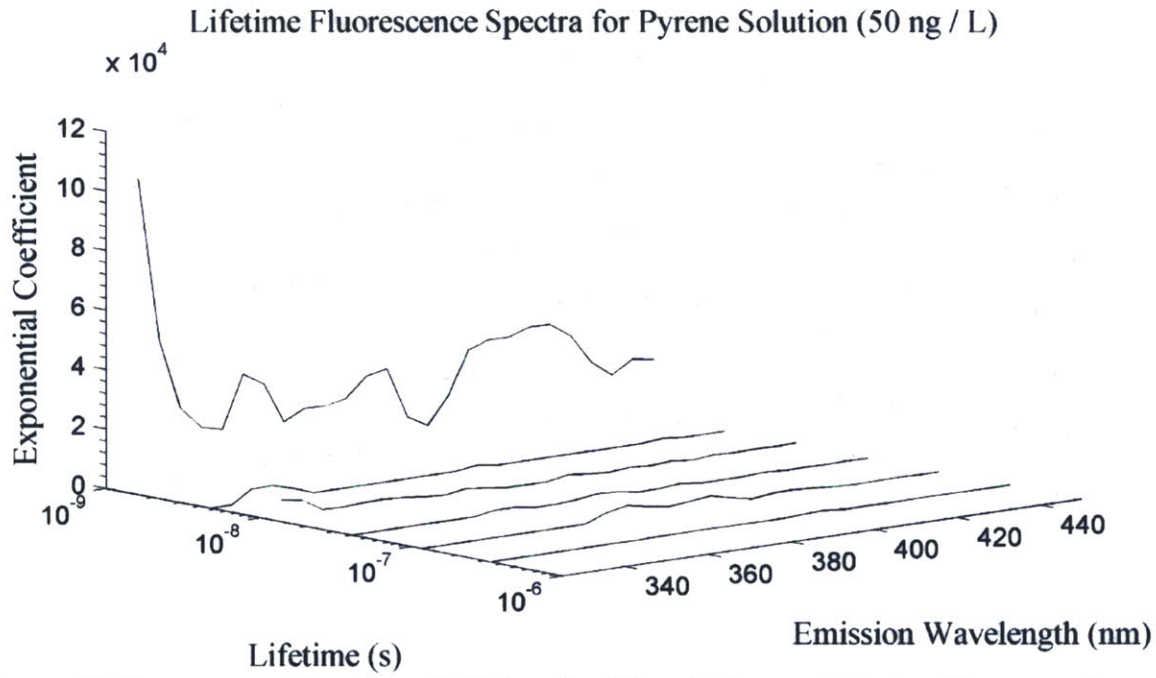

Figure 5.8 Spectra as a Function of Lifetime for 50 ng / l Pyrene Solution. The same data as Figure 5.7 but condensed and plotted as function wavelength. The spectra at 130 ns shows peaks in the wavelength range expected for pyrene.

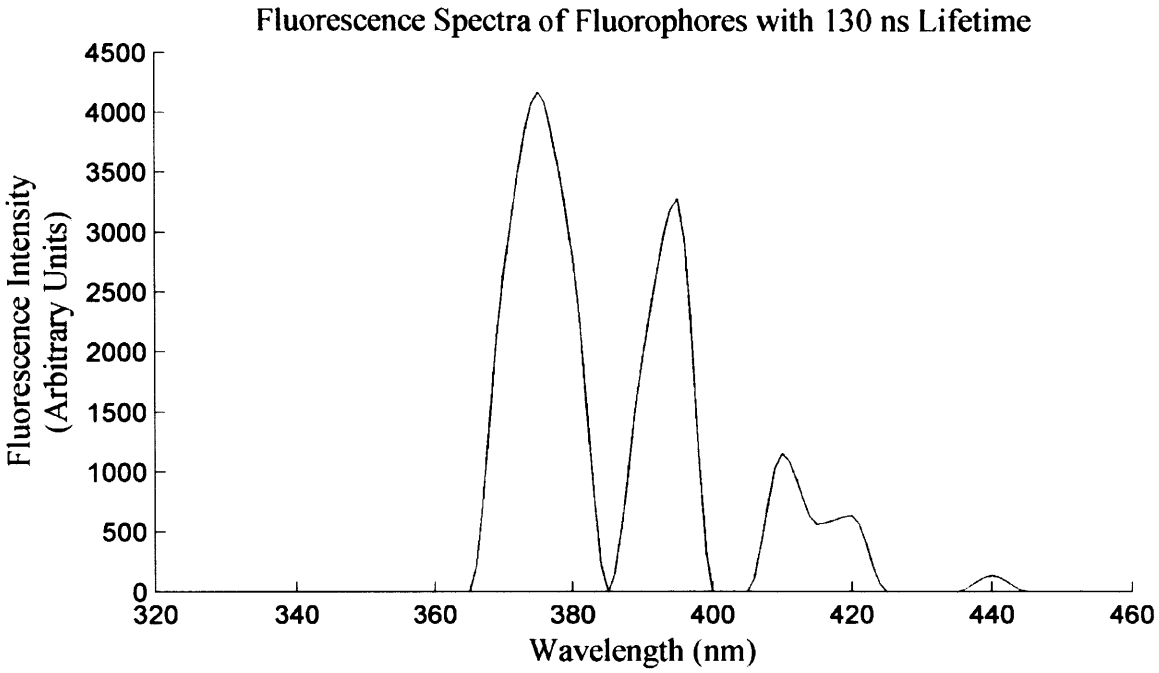

Figure 5.9 Spectrum of 130 ns Lifetime Fluorescence. The data shows fluorescence peaks at 375, 395 and 410 nm, which matches the expected values for pyrene.

Chapter 6

Conclusion

In this thesis, three new instruments for the investigation of the chemistry of natural waters are discussed. Each instrument exploits the optical properties of aqueous mixtures to sense the presence of chemical compounds. The combination of steady state fluorescence, lifetime fluorescence, and absorbance measurements all taken simultaneously in situ provides an unprecedented view of aquatic environments.

The flowcell presented in Chapter 2 is a novel design with broad future applications. It enables the use of up to 6 fluorescence excitation sources and 1 absorbance lamp in a small package that can withstand greater than 10 bars of pressure. Its generic optical window design makes it straightforward to reconfigure the sensor for many different types of scientific missions. For example, the fluorescence lifetime instrument in Chapter 5 used the same flowcell with minimal modifications; a laser source was simply swapped with one of the excitation LEDs. The software, iLEDLIF, is equally adaptable to instrument revisions. The modular design of the code makes it straightforward to write drivers for any new components that communicate over common protocols such as serial or I^2C. For simpler reconfigurations of the instrument, such as changing the LED excitation wavelengths, only edits to the configuration file are required. The LEDIF flowcell instrument lays the foundation for continued development of optical-type sensors deployable on AUVs.

The work described in Chapter 3 highlights how in situ instrumentation can impact some of the most important environmental work being done today. Both global climate change and the destruction of unique ecosystems are directly linked on the island of Borneo. The near total deforestation of tropical rainforests in Southeast Asia is tragedy enough; the fact that the burning and decomposition of the peat contributes to the release of greenhouse gasses is an additional insult. The instrument we developed to characterize DOM transport in peatland ecosystems is one small piece of research currently underway that will help scientists understand this very complex biogeochemical system. During the instrument's first two deployments we identified river DOM concentration changes occurring on the scale of hours, indicating the need for

continued persistent sensing. The field work also highlighted improvements that can be made to the instrument to increase its accuracy and sensitivity.

The instruments of Chapter 2 and 3 demonstrate two different modes of in situ investigation. In Chapter 2, the instrument LEDIF is deployed aboard an AUV and demonstrates the ability to quickly produce high resolution (1 m) three dimensional maps of chemical information. In Chapter 3, the DOM instrument is moored in a single place, but captures long time series of data. Future environmental studies will continue to increase the deployment of both mobile and fixed sensor platforms to understand systems on finer time and spatial scales.

In Chapter 4, the design of a generic high speed data acquisition board is shown. This circuit was developed to address a broad need in our own lab and in the labs of other sensor researchers. Its size, power, and cost specifications all exceed any similar data acquisition systems commercially available. More importantly, the commercial options just do not fit on the AUV platforms, immediately limiting the types of sensors that could be developed before this work. The board was designed with numerous future improvements in mind that require minimal, if any, changes to the PCB. First, additional development of FPGA code can implement other forms of digital signal processing. For example, potentially the exponential fitting discussed in Chapter 5 could be completely performed on the data acquisition board. The other improvements to the board require upgrading the ADC and clock chips. Pin compatible versions of all necessary ICs exist up to 3.6 GHz, which would nearly quadruple the current data capture rate. The availability of this board expands the possibility for miniaturization of numerous new sensors.

The high speed data board has already enabled the development of the fluorescence lifetime sensor described in Chapter 5. This instrument measures the decay rates of fluorophores present in aqueous solutions, providing an additional dimension of data on which to identify chemical compounds. The method is particularly useful in separating out low concentration components with long lifetimes from the large short-lived background fluorescence signals present in most natural waters. Demonstrations with solutions of pyrene at environmentally relevant concentrations validated the instrument performance. Future work remains in order to package the current components onto an AUV or other in situ platform. As mentioned, this can leverage the existing LEDIF flowcell and code, combining the advantages of this method with a previously field tested platform.

The development of new field instruments is challenging. External variables and Murphy's law constantly test every aspect of the design, from the simplest screw connection to the most complicated GHz circuit. However, the future of environmental research lies in pervasive sensing of the world at increasingly fine spatial and temporal scales. The work discussed here provides the environmental science and engineering community with additional research tools and new ideas for the continued advancement of in situ environmental sensors.

Appendix A

Validating LEDIF Field Performance

A.1 Chlorophyll a Calibration

The LEDIF flowcell aboard the STARFish AUV has been calibrated for chlorophyll a concentrations. Results from the calibration are shown in Figure A.1. Fluorescence counts are the counts recorded on the spectrometer at the chlorophyll peak of 680 nm with an excitation of 405 nm. The resulting conversion is

$$Chlorophyll\ a\ (ppm) = 0.043 * Counts_{\lambda=680} - 2.3.$$

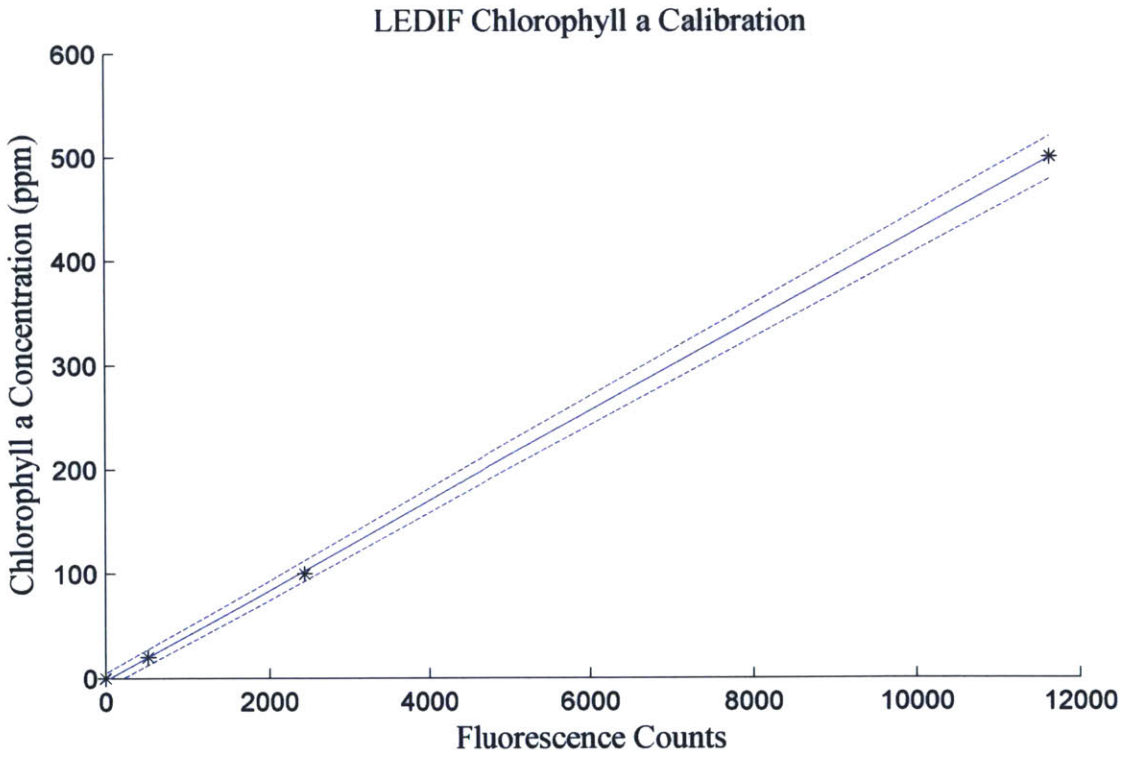

Figure A.1 Figure A.1 Chlorophyll a Calibration. The calibration curve is shown with estimated error bars based on the 95% confidence intervals of the fit parameters.

A.2 Field Results

LEDIF was used to collect field data at an anonymous lake location on two different occasions. On the first day, chlorophyll fluorescence intensities ranged between 740 and 1140 counts, corresponding to chlorophyll a concentrations of 30 and 45 ppm. On the second day, the chlorophyll fluorescence intensities ranged between 600 and 1500 counts, corresponding to chlorophyll a concentrations of 24 and 62 ppm. These values agree with measurements from similar water bodies described by Clews [1].

A.3 References

[1] E. Clews, E. Low, C. C. Belle, P. a. Todd, H. S. Eikaas, and P. K. L. Ng, "A pilot macroinvertebrate index of the water quality of Singapore's reservoirs," *Ecol. Indic.*, vol. 38, pp. 90–103, Mar. 2014.

Appendix B

Spectral Intensity Distributions for LEDIF and DOM Instrument LEDs

B.1 260 nm LED

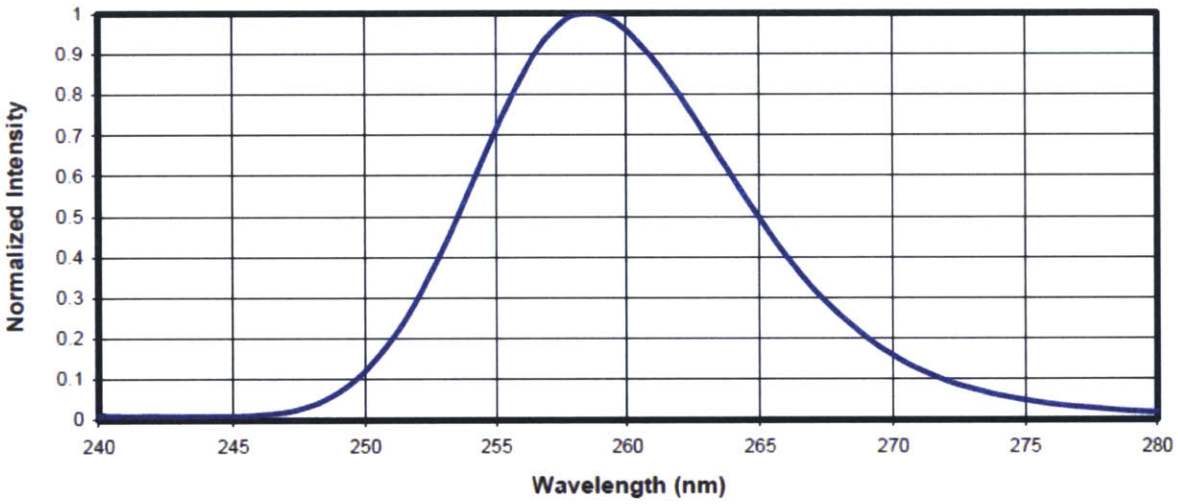

B.2 285 nm LED

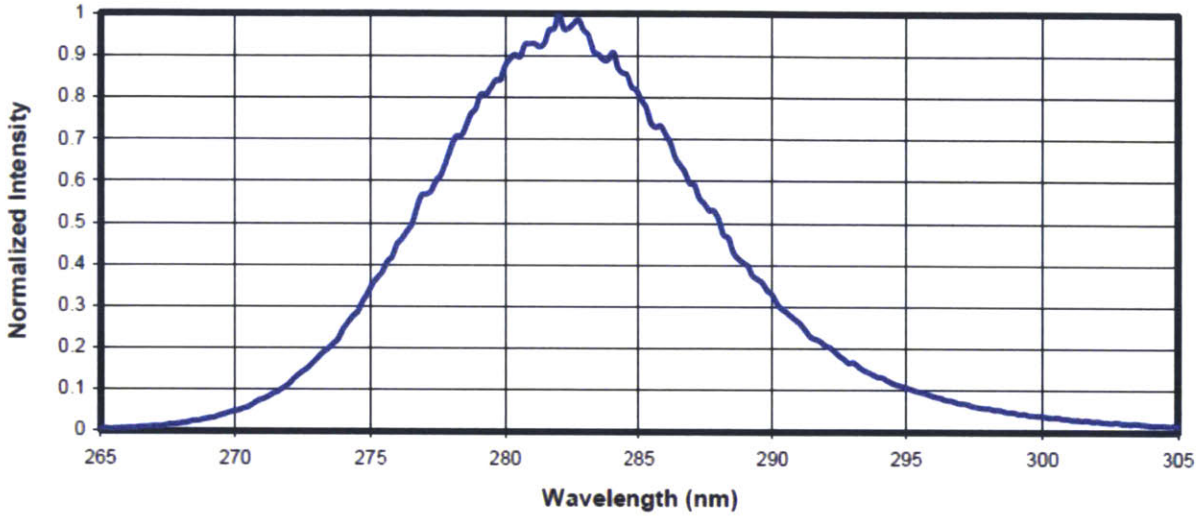

B.3 315 nm LED

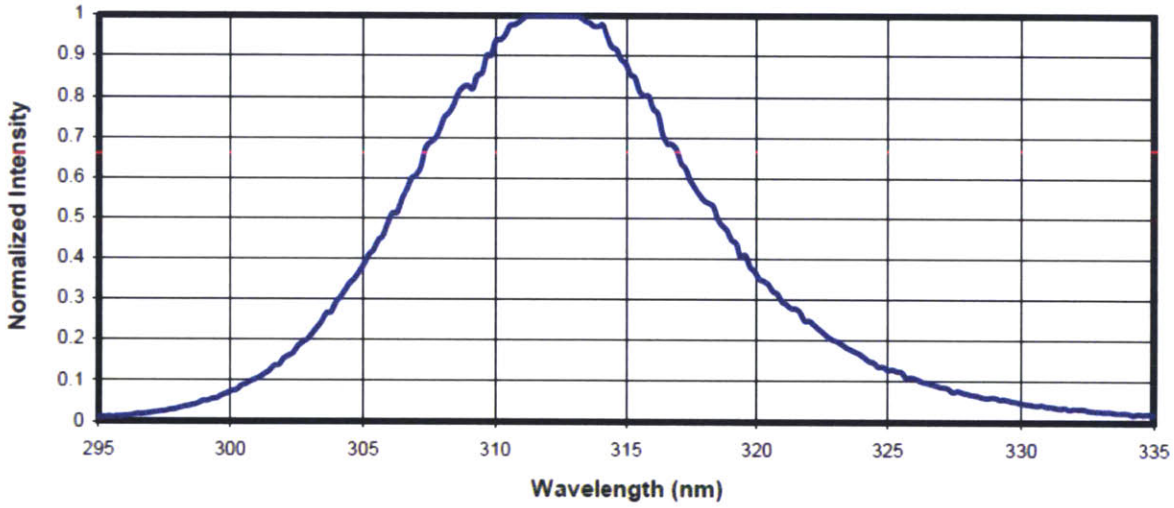

B.4 340 nm LED

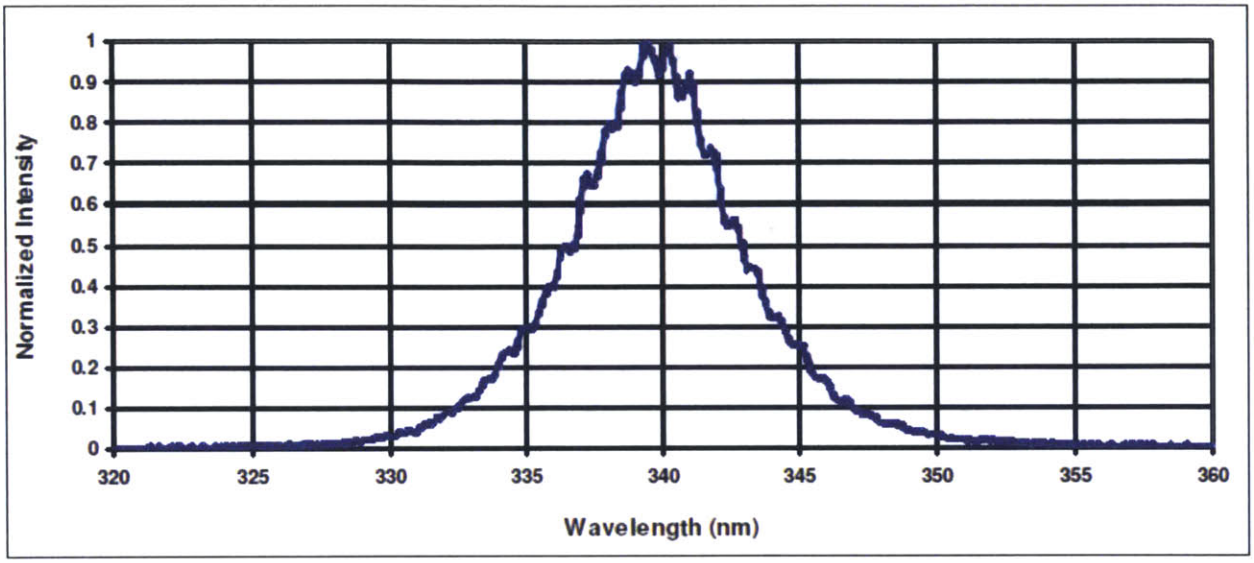

B.5 370 nm LED

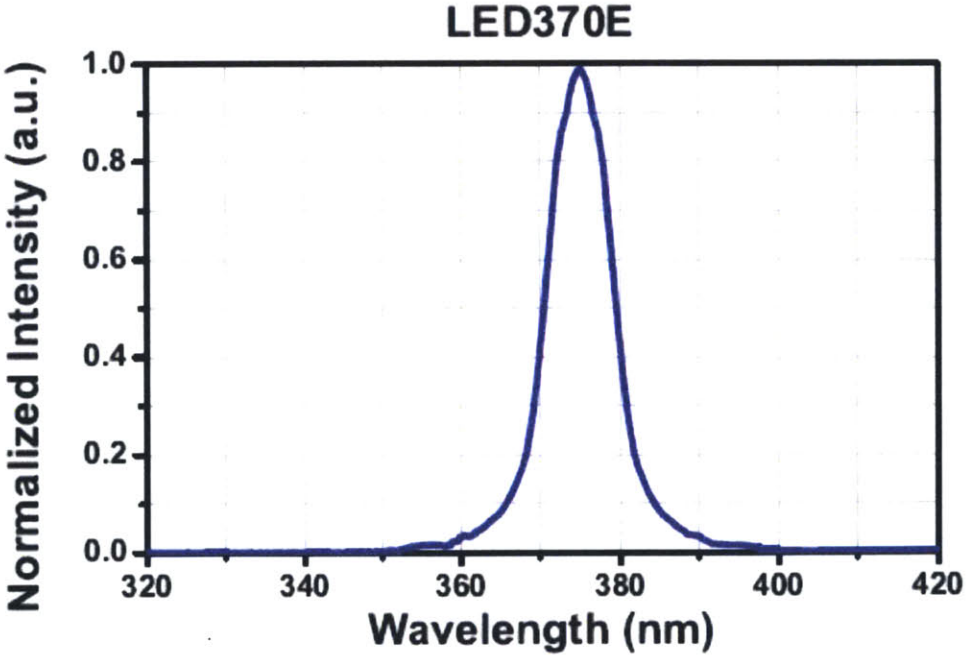

B.6 390 nm LED

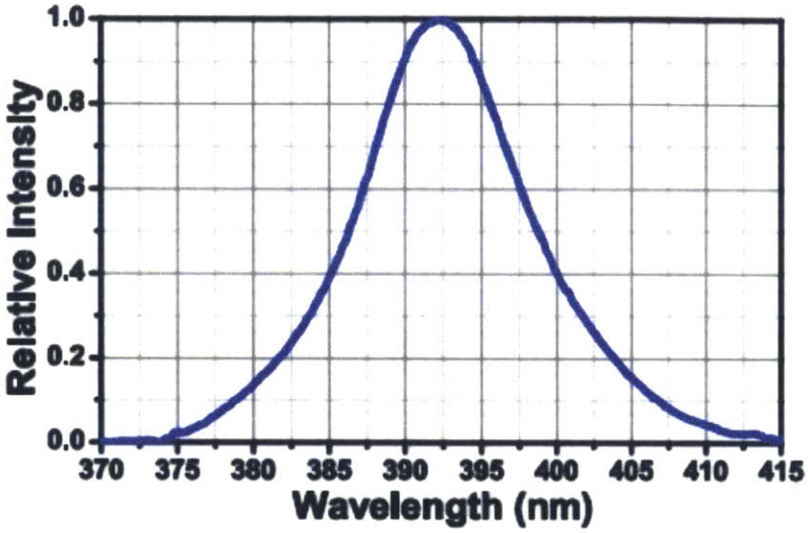

B.7 405 nm LED

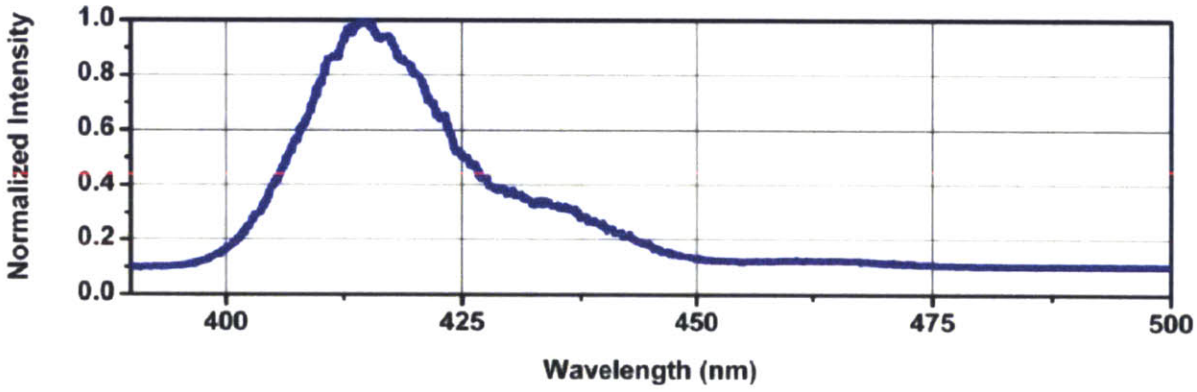

B.8 430 nm LED

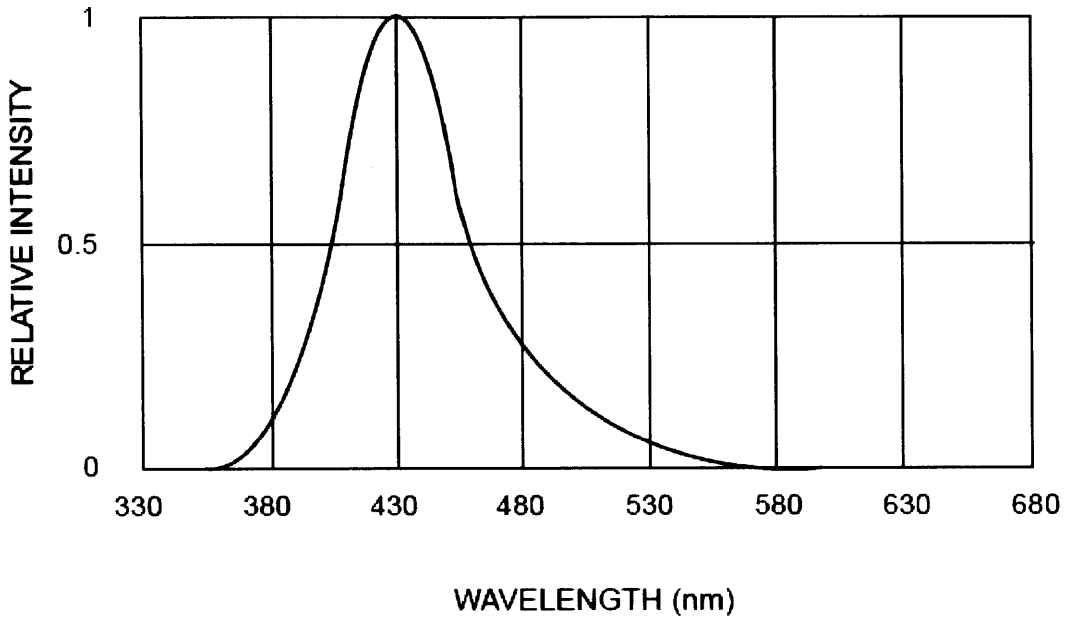
1
0.5
0
RELATIVE INTENSITY
330
380
430
480
530
580
630
680
WAVELENGTH (nm)

Appendix C

Monte Carlo Photon Absorbance and Fluorescence Simulation

The following code was written in MATLAB to perform simulations of photons moving through absorbing and fluorescing material. Since these simulations require billions of iterations, all math operations have been vectorised.

```
function PhotonSimVectorized( abs, fl, numPhotonsToLaunch, fname, saveData)
%PhotonSim Simulate photon moving through absorbing and fluorescing
%material

%    abs: an absorbance standard struct
%        abs.wl: a vector of wavelength values
%        abs.data: a vector of absorbance values such that the absorbance at
%        abs.wl(i) equals abs.data(i)
%    fl: a fluorescence standard struct
%        fl.wl: a vector of wavelength values
%        fl.eCDF: a matrix of i rows and j columns of cumulative distribution
%        functions providing the probability that a fluoresced photon will
%        have a specific wavelength
%        Each row of eCDF is associated with the wavelength of the photon
%        that was absorbed, and each column is the wavelength associated with
%        resulting fluorescence.
%        Ex: fl.eCDF(i, :) = the fluoresnce wavelength cumulative  probability
%        distribution for a photon with wavelength i that was absorbed
%        Ex: fl.eCDF(i, j) = the cumulative probability that after a photon
%        with wavelength i has been absorbed, it will fluoresce at
%        wavelength fl.wl(j)
%        Note: The actual wavelengths associated with the absorbed photon
%        are defined below in the code - see tCDFStart - and are assumed to
%        increment by 1 above that.
%    numPhotonsToLaunch: the number of photons to simulate
%    fname: the file name to save the results
%    saveData: 0 or 1 flag to save extra data

    % Create the detector
    % detector type, detector radius, x-offest, y-offset, acceptance angle
    d = CreateDetector('circle', 0.06, 0.648, 0, degtorad(11.5));
    % 0.648 is actual spacing in PEAT-LEDIF

    % initialze variable to store the wavelength and fluoresnce number of
    % detected photons
```

```
    detPhotons = zeros(max(1000, round(numPhotonsToLaunch*10000/100000000)),
2);

    %initialize main counter variables
    absorbed = 0;
    missed = 0;
    detected = 0;

    %set the excitation wavelength
    excWl = 375;

    %Set the height of the LED - used to make light source more realistic
    %(less of a point source)
    ledHeight = 0.5;

    %Wavelength that index 1 of the CDFs start at
    tCDFStart = 350;

    %Define the maximum size for the intermediate arrays
    maxC = 100000;  %this seems like a good balance of memory/speed

    %Define the maximum absorbable wavelength that produces fluorescence
    maxAbsorbabelWL = tCDFStart + size(fl.eCDF, 1)-1;

    %ps is a three-dimension array of photon position and direction
    % [ x dx;
    %   y dy;
    %   z dz]
    ps = zeros(3, 2, maxC);

    %dS is a 2x1 matrix defined as [1; photon_step_size];
    %dS makes calculating the new photon position simply ps*dS
    dS = ones(2, 1, maxC);

    %store the wavelength of the photons described by ps
    wl = zeros(maxC, 1);

    %stores the absorption coefficients for photons - each wavelength has a
    %unique coefficient
    mu_a = zeros(maxC, 1);


    %This for loop controls the total number calculations to perform
    for iter = 1:maxC:numPhotonsToLaunch
        if(saveData)
            fullPhotonData = cell(maxC,1);
            dSSaved = cell(maxC, 1);
            wlSaved = cell(maxC, 1);
            detInd = [];
        end
        %At the start of each for loop iteration, reset the main variables
        %set all x and y positions to 0, and z to - ledHight
        ps(1, 1, :) = 0;
        ps(2, 1, :) = 0;
```

```
ps(3, 1, :) = -ledHeight;

%Generate arrays of random numbers to use for elevation and azimuth
%Light coming out of LED is normally distributed from the Z axis
elev = normrnd(pi/2, degtorad(15), maxC, 1);
%Light is uniformly around the z axis (e.g. any point in the x, y
%plane
az = rand(maxC, 1).*2.*pi;

% equations taken from matlab sph2cart function
% used to find unit vector
ps(3, 2, :) = sin(elev);
rcoselev = cos(elev);
ps(1, 2, :) = rcoselev .* cos(az);
ps(2, 2, :) = rcoselev .* sin(az);

%The initial mu is always the same because of the excitation
%wavelength
%The index is the wavelength offset by the wavelength of the first
%index
initial_mu = abs.data(round(excWl) - abs.wl(1) + 1);

%Calculate the initial first step size - it is a combination of
%first moving to the z=0 plane and then the random step
%To test, set initial_mu equal to inf
%Step size is -ln(rand) / absorption coefficient
dS(2, 1, :) = ledHeight/ps(3,2,:) + reshape(-log(rand(maxC, 1))...
    ./initial_mu, 1, 1, maxC);

%move each photon to the z = 0 plane and also to first absorbance
%event
for q = 1: maxC
    if(saveData)
       fullPhotonData{q,1} = ps(:,:,q);
       dSSaved{q, 1} = dS(2,1,q);
    end
    ps(:,1, q) = ps(:, :, q) * dS(:, :, q);
end

%The new wavelength is found by picking a random number and using
%it to select the wavelength from an inverse cdf for the excitaton
%wavelength

%efficiently find new wavelength of photons - this only works
%because the excitation wavelength is the same for all photons the
%first absorbance event

%generate random numbers
A = rand(maxC,1);
%sort the random numbers, keeping track of the indexes
[B, ind] = sort(A);
j = 1;
for i = 1: maxC
    searching = 1;
    %Go through and match the random number to its cdf wavelength
```

```
    while(searching)
       if(B(i) < fl.eCDF(excWl - tCDFStart + 1, j))
            wl(ind(i)) = fl.wl(j);
            searching = 0;
       else
           j = j + 2;%Plus 2 to stay with integer wavelength values
       end
    end
end

%lookup absorbance values for all photons
mu_a(:, 1) = abs.data(wl - abs.wl(1) + 1);

%find new step size for each photon
dS(2, 1, :) = reshape(-log(rand(maxC, 1))./mu_a(:, 1), 1, 1, maxC);

%Find new direction for photon
%Make sure that it's an even distribution (just picking random
%between 0 and pi does not give randomly distributed values on
%sphere)
elev = asin(2.*rand(maxC, 1)-1);
az = rand(maxC, 1).*2.*pi;

% equations taken from matlab sph2cart function
% used to find unit vector
ps(3, 2, :) = sin(elev);
rcoselev = cos(elev);
ps(1, 2, :) = rcoselev .* cos(az);
ps(2, 2, :) = rcoselev .* sin(az);

%move each photon to the second absorbance event
%As far as I can tell, there is no way to vectorize this
for q = 1: maxC
   if(saveData)
       fullPhotonData{q,1} = [fullPhotonData{q,1}; ps(:,:,q)];
       dSSaved{q, 1} = [dSSaved{q,1}; dS(2,1,q)];
       wlSaved{q,1} = wl(q);
   end
   ps(:,1, q) = ps(:, :, q) * dS(:, :, q);
end

%At this point in the code, every photon is at the site of the
%second absorbance event

%still alive is a logical array to track if the photons are still
%being absorbed/fluoresced
stillAlive = true(1, 1, maxC);

%absEvents keeps track of the number of times photons are
%absorbed/fluoresced
absEvents = 1;

%loop until all the photons have been detected, missed, or totally
%absorbed
while (sum(stillAlive) > 0)
```

```
            % Identify all photons that are back across the z plane - this
            % is a requirement for the possibility of being detected
            inZPlane = stillAlive & (ps(3,1,:) < 0);

            % Of the photons with z<0, find photons with acceptable angles
            angleInRange =  inZPlane & (acos(ps(3, 2, :)) > (pi - d.angle));

            % For photons that are possibly detected, move them back to z=0
            % to test if they fall in the area of the detector
            % This length is simply the ratio of the z position and dz
            tempDs = ps(3, 1, :) ./ ps(3,2, :).*angleInRange;

            %check if the position of the photon (when z=0) falls within the
            %detector area
            pDetections = angleInRange & (((ps(1,1,:) - tempDs.*ps(1,2,:)) ...
                - d.x).^2 + ((ps(2,1,:) - tempDs.*ps(2,2,:)) -d.y).^2 <
d.size^2);

            if(saveData)
                ii = find(inZPlane);
                for j = 1:numel(ii)
                    a =[ps(:,1,ii(j)) [0; 0; 0]];
                    x = (ps(1,1,ii(j)) - tempDs(ii(j)).*ps(1,2,ii(j)));
                    y = (ps(2,1,ii(j)) - tempDs(ii(j)).*ps(2,2,ii(j)));
                    b =[x 0; ...
                        y 0; ...
                        0 0];
                    t = [a; b];
                    fullPhotonData{ii(j),1} = [fullPhotonData{ii(j),1}; t];
                    dSSaved{ii(j), 1} = [dSSaved{ii(j),1}; dS(2,1,ii(j))];
                    wlSaved{ii(j), 1} = [wlSaved{ii(j), 1}; wl(ii(j))];
                end
            end

            %store the detections
            sumDetections = sum(pDetections);
            if(sumDetections)
                detPhotons(detected+1:detected+sumDetections, 1) =
wl(pDetections);
                detPhotons(detected+1:detected+sumDetections, 2) = absEvents;
                detected = detected + sumDetections;
                if(saveData)
                    detInd = [detInd; find(pDetections)];
                end
            end

            %increment the number of absorbance events
            absEvents = absEvents + 1;

            %A photon is "missed" if it passes the x-y plane but does not
            %hit the detector
            missed = missed + sum(inZPlane) - sum(pDetections);

            %any photon that crossed the x-y plane are now inactive
```

```
            stillAlive(inZPlane) = false;

            %Find photons which are completely absorbed and make then
            %inactive
            absorbedPhotons = stillAlive & reshape((wl > maxAbsorbabelWL), ...
                1, 1, maxC);
            absorbed = absorbed + sum(absorbedPhotons);
            stillAlive(absorbedPhotons) = false;

            %Any photons still alive are given new wavelength
            %Operation non-vectorizable because different CDF for each
            %wavelength
            totalStillAlive = sum(stillAlive);
            %get all indexes for active photons
            saInd = find(stillAlive);
            %select random numbers for picking new wavelength
            tRand = rand(totalStillAlive, 1);
            for c=1:totalStillAlive
                %use the photon's current wavelength to select which CDF to
                %use
                %Since the cdf is sorted, the fastest way to find the index
                %of the new wavelength is just to sum the total number of
                %values less than the random number
                ind = (fl.eCDF(wl(saInd(c)) - tCDFStart + 1, :)  <
tRand(c,1));
                %store the new wavelength
                wl(saInd(c)) = floor(fl.wl(sum(ind)));
            end

            %look up the new absorption coefficients for the new wavelengths
            mu_a(stillAlive, 1) = abs.data(wl(stillAlive) - abs.wl(1) + 1);

            %find new step size for each alive photon
            dS(2, 1, stillAlive) = reshape(-log(rand(totalStillAlive, 1))./...
                mu_a(stillAlive, 1), 1, 1, totalStillAlive);

             %Find new direction for photon
             %Make sure that it's an even distribution (just picking random
             %between 0 and pi does not give randomly distributed values on
             %sphere)
             elev = asin(2.*rand(totalStillAlive, 1)-1);
             az = rand(totalStillAlive, 1).*2.*pi;

             % equations taken from matlab sph2cart function
             % used to find unit vector
             ps(3, 2, stillAlive) = sin(elev);
             rcoselev = cos(elev);
             ps(1, 2, stillAlive) = rcoselev .* cos(az);
             ps(2, 2, stillAlive) = rcoselev .* sin(az);

            %move each photon to the second absorbance event
            for q = 1: totalStillAlive
                if(saveData)
                    fullPhotonData{saInd(q),1} =
[fullPhotonData{saInd(q),1};...
```

```
                    ps(:,:,saInd(q))];
                dSSaved{saInd(q), 1} = [dSSaved{saInd(q),1};
dS(2,1,saInd(q))];
                wlSaved{saInd(q),1} = [wlSaved{saInd(q),1}; wl(saInd(q))];
            end
            ps(:,1, saInd(q)) = ps(:, :, saInd(q)) * dS(:, :, saInd(q));
        end

        %check for possible overrun on detected photon array
        if(detected > numel(detPhotons)/2 - 50)
            detPhotons = [detPhotons; zeros(round(numPhotonsToLaunch*...
                10000/100000000), 2)];
        end
    end
    dil = numel(detInd);
    if(saveData && dil > 0)
        tempname = strrep(fname, '.mat', '');
        tempname = strcat(tempname, 'FD', num2str(round(iter/maxC)),
'.mat');
        pData = cell(dil,1);
        pWl = cell(dil, 1);
        pDS = cell(dil, 1);
        for di = 1:dil
            pData(di, 1)  = fullPhotonData(detInd(di), 1);
            pWl(di, 1) = wlSaved(detInd(di), 1);
            pDS(di, 1) = dSSaved(detInd(di), 1);
        end
        save(tempname, 'pData', 'pWl', 'pDS');
    end
    save(fname, 'detected', 'missed', 'absorbed', 'detPhotons');
end
end


function [ detector ] = CreateDetector( type, size, x, y, acceptanceAngle )
%CreateDetector Create the detector structure
%   type: either "circle" or 'square'
%   size: if type is circle, this is the radius (in cm); if type is square
%   this is [x_length y_length]
%   x: x location of detector (cm)
%   y: y location of detector (cm)
%   acceptanceAngle: The angle of accepted photons in radians

    detector = struct();
    detector.type = type;
    detector.size = size;
    detector.x = x;
    detector.y = y;
    detector.angle = acceptanceAngle;

end
```

Appendix D

DOM Instrument Microcontroller Code

The following code is used to control the instrument described in Chapter 3. It includes the main instrument code along with libraries for control of a real time clock and LED driver.

D.1 Main Instrument Code

D.1.1 Header File

```
/**
Description:      A header file that defines all pin connections and global
constants for the Brunei Controller board version 2.

Author:           Schuyler Senft-Grupp
Version:          1.0
Date:             1/20/14

**/

#ifndef __BRUNEI_CONTROLLER__
#define __BRUNEI_CONTROLLER__

#include <Arduino.h>


/*********************************************
//GLOBAL CONSTANTS
*********************************************/
const unsigned int BATTERY48_NOT_CONNECTED_LEVEL = 100;    // Minimum ADC
value that we assume means battery is not connected
const unsigned int BATTERY48_WARNING_LEVEL = 570;          // Set to 43 volts
- but not actually implemented yet
const uint16_t MAX_INTEGRATION_TIME = 10000;               // The maximum
allowed USB4000 integration time
const uint16_t MIN_INTEGRATION_TIME = 10;                  // The minimum
allowed USB4000 integration time
const uint8_t MAX_LOOP_ERRORS = 5;                         // The number of
errors in loop() before power cycling
const uint8_t MINIMUM_ALARM_SECCONDS = 5;.                 // The minimum time
the alarm can be set for in seconds

const byte ACK = 6;       //ASCII ack used by USB4000
const byte NAK = 21;      //ASCII nak used by USB4000
```

```
const uint8_t WITH_CRLF = 1;
const uint8_t NO_CRLF = 0;

// COLOR DEFINITIONS FOR STATUS LEDs
const uint8_t RED =     0b00000110;
const uint8_t GREEN =   0b00000101;
const uint8_t BLUE =    0b00000011;
const uint8_t YELLOW =  0b00000100;
const uint8_t TEAL =    0b00000001;
const uint8_t PURPLE =  0b00000010;
const uint8_t WHITE =   0b00000000;
const uint8_t BLACK =   0b00000111;

// ERROR VALUES
const uint8_t SD_FAIL = (1<<3) | RED;
const uint8_t FILE_FAIL = (3<<3) | RED;
const uint8_t USB4000_FAIL = (5<<3) | RED;
const uint8_t BATTERY48_NOT_CONNECTED = (3<<3) | YELLOW;
const uint8_t USB4000_ERROR_1 = (1<<3) | TEAL;
const uint8_t USB4000_ERROR_2 = (2<<3) | TEAL;
const uint8_t USB4000_ERROR_3 = (3<<3) | TEAL;
const uint8_t USB4000_ERROR_4 = (4<<3) | TEAL;
const uint8_t USB4000_ERROR_5 = (5<<3) | TEAL;

/*****************************************
//PIN ASSIGNMENTS
*****************************************/

//Spectrometer serial communication
const uint8_t SpecRx = 0;
const uint8_t SpecTx = 1;
//Spectrometer scan trigger
const uint8_t specTrigger = 4;

// RTC Alarm and battery charger status are both pin 3
// This pin is pulled up to the Arduino Voltage
// It is pulled down EITHER when the RTC Alarm goes off
// or if the battery is charging
const uint8_t rtcAlarmAndChargeStatus = 3;

//Specialized pins for excitation LEDs
const uint8_t ledOutputEnable = 2;
const uint8_t ledLatchEnable = 5;

//Pull selfReset High to reset the microcontroller
const uint8_t selfReset = 6;

//Pins to enable DC-DC voltage regulators
const uint8_t twelveVoltEnable = 8;
const uint8_t fiveVoltEnable = 9;

//Chip Select pins for SD card and RTC
const uint8_t csSD = A0;
const uint8_t csRTC = A1;

//Status LEDs - pull low to turn on
```

```
const uint8_t redLED = 7;
const uint8_t greenLED = A3;
const uint8_t blueLED = A2;

//Analog input pins for reading battery voltages
const uint8_t batteryVoltage48 = A4;
const uint8_t batteryVoltage37 = A5;

void SetLEDColor(const uint8_t *color){
  digitalWrite(redLED,        bitRead(*color, 0));
  digitalWrite(greenLED,      bitRead(*color, 1));
  digitalWrite(blueLED,       bitRead(*color, 2));
}

// Turn on the LED to a color for "timing" milliseconds
// Turn off LED when done
void SetLEDColorWithDelay(const uint8_t *color, int timing) {
    SetLEDColor(color);
    delay(timing);
    SetLEDColor(&BLACK);
}

//Blink an LED color "blinks" number of times
void Blink (uint8_t color, int timing, int blinks){
  for(int i = 0 ; i< blinks; i++){
    SetLEDColorWithDelay(&color, timing);
    delay(timing);
  }
}

#endif
```

D.1.2 Main Code and Helper Functions

```
/*Instructions for trigger mode 3 - external hardware trigger

To take a scan send
'S' with no carriage return or line feed
This makes the USB4000 ready to be triggerd from the external signal
Once it is triggered, it will integrate for the given time, and then return
the data once it's done
*/

//Import header with all pin assignments, global constants, and several
helper functions
#include <BruneiController.h>

#include <SPI.h>
#include <SD.h>
#include <RTC_DS3234.h>
#include <TLC_5916.h>
#include <avr/sleep.h>

/*********************************************
```

```
//GLOBAL VARIABLES
*****************************************/
uint8_t loopIteration = 0;          // keeps track of the number of times
through loop()
uint8_t loopErrors = 0;             // counts the number of times an error is
encounterd in loop()
uint8_t errorValue = 0;             // holds an error value between 1 and 31,
and an LED color
                                    // error value is stored in bits 7 to 3
                                    // color is stored in bits 2 to 0

//Default data logging settings (Consider removing initial values to free up
SRAM)
uint8_t dataLogSeconds = 15;
uint8_t dataLogMinutes = 0;
uint8_t dataLogHours = 0;

uint16_t lampWarmUpTime = 1000;  // Lamp warm up time in milliseconds
uint16_t ledWarmUpTime = 100;   // LED warm up/stabilization time in
milliseconds
boolean waitForFullCharge = false;   // if this is true, then the sensor will
stay on until the 3.7v battery completes charging

//USB4000 settings
uint16_t BOXCAR_WIDTH = 5;    //Values greater than 3 slow down transfer
speeds
                              //Slower transfer speeds are good so that the SD
card can keep up
uint16_t PIXEL_TRANSFER_SPACING = 10;
uint16_t currentIntegrationTime = 0;

//index of LED_NAMES + 1 is the bit address of that LED on the TLC_5916
char* const LED_NAMES [] ={"LED365", "LED430", "LED405", "LED390", "LED370",
"AbsLOW", "AbsHI_", "Turbid"};
uint8_t const LED_CURRENT_GAIN [] = {CG_20, CG_30, CG_30, CG_100, CG_30,
CG_10, CG_10, CG_10};
uint16_t ledIntegrationTime [] = {5000, 5000, 5000, 5000, 5000, 10000, 5000,
1000};  //array for initial integration times for each LED
                                                                        //the
last one is for absorbance source
boolean recordingDarkSpectrum = false;
uint8_t darkSpectrum = 0b0;             // each bit refers to a dark spectrum
recorded for
                                        // the integration time specified by
that bit index

boolean configParamsChanged = false;

RTCDateTime currentTime;  //global variable to store the current date and
time
RTCDateTime alarmTime;    //global variable to store the current alarm time

char dateStr[ ] = "00/00/00 00:00:00";          // a character array for
printing date/time
char dataFileName[ ] = "files/MM_DD_YY.txt";    // a character array for the
file name
```

```
File dataFile;                                  // A File variable to point
to the currently open file

//helper variables
int bytesRead;
char dataBuffer[8];
int incomingByte;
char data = 0;
uint8_t openTries = 0;
uint8_t usb4000Tries = 0;
uint8_t startLoc = 0;

uint16_t bv37Analog;
uint16_t bv48Analog;

/*****************************************************************************
Setup() runs once on startup. It does the foloowing:
1. Initializes all I/O pins
2. Initializes serial and SPI communication
3. Gets the current date/time from the real-time clock
4. Begins communication with the SD card. Opens or creates the data file
5. Reads from a config file
6. Initializes communication with the USB4000 spectrometer. Sets the boxcar,
     pixel mode, and trigger modes for spectrum collection.
7. Performs basic error checking to make sure everything is working properly
*****************************************************************************/
void setup(){
  Serial.begin(9600);

  //Initialize pins
  pinMode(fiveVoltEnable, OUTPUT);
  pinMode(twelveVoltEnable, OUTPUT);
  pinMode(selfReset, OUTPUT);
  digitalWrite(selfReset, LOW);

  pinMode(specTrigger, OUTPUT);
  digitalWrite(specTrigger, LOW);

  pinMode(greenLED, OUTPUT);
  pinMode(blueLED, OUTPUT);
  pinMode(redLED, OUTPUT);
  SetLEDColor(&BLACK);

  //read the battery voltages
  analogReference(INTERNAL);  //set the analog reference to the internal 1.1
volts
  delay(10);
  for(uint8_t i = 0; i<5; i++){     // The arduino website claims that after
changing reference sources
    analogRead(batteryVoltage37);   // the first few analog reads can be off
  }
  delay(10);
  bv37Analog = analogRead(batteryVoltage37);

  analogRead(batteryVoltage48);
  delay(10);
  bv48Analog = analogRead(batteryVoltage48);
```

```
  //turn on the 5V DC-DC converter. This automatically turns on the USB4000
  digitalWrite(fiveVoltEnable, HIGH);

  //Cycle through colors
  SetLEDColorWithDelay(&RED,     250);
  SetLEDColorWithDelay(&YELLOW,  250);
  SetLEDColorWithDelay(&GREEN,   250);
  SetLEDColorWithDelay(&TEAL,    250);
  SetLEDColorWithDelay(&BLUE,    250);
  SetLEDColorWithDelay(&PURPLE,  250);
  SetLEDColorWithDelay(&WHITE,   250);
  SetLEDColorWithDelay(&BLACK,   250);

  //Initialize chip select control pinspins
  pinMode(10, OUTPUT);         //Arduino defined chip select
  pinMode(csSD, OUTPUT);       //SD card chip select
  digitalWrite(csSD, HIGH);
  pinMode(csRTC, OUTPUT);      //Real time clock chip select
  digitalWrite(csRTC, HIGH);

  SPI.begin();  //start SPI communication

  //see if the SD card is present and can be initialized:
  if (!SD.begin(csSD)) {
    errorValue = SD_FAIL;
    goto initializeError;
  }else{
    Blink(GREEN, 500, 1);    //1st green blink
  }

  RTC.begin(csRTC);                    //initialize RTC with chip select pin
  RTC.clearAlarmFlags();               //clear the alarm flags because we
don't know what state the RTC was in
  currentTime = RTC.getRTCDateTime();  //need to do this initial read -
otherwise strange bug occurs
                                       //where SD.open() fails the first
time.

  dateTime2String(&currentTime);       //convert date and time to human
readable string
                                       //which is stored in the variable
dateStr

  //If a configuration file exists, load its info
  //Try to open the config file for reading
  openTries = 0;
  do{
    dataFile = SD.open("CONFIG.TXT", FILE_READ);
    openTries++;
  }while(!dataFile && openTries < 4);

  if(dataFile){
    Blink(GREEN, 500, 1);    //2nd green blink
    while(dataFile.available()){
      data = dataFile.read();
      if (data == 'B'){
```

```
        BOXCAR_WIDTH = (uint16_t)dataFile.parseInt();
      }else if (data == 'C'){
        waitForFullCharge = (dataFile.parseInt() != 0);
      }else if (data == 'H'){
        dataLogHours = (uint16_t)dataFile.parseInt();
      }else if (data=='L'){
        ledWarmUpTime = (uint16_t)dataFile.parseInt();
      }else if (data == 'M'){
        dataLogMinutes = (uint16_t)dataFile.parseInt();
      }else if (data == 'P'){
        PIXEL_TRANSFER_SPACING = (uint16_t)dataFile.parseInt();
      }else if (data == 'S'){
        dataLogSeconds = (uint16_t)dataFile.parseInt();
      }else if (data =='W'){
        lampWarmUpTime = (uint16_t)dataFile.parseInt();
      }else if(data >= 'a' && data <= 'h'){
        ledIntegrationTime[data - 'a'] = (uint16_t) dataFile.parseInt();
      }
    }
    dataFile.close();
  }else{
    Blink(PURPLE, 300, 3);  //Let user know that the config file wasn't read
  }

  //error check to make sure integration times are in correct range
  for(int i = 0; i<7; i++){
    int j = constrain(ledIntegrationTime[i], MIN_INTEGRATION_TIME,
MAX_INTEGRATION_TIME);
    if(j != ledIntegrationTime[i]){
     ledIntegrationTime[i] = j;
     configParamsChanged = true;
    }
  }

  //Open the logfile - if this is the first time, then add a header line
  dataFile = SD.open("LOGFILE.TXT", FILE_WRITE);
  if(dataFile.size() < 5){
    dataFile.print("Date\tTime\t3.7V Battery\t48V
Battery\tCharging\tErrors");
  }

  //print some status information
  dataFile.println("");
  dataFile.print(dateStr);  //Measurement date and time
  dataFile.print('\t');
  dataFile.print(((float)bv37Analog)*0.00466);  //3.7 battery voltage =
bv37Analog/1023*1.1*(325/75)
  dataFile.print('\t');
  dataFile.print(((float)bv48Analog)* 0.0555 + 0.7491);  //48 battery voltage
= bv48Analog/1023*1.1*(4990/100)
  dataFile.print('\t');

digitalRead(rtcAlarmAndChargeStatus)?dataFile.print("No\t"):dataFile.print("Y
es\t"); //if the 3.7v battery is charging
  dataFile.close();

  //set the file name to the current date
```

```
  dataFileName [6] = currentTime.months/10 + '0';
  dataFileName [7] = currentTime.months%10 + '0';
  dataFileName [9] = currentTime.days/10 + '0';
  dataFileName [10] = currentTime.days%10 + '0';
  dataFileName [12] = currentTime.year/10 + '0';
  dataFileName [13] = currentTime.year%10 + '0';

  //If the directory 'files' does not exist, create it
  if(!SD.exists("files")){
    SD.mkdir("files/");
  }

  //Try to open the data file for writing/appending new data
  openTries = 0;
  do{
    dataFile = SD.open(dataFileName, FILE_WRITE);
    openTries++;
  }while(!dataFile && openTries < 4);

  if(!dataFile){                          //If unable to open the file, alert
to an error
    errorValue = FILE_FAIL;
    goto initializeError;
  }

  pinMode(rtcAlarmAndChargeStatus, INPUT);          //Interrupt pin for RTC
alarm

  //Start the TLLC5916 LED driver with pins 5 and 7 controlling the SPI
communications
  tlc5916.begin(ledOutputEnable,ledLatchEnable);

  delay(500);
  //Wait for spectrometer to finish initializing
  //If everything goes well, green LED will blink 6 times
  Blink(BLUE, 500, 5);

  usb4000Tries = 0;
  do{
    Blink(BLUE, 500<<usb4000Tries, 1);
    clearSerial();
    Serial.write(' ');
    Serial.flush();
    delay(50);
    incomingByte = Serial.read();
    usb4000Tries++;
  }while(incomingByte != NAK && usb4000Tries < 4);

  //Check if there has been a major failure with the USB4000 startup - if so,
restart
  if(incomingByte != NAK){
    errorValue = USB4000_FAIL;
    goto initializeError;
  }

  //Set boxcar average
  Serial.write('B');
```

```
  Serial.write(highByte(BOXCAR_WIDTH));
  Serial.write(lowByte(BOXCAR_WIDTH));
  delay(10);
  if(Serial.read() != ACK){
    errorValue = USB4000_ERROR_1;
    goto initializeError;
  }

  //set Pixel Mode
  Serial.write('P');
  Serial.write(0);
  Serial.write(1);
  Serial.write(highByte(PIXEL_TRANSFER_SPACING));
  Serial.write(lowByte(PIXEL_TRANSFER_SPACING));
  Serial.flush();
  delay(100);
  if(Serial.read() != ACK){
    errorValue = USB4000_ERROR_2;
    goto initializeError;
  }

  //Set trigger to 2 external synchronization
  Serial.write('T');
  Serial.write(0);
  Serial.write(3);
  Serial.flush();
  delay(100);
  if(Serial.read() != ACK){
    errorValue = USB4000_ERROR_3;
    goto initializeError;
  }

  //change the spectrometer to ASCII mode
  Serial.write('a');
  Serial.write('A');
  Serial.flush();
  if(!asciiACKRead(NO_CRLF)){
    errorValue = USB4000_ERROR_4;
    goto initializeError;
  }

initializeError:
  if(errorValue > 0){
    Blink(errorValue & 0b00000111, 500, errorValue >> 3);
    digitalWrite(selfReset, HIGH);
  }

  //If program gets here, then everything is working fine
  Blink(GREEN, 300, 3);
}

void loop(){
  recordingDarkSpectrum = false;
  //If we don't need to change the integration time, then we already
  //must have the dark spectrum as well, so skip ahead
  if(currentIntegrationTime == ledIntegrationTime[loopIteration]){
    goto doneSettingIntegration;
```

```
  }

  //check if the darkSpectrum bit has been set for this iteration
  if(!(1<<(loopIteration) & darkSpectrum)){
      recordingDarkSpectrum = true;
  }

  //Go through and set the flag for all other scans with the same integration
time
  for(uint8_t i = loopIteration; i < 8; i++){
   if(ledIntegrationTime[loopIteration] == ledIntegrationTime[i]){
    darkSpectrum = darkSpectrum | 1<<i;
   }
  }

  //Convert binary value into ASCII characters
  dataBuffer[0] = ledIntegrationTime[loopIteration]/10000;
  dataBuffer[1] = (ledIntegrationTime[loopIteration]%10000)/1000;
  dataBuffer[2] = (ledIntegrationTime[loopIteration]%1000)/100;
  dataBuffer[3] = (ledIntegrationTime[loopIteration]%100)/10;
  dataBuffer[4] = (ledIntegrationTime[loopIteration]%10);

  //Remove the leading zeros
  startLoc = 0;
  while(dataBuffer[startLoc] == 0){
    startLoc++;
  }

  //Set the spectrometer integration time
  Serial.write('I');
  Serial.flush();
  delay(10);

  Serial.read();

  while(startLoc<5){
    Serial.write(dataBuffer[startLoc] + '0');
    Serial.flush();
    delay(10);
    Serial.read();//read the echoed character
    startLoc++;
  }
  dataFile.flush();

  Serial.write(13);
  Serial.flush();
  delay(20);

  //check that command received successfully
  if(!asciiACKRead(WITH_CRLF)){
    errorValue = USB4000_ERROR_1;
    Blink(errorValue & 0b00000111, 500, errorValue >> 3);
    loopErrors++;
    clearSerial();
    goto endloop;
  }
```

```
  currentIntegrationTime = ledIntegrationTime[loopIteration];
  delay(100);

doneSettingIntegration:

  if(recordingDarkSpectrum){
    dataFile.print("Dark  ");
  }else{
    dataFile.print(LED_NAMES[loopIteration]);
  }
  dataFile.write(' ');
  dataFile.print(dateStr);

  //Check that the USB4000 is ready to take a scan
  if(!USB4000Ready()){
    errorValue = USB4000_ERROR_2;
    Blink(errorValue & 0b00000111, 500, errorValue >> 3);
    loopErrors++;
    goto endloop;
  }

  //Turn on blue LED to let user know that integration taking place
  SetLEDColor(&BLUE);

  //Turn on Excitation Source
  if(recordingDarkSpectrum){
    //do nothing
  }else if(loopIteration < 5 ){
    tlc5916.disableOutput();
    tlc5916.ezSetCurrentConfigurationCode(LED_CURRENT_GAIN[loopIteration]);
    tlc5916.ezSetPinsOnOff(1 << loopIteration);
    tlc5916.enableOutput();
    dataFile.flush();
    delay(ledWarmUpTime);
  }else if(loopIteration < 7){            //Absorbance measurements low and
high
    digitalWrite(twelveVoltEnable, HIGH);  //turn on lamp
    delay(lampWarmUpTime);                  // give time to warm up
  }else{  //turbidity measurement
    tlc5916.disableOutput();
    tlc5916.ezSetCurrentConfigurationCode(LED_CURRENT_GAIN[loopIteration]);
    tlc5916.ezSetPinsOnOff(0b00011111);    //turn on all LEDs
    tlc5916.enableOutput();
    dataFile.flush();
  }

  //Start the scan
  Serial.write('S');
  Serial.flush();

  //USB4000 should immediately respond with 2 bytes
  //The first value is 'S' echo
  //The second value is etx or stx
  dataBuffer[0] = 0;
  dataBuffer[1] = 3;
  bytesRead = Serial.readBytes(dataBuffer, 2);
```

```
  if(dataBuffer[0] != 'S' || dataBuffer[1] == 3){  //error with Spec
    tlc5916.disableOutput();  //turn off LED
    digitalWrite(twelveVoltEnable, LOW); //turn off absorbance source
    errorValue = USB4000_ERROR_3;
    Blink(errorValue & 0b00000111, 500, errorValue >> 3);
    clearSerial();
    loopErrors++;
    goto endloop;
  }

  delay(30);  //need this for low integration times

  Serial.setTimeout(ledIntegrationTime[loopIteration] + 500);  //set the
timeout to the integration time plus 0.5 second

  //Trigger the spectrometer to start scan
  digitalWrite(specTrigger, HIGH);
  delay(1);
  digitalWrite(specTrigger, LOW);

  //wait here until spectrum begins transmitting - will timeout if nothing
received
  bytesRead = Serial.readBytes(dataBuffer, 5);

  //Gets here once the USB4000 starts transmitting data
  tlc5916.disableOutput();  //turn off LED once scan has been captured
  digitalWrite(twelveVoltEnable, LOW); //turn off absorbance source
  SetLEDColor(&BLACK);

  if(bytesRead == 0){ //the read operation timedout so there must have been
an error
    errorValue = USB4000_ERROR_4;
    Blink(errorValue & 0b00000111, 500, errorValue >> 3);
    clearSerial();
    loopErrors++;
    goto endloop;
  }

  Serial.setTimeout(20);    //set the serial timeout to 20ms (probably can be
shorter)
  while(Serial.readBytes(dataBuffer, 1)){
   digitalWrite(greenLED, LOW);
   if(dataBuffer[0] == 13 || dataBuffer[0] == '>' || dataBuffer[0] == 10){
      //do nothing
   }else{
     dataFile.write(dataBuffer[0]);
   }
   digitalWrite(greenLED, HIGH);
  }
  dataFile.println("");
  dataFile.flush();  //make sure all the data was written to the SD card

  if(!recordingDarkSpectrum){
    loopIteration++;
  }

  if(loopIteration >= 8){
```

```
    while(waitForFullCharge && !digitalRead(rtcAlarmAndChargeStatus)){ //if
set, wait here until battery is charged
      digitalWrite(blueLED, !digitalRead(blueLED));
    };
    dataFile.close();
    dataFile = SD.open("LOGFILE.TXT", FILE_WRITE);
    dataFile.print("C:");

digitalRead(rtcAlarmAndChargeStatus)?dataFile.print("No\t"):dataFile.print("Y
es\t"); //if the 3.7v battery is charging
    dataFile.close();
    writeConfigFile();                    //update the config file with any
changes
    Blink(WHITE, 100, 3);                 //All Done

    //The RTC neesd to hav 5V applied ot it to set the alarm - I don't know
why.
    delay(1000);
    RTC.clearAlarmFlags();                //clear the alarm flags so that they
can be triggered later
    //currentTime = RTC.getAlarm1();      //Get the previous time that the
alarm was set for
    setRTCAlarm(dataLogSeconds, dataLogMinutes, dataLogHours);
//set the alarm for some time from now

    Serial.end();
    pinMode(SpecTx, INPUT);
    pinMode(SpecRx, INPUT);
    //Now turn off the 5V supply and wait before setting the interrupt
    digitalWrite(fiveVoltEnable, LOW);      //turn off the five volt dc-dc
converter - now we are operating from the 3.7v battery
    delay(1000);

    sleepNow();     //go to sleep
    //Next 2 lines were required with v1 hardware - should no longer be
necessary
//    digitalWrite(fiveVoltEnable, HIGH);     //if we get here, then we just
woke up - we need the 5V line to do the reset
//    delay(10);
    digitalWrite(selfReset, HIGH);    //After wake up, reset the arduino
  }
  loopErrors = 0;

endloop:
  //If there have been repeated loop errors, we will try to restart
  if(loopErrors >= MAX_LOOP_ERRORS){
    dataFile.close();
    //Open the logfile - if this is the first time, then add a header line
    dataFile = SD.open("LOGFILE.TXT", FILE_WRITE);
    dataFile.print("E:");
    dataFile.print(errorValue, BIN);
    dataFile.close();
    writeConfigFile();
    digitalWrite(selfReset, HIGH);
  }

  if(loopErrors > 0 && recordingDarkSpectrum){
```

```
    darkSpectrum &= ~(1<<loopIteration);
  }
  digitalWrite(greenLED, LOW);
}

void writeConfigFile(){
  if(!configParamsChanged){
    return;
  }

  SD.remove("config.txt");  //remove the current config file
  dataFile = SD.open("config.txt", FILE_WRITE);
  dataFile.print("B=");
  dataFile.println(BOXCAR_WIDTH);
  dataFile.print("C=");
  dataFile.println(waitForFullCharge);
  dataFile.print("H=");
  dataFile.println(dataLogHours);
  dataFile.print("L=");
  dataFile.println(ledWarmUpTime);
  dataFile.print("M=");
  dataFile.println(dataLogMinutes);
  dataFile.print("P=");
  dataFile.println(PIXEL_TRANSFER_SPACING);
  dataFile.print("S=");
  dataFile.println(dataLogSeconds);
  dataFile.print("W=");
  dataFile.println(lampWarmUpTime);

  for(int i = 0; i < 8; i ++){
    dataFile.print((char)('a' + i));
    dataFile.print('=');
    dataFile.println(ledIntegrationTime[i]);
  }
  dataFile.close();
}

//convert the RTCDateTime structure to human readable string
void dateTime2String(RTCDateTime * dt){

  //"00 / 00 / 00   00 : 00 : 00"
  // 01 2 34 5 67 8 90 1 23 4 56
  dateStr[6] = dt->year/10 + '0';
  dateStr[7] = dt->year%10 + '0';

  dateStr[0] = dt->months/10 + '0';
  dateStr[1] = dt->months%10 + '0';

  dateStr[3] = dt->days/10 + '0';
  dateStr[4] = dt->days%10 + '0';

  dateStr[9] = dt->hours/10 + '0';
  dateStr[10] = dt->hours%10 + '0';

  dateStr[12] = dt->minutes/10 + '0';
  dateStr[13] = dt->minutes%10 + '0';
```

```
  dateStr[15] = dt->seconds/10 + '0';
  dateStr[16] = dt->seconds%10 + '0';
}

//Interrupt service routine called when the RTC alarm interrupt fires
void rtcAlarmISR(){
  //nothing to do here
}

//Function to help set the RTC alarm
//Sets the alarm to a time (seconds, minutes, hours) from the current time
//input variables can be arbitrary numbers but limiited to 255 by variable
size
//must be at least 5 seconds
void setRTCAlarm(uint8_t ss, uint8_t mm, uint8_t hh){
  if(hh == 0 && mm == 0 && ss < MINIMUM_ALARM_SECCONDS)
    ss=MINIMUM_ALARM_SECCONDS;

  alarmTime.seconds = currentTime.seconds + ss;
  alarmTime.minutes = currentTime.minutes + mm + alarmTime.seconds/60;
  alarmTime.hours = currentTime.hours + hh + alarmTime.minutes/60;

  alarmTime.seconds = alarmTime.seconds%60;
  alarmTime.minutes = alarmTime.minutes%60;
  alarmTime.hours = alarmTime.hours%24;

  //set the alarm
  RTC.setAlarm1(alarmTime.seconds, alarmTime.minutes, alarmTime.hours);
}

void sleepNow(){          // here we put the arduino to sleep
  /* Now is the time to set the sleep mode. In the Atmega8 datasheet
   * http://www.atmel.com/dyn/resources/prod_documents/doc2486.pdf on page 35
   * there is a list of sleep modes which explains which clocks and
   * wake up sources are available in which sleep mode.
   *
   * In the avr/sleep.h file, the call names of these sleep modes are to be
found:
   *
   * The 5 different modes are:
   *     SLEEP_MODE_IDLE         -the least power savings
   *     SLEEP_MODE_ADC
   *     SLEEP_MODE_PWR_SAVE
   *     SLEEP_MODE_STANDBY
   *     SLEEP_MODE_PWR_DOWN     -the most power savings
   *
   * For now, we want as much power savings as possible, so we
   * choose the according
   * sleep mode: SLEEP_MODE_PWR_DOWN
   *
   */

  set_sleep_mode(SLEEP_MODE_PWR_SAVE);   // Set which sleep mode to enter
  sleep_enable();                        // Enable the sleep bit in the mcucr
register
  attachInterrupt(1, rtcAlarmISR, LOW); // Use interrupt 1 (pin 3) and run
function
```

```
                                        // rtcAlarmISR when pin 3 gets LOW
  sleep_mode();                         // Put device to sleep!!

  //******THE PROGRAM CONTINUES FROM HERE AFTER WAKING UP*********//

  sleep_disable();    // disable sleept first thing after waking from sleep:
  detachInterrupt(1); // disables interrupt 1 on pin 3 so the
  // rtcAlarmISR code will not be executed
   // during normal running time.
}

//check if USB4000 is responding while in ASCII mode
boolean USB4000Ready(){
  char bytes [6];
  int numBytesRead;
  uint8_t expectedNumBytes = 6;
  Serial.write(' ');
  Serial.flush();   //wait for transmission to complete
  Serial.setTimeout(100);  //set the timeout to something reasonable
  numBytesRead = Serial.readBytes(bytes, expectedNumBytes);
  if(numBytesRead != expectedNumBytes)
    return false;

  return (bytes[1] == 21);
}

void clearSerial(){
  while(Serial.available() > 0){        //clear the serial port
    Serial.read();
    delay(10);
  }
}

boolean asciiACKRead(uint8_t mode){
  char bytes [7];
  int numBytesRead;
  uint8_t expectedNumBytes = 7;
  if(mode == NO_CRLF)
    expectedNumBytes = 5;

  Serial.setTimeout(1000);  //I found that 300ms was not enough. 1000ms seems
to be enough
  numBytesRead = Serial.readBytes(bytes, expectedNumBytes);
  if(numBytesRead != expectedNumBytes){
    return false;
  }

  if(mode == WITH_CRLF && bytes[2] == ACK)
    return true;
  if(mode == NO_CRLF && bytes[0] == ACK)
    return true;

  return false;
}
```

D.2 Real Time Clock (RTC) Library

D.2.1 Header File

```
//Written by Schuyler Senft-Grupp skysg@mit.edu
//3/27/12
//Feel free to use this code however you wish!

//This library makes several assumptions and does not take full advantage of
all the RTC DS3234 features.
//Below is a list of some of these limitations:
// 1. times are all assumed to be 24 hours (i.e. no AM/PM)
// 2. there are several alarm modes - the only one implemented here is a
match with seconds/minutes/hours
// 3. only Alarm1 can be set

#ifndef __RTC_DS3234_H__
#define __RTC_DS3234_H__

#include <stdio.h>

typedef struct {
      uint8_t seconds, minutes, hours, days, months, year;
}RTCDateTime;

class RTC_DS3234{
public:
      void begin(uint8_t cs);
      void setRTCDateTime(uint8_t ss, uint8_t mm, uint8_t hh, uint8_t d,
uint8_t month, uint8_t year);
      RTCDateTime getRTCDateTime();
      void setAlarm1(uint8_t ss, uint8_t mm, uint8_t hh);
      RTCDateTime getAlarm1();
      void clearAlarmFlags();

private:
      uint8_t _cs;
      uint8_t dataArray [7];
      uint8_t oldSPISettings;

      void readWrite(uint8_t address, uint8_t dataLength);
      uint8_t bcd2bin (uint8_t val);
      uint8_t bin2bcd (uint8_t val);

};

extern RTC_DS3234 RTC;

#endif // __RTC_DS3234_H__
```

D.2.2 RTC Library Code

```
//Written by Schuyler Senft-Grupp skysg@mit.edu
//3/27/12
//Feel free to use this code however you wish!

#include "RTC_DS3234.h"
#include <SPI.h>

RTC_DS3234 RTC;

//RTC DS3234 register addresses
const uint8_t DT_READ = 0x00;
const uint8_t DT_WRITE = 0x80;
const uint8_t A1_READ = 0x07;
const uint8_t A1_WRITE = 0x87;
const uint8_t A2_READ = 0x0B;
const uint8_t A2_WRITE = 0x8B;
const uint8_t CONTROL_READ = 0x0E;
const uint8_t CONTROL_WRITE = 0x8E;
const uint8_t STATUS_READ = 0x0F;
const uint8_t STATUS_WRITE = 0x8F;

//RTC DS3234 register bit functions
const uint8_t A1IE = 0;
const uint8_t A2IE = 1;
const uint8_t INTCN = 3;
const uint8_t A1F = 0;
const uint8_t A2F = 1;


//function to initialize the RTC
//this should be called before any other functions
void RTC_DS3234::begin(uint8_t cs){
      _cs = cs;
      pinMode(_cs, OUTPUT);                     //set chip select pin as
output
      digitalWrite(_cs, HIGH);                  //set chip select high to
disable SPI communications
      dataArray[0] = 0b00000101;                //{_BV(INTCN) | _BV(A1IE)};
      readWrite(CONTROL_WRITE, 1);        //Write to control register to turn
on alarm 1 interrupts
      delay(10);                                      //not sure this is
necessary
}

//Set the RTC date and time
//This should rarely be necessary
void RTC_DS3234::setRTCDateTime(uint8_t ss, uint8_t mm, uint8_t hh, uint8_t
d, uint8_t m, uint8_t y){
      dataArray[0] = bin2bcd(ss);
      dataArray[1] = bin2bcd(mm);
      dataArray[2] = bin2bcd(hh);
      dataArray[3] = 1;
      dataArray[4] = bin2bcd(d);
      dataArray[5] = bin2bcd(m);
```

```
      dataArray[6] = bin2bcd(y);
      readWrite(DT_WRITE, 7);
}

//read the date and time from the RTC
//data is returned in a RTCDateTime struct (see header file)
RTCDateTime RTC_DS3234::getRTCDateTime(){
      readWrite(DT_READ, 7);
      return (RTCDateTime) {bcd2bin(dataArray[0]), bcd2bin(dataArray[1]),
                                          bcd2bin(dataArray[2]),
bcd2bin(dataArray[4]),
                                          bcd2bin(dataArray[5]),
bcd2bin(dataArray[6])};
}

//sets Alarm1 on the RTC
//the alarm interrupt pin will go low when the RTC seconds/minutes/hours
matches the values ss, mm, hh
//after the alarm has been triggered, the user must call clearAlarmFlags to
manually reset the pin to high
void RTC_DS3234::setAlarm1(uint8_t ss, uint8_t mm, uint8_t hh){
      dataArray[0] = bin2bcd(ss);
      dataArray[1] = bin2bcd(mm);
      dataArray[2] = bin2bcd(hh);
      dataArray[3] = 0b10000000;
      readWrite(A1_WRITE, 4);
}

//returns the value that Alarm1 is set to
RTCDateTime RTC_DS3234::getAlarm1(){
      readWrite(A1_READ, 4);
      return (RTCDateTime) {bcd2bin(dataArray[0]), bcd2bin(dataArray[1]),
bcd2bin(dataArray[2]), dataArray[3],0,0};
}

//clears the alarm flags in the status register
//this function should be called once soon after the call to begin()
//and MUST be called after the alarm is triggered in order to allow the alarm
to be triggered again in the future
void RTC_DS3234::clearAlarmFlags(){
      readWrite(STATUS_READ, 1);                //read the value of the
status register
      dataArray[0] = dataArray[0] & ~(_BV(A1F) | _BV(A2F)); //set only the
alarm flags back to zero without changing any of the other bits
      readWrite(STATUS_WRITE, 1);               //write the new status
register
}

//simultaneously reads and writes to the RTC
//the values in dataArray are written to the RTC, and the bytes read are
stored in dataArray
void RTC_DS3234::readWrite(uint8_t address, uint8_t dataLength){
      oldSPISettings = SPCR; //store the old SPI control register settings
      SPI.setBitOrder(MSBFIRST); //Set the SPI settings for the DS3234
      SPI.setDataMode(SPI_MODE1);

      digitalWrite(_cs, LOW); //Enable the device for communication
```

```
      SPI.transfer(address);  //Send the register address to read/write to

      for(uint8_t i = 0; i<dataLength; i++){
            dataArray[i] = SPI.transfer(dataArray[i]); //Read/write all
values in array
      }

      digitalWrite(_cs, HIGH); //Disable the device for SPI communication
      SPCR = oldSPISettings;  //Reset the SPI settings
}

//convert binary coded decimal to binary
uint8_t RTC_DS3234::bcd2bin (uint8_t val)
{
    return val - 6 * (val >> 4);
}

//convert binary to binary coded decimal
uint8_t RTC_DS3234::bin2bcd (uint8_t val)
{
    return val + 6 * (val / 10);
}
```

D.3 LED Driver Library

D.3.1 Header File

```
//Written by Schuyler Senft-Grupp skysg@mit.edu
//3/27/12
//Feel free to use this code however you wish!


#ifndef __TLC_5916_H__
#define __TLC_5916_H__

#include <stdio.h>
#include "pins_arduino.h"

const uint8_t CG_100=0b11111111;
const uint8_t CG_90=0b11001111;
const uint8_t CG_80=0b01100111;
const uint8_t CG_70=0b10011011;
const uint8_t CG_60=0b00110011;
const uint8_t CG_50=0b00000011;
const uint8_t CG_40=0b01100101;
const uint8_t CG_30=0b11001110;
const uint8_t CG_20=0b10110010;
const uint8_t CG_10=0b10110000;


class TLC_5916{
```

```
public:
      void begin(uint8_t oe, uint8_t le);
      void enableOutput();
      void disableOutput();
      bool ezSetPinsOnOff(uint8_t vals);
      bool ezSetCurrentConfigurationCode(uint8_t vals);
      bool ezReadErrorStatus(uint8_t vals);

private:
      uint8_t _oePin;
      uint8_t _lePin;
      uint8_t oldSPISettings;
      uint8_t oldSPSRSettings;

      void changeToSpecialMode();
      void changeToNormalMode();
      void readWrite(uint8_t vals);
      void specialWrite(uint8_t oeValues, uint8_t leValues, uint8_t
dataLength);

};

extern TLC_5916 tlc5916;

#endif __TLC_5916_H__
```

D.3.2 LED Driver Main Code

```
#include "TLC_5916.h"
#include <SPI.h>

const uint8_t OE_SPECIAL_MODE = 0b10111111;
const uint8_t LE_SPECIAL_MODE = 0b00010000;
const uint8_t OE_NORMAL_MODE = 0b10111111;
const uint8_t LE_NORMAL_MODE = 0b00000000;

TLC_5916 tlc5916;

void TLC_5916::begin(uint8_t oe, uint8_t le){
      _oePin = oe;
      _lePin = le;
      pinMode(_oePin, OUTPUT);
      digitalWrite(_oePin, HIGH);
      pinMode(_lePin, OUTPUT);
      digitalWrite(_lePin, LOW);
}

void TLC_5916::enableOutput(){
      digitalWrite(_oePin, LOW);
}

void TLC_5916::disableOutput(){
      digitalWrite(_oePin, HIGH);
}
```

```
bool TLC_5916::ezSetPinsOnOff(uint8_t pinsToTurnOnOff){
      readWrite(pinsToTurnOnOff);    //shift the data into the chips
      digitalWrite(_lePin, HIGH);    //latch the data
      delay(1);
      digitalWrite(_lePin, LOW);
}

bool TLC_5916::ezSetCurrentConfigurationCode(uint8_t vals){
      uint8_t isOE;
      isOE = digitalRead(_oePin);
      changeToSpecialMode();
      readWrite(vals);
      digitalWrite(_lePin, HIGH);
      digitalWrite(_lePin, LOW);
      changeToNormalMode();
      digitalWrite(_oePin, isOE);
}

bool TLC_5916::ezReadErrorStatus(uint8_t errorVals){
      changeToSpecialMode();
      specialWrite(0b10000000, 0, 5);
      digitalWrite(_oePin, HIGH);//Pull OE high to latch error codes to shift
register
      readWrite(errorVals);    //Shift in the error values
      changeToNormalMode();
}

void TLC_5916::changeToSpecialMode(){
      specialWrite(OE_SPECIAL_MODE ,  LE_SPECIAL_MODE, 5);
}

void TLC_5916::changeToNormalMode(){
      specialWrite(OE_NORMAL_MODE ,  LE_NORMAL_MODE, 5);
}

void TLC_5916::readWrite(uint8_t vals){
      oldSPISettings = SPCR;  //store the old SPI control register settings
      oldSPSRSettings = SPSR;
      SPI.setBitOrder(MSBFIRST); //Set the SPI settings for the TLC_5916
      SPI.setDataMode(SPI_MODE0);
      SPI.setClockDivider(SPI_CLOCK_DIV128);

      SPI.transfer(vals);      //Read/write all values in array

      SPCR = oldSPISettings;         //Reset the SPI settings
      SPSR = oldSPSRSettings;
}

void TLC_5916::specialWrite(uint8_t oeValues, uint8_t leValues, uint8_t
dataLength){
      oldSPISettings = SPCR;
      oldSPSRSettings = SPSR;
      SPI.end();//stop the SPI so that we can manually control the clock pin
      uint8_t bitMask = 0b10000000;
      for(uint8_t i = 0; i<dataLength; i++){
            digitalWrite(13, LOW);
            digitalWrite(_oePin, 1 && (bitMask & oeValues));
```

```
      digitalWrite(_lePin, 1 && (bitMask & leValues));
      digitalWrite(13, HIGH);
      bitMask = bitMask>>1;
}
SPI.begin();              //restart SPI
SPCR = oldSPISettings;    //restore old SPI settings
SPSR = oldSPSRSettings;

}
```

Appendix E

Design Files for Gigahertz Data Acquisition Circuit Board

This appendix contains the schematics and bill of materials for the gigahertz data acquisition board described in Chapter 4. For a digital copy of all files (schematics, bill of materials, board layout), please email skysg@alum.mit.edu. The digital files can be directly sent to a manufacturer (e.g. Advanced Assembly) to have the components ordered, board printed, and board assembled.

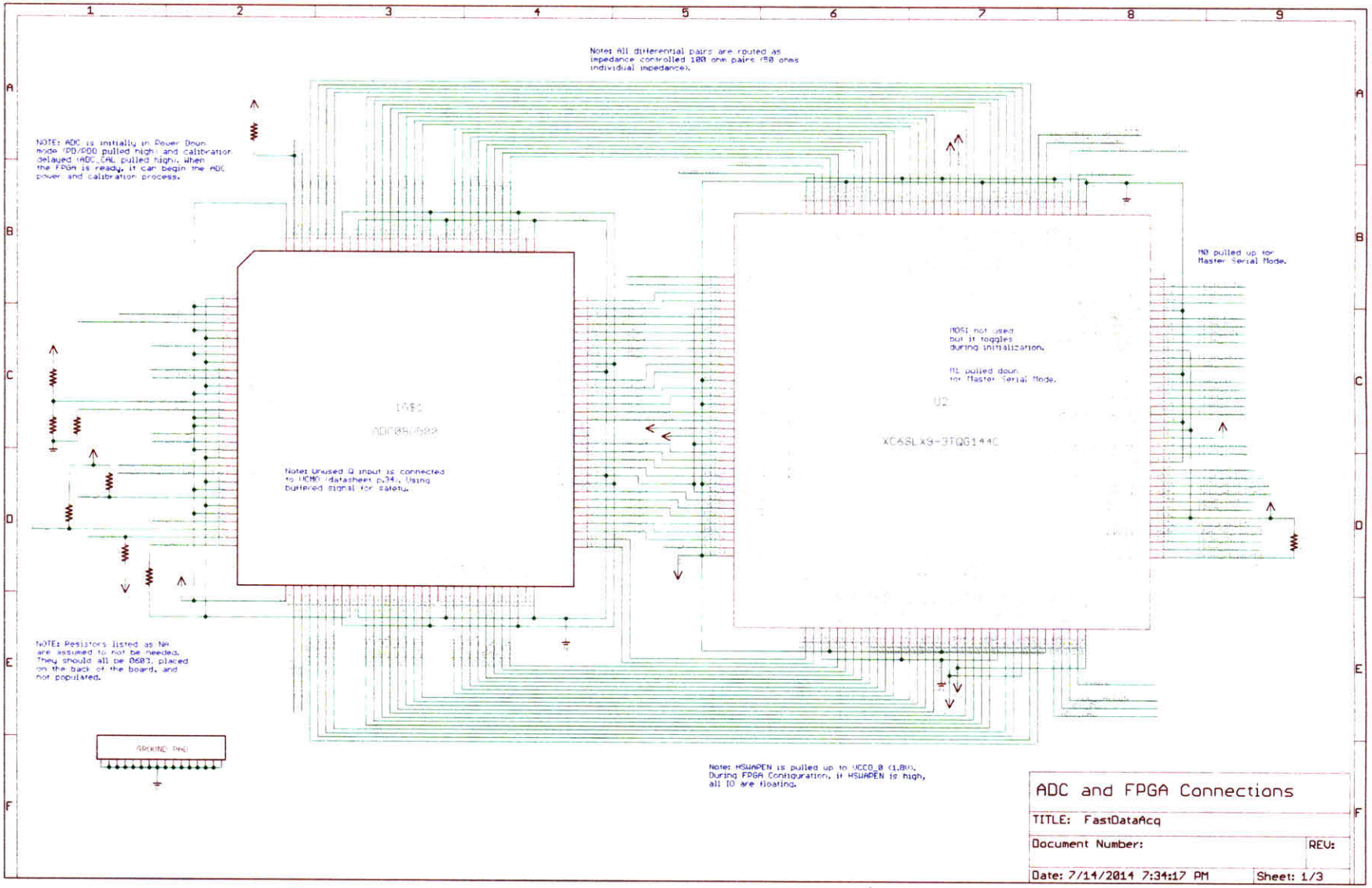
Note: All differential pairs are routed as impedance controlled 100 ohm pairs (50 ohms individual impedance).
NOTE: ADC is initially in Power Down mode (PD/PDD pulled high) and calibration delayed (ADC_CAL pulled high). When the FPGA is ready, it can begin the ADC power and calibration process.
M0 pulled up for Master Serial Mode.
MOSI not used but it toggles during initialization.
M1 pulled down for Master Serial Mode.
U2
XC6SLX9-3TQG144C
Note: Unused Q input is connected to HDMI datasheet p.34. Using buffered signal for safety.
NOTE: Resistors listed as NA are assumed to not be needed. They should all be 0603, placed on the back of the board, and not populated.
GROUND PAD
Note: HSWAPEN is pulled up to VCCO_0 (1.8V). During FPGA Configuration, if HSWAPEN is high, all IO are floating.
ADC and FPGA Connections
TITLE: FastDataAcq
Document Number:
REV:
Date: 7/14/2014 7:34:17 PM
Sheet: 1/3

Power Regulation

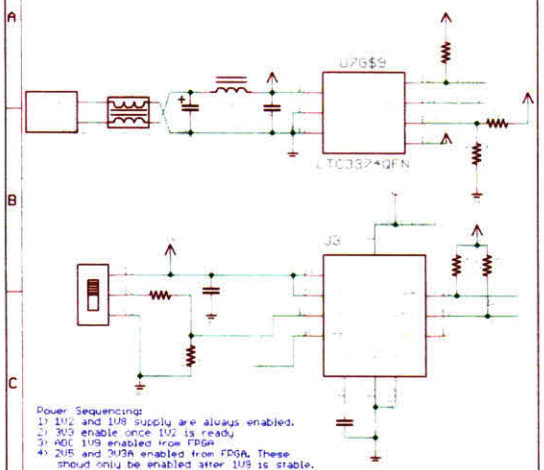

Power Sequencing:
1) 1V2 and 1V8 supply are always enabled.
2) 3V3 enable once 1V2 is ready
3) ADC 1V9 enabled from FPGA
4) 2V5 and 3V3A enabled from FPGA. These should only be enabled after 1V8 is stable.

FPGA & Digital Power

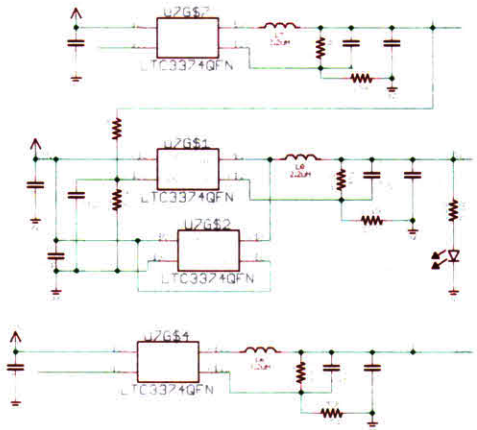

Note: Ven is 420mV. Resistor divider should account for transient droop of at least 100mV.

Note: 1V8 must be enabled before FPGA starts config process so that HSWAPEN is high and all FPGA pins are tri-stated.

ADC and Analog Power

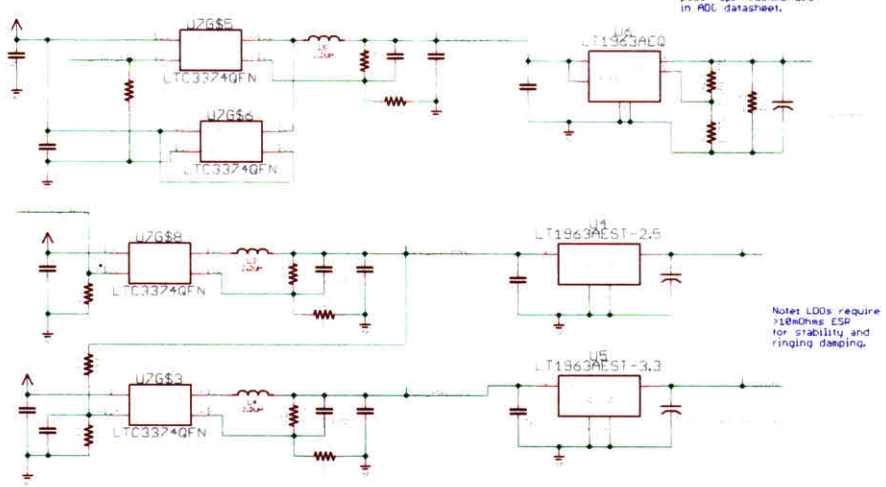

Note: 100 ohm resistor damps overshoot on power up. Recommended in ADC datasheet.

Note: LDOs require >10mOhms ESR for stability and ringing damping.

ADC Bypassing

Each analog and digital supply pin is bypassed with a 0.1 uF capacitor. A 33uF capacitor is also placed within 1" of pins. Ferrite chokes isolate each supply from each other.

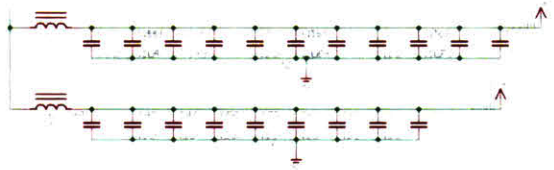

FPGA Bypassing

Vccint bypassing

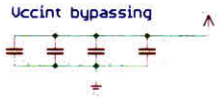

Vccaux bypassing

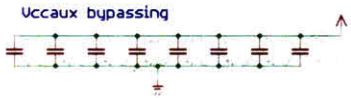

Vcc0 bypassing

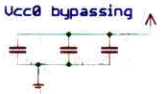

Vcc1 bypassing

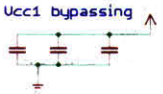

Vcc2 bypassing

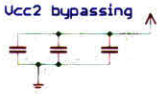

Vcc3 bypassing

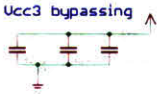

Power Supply and Bypassing	
TITLE: FastDataAcq	
Document Number:	REV:
Date: 7/14/2014 7:34:17 PM	Sheet: 2/3

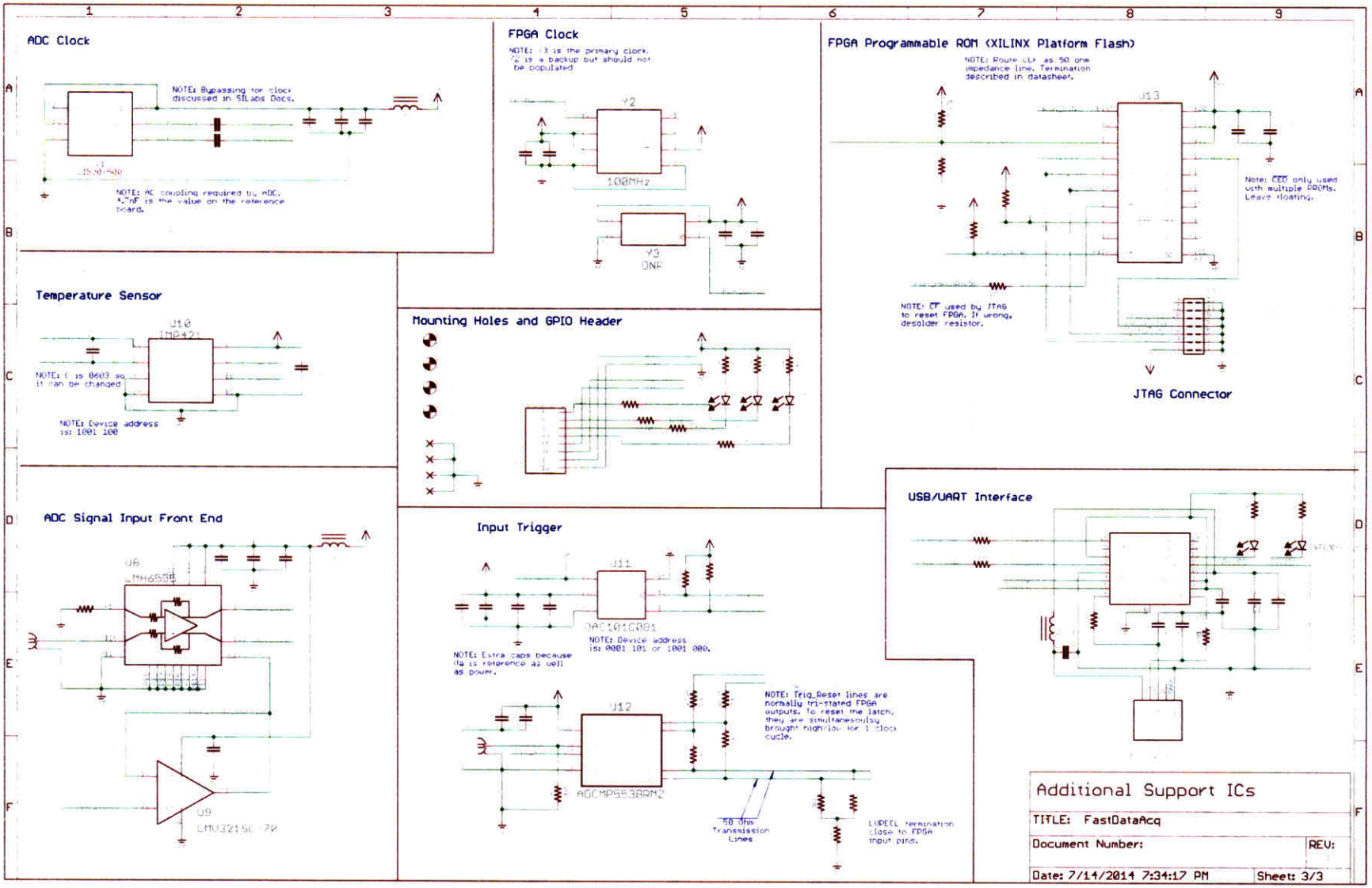
ADC Clock
NOTE: Bypassing for clock discussed in SiLabs Docs.
NOTE: AC coupling required by ADC. 4.7nF is the value on the reference board.
FPGA Clock
NOTE: Y3 is the primary clock. Y2 is a backup but should not be populated
Y2
100MHz
Y3
DNP
FPGA Programmable ROM (XILINX Platform Flash)
NOTE: Route CLK as 50 ohm impedance line. Termination described in datasheet.
J13
Note: CE0 only used with multiple PROMs. Leave floating.
NOTE: CF used by JTAG to reset FPGA. If wrong, desolder resistor.
JTAG Connector
Temperature Sensor
U10
TMP421
NOTE: C is 0603 so it can be changed
NOTE: Device address is: 1001 100
Mounting Holes and GPIO Header
ADC Signal Input Front End
U8
LMH6559
U9
LMV321SC
Input Trigger
U11
DAC101C081
NOTE: Device address is: 0001 101 or 1001 000.
NOTE: Extra caps because Va is reference as well as power.
U12
ADCMP553BRM2
NOTE: Trig_Reset lines are normally tri-stated FPGA outputs. To reset the latch, they are simultaneously brought high/low for 1 clock cycle.
50 Ohm Transmission Lines
LVPECL Termination close to FPGA input pins.
USB/UART Interface
Additional Support ICs
TITLE: FastDataAcq
Document Number:
REV:
Date: 7/14/2014 7:34:17 PM
Sheet: 3/3

Bill of Materials

Parts	Value	MFG PN	Digikey PN	SUPPLIER	Qty
C1, C2, C3, C4, C8, C16, C17, C18, C19, C20, C21,	10uF		445-4112-1-ND	DIGIKEY	12
C10, C11, C14, C27, C28, C29	10pF		445-1769-1-ND	DIGIKEY	6
C12, C13, C15, C30, C31, C32, C39, C40, C83, C88	33uF		445-8238-1-ND	DIGIKEY	10
C24, C25, C26	22uF 150mOhm ESR		P16231CT-ND	DIGIKEY	3
C33, C34, C35, C36, C41, C51, C52, C53, C57, C61,					
C66, C69, C72, C74, C89, C105	4.7uF	CL05A475MQ5NRNC	1276-1056-1-ND	DIGIKEY	16
C37, C38, C42, C43, C46, C56, C58, C62, C63, C76	0.47uF		1276-1779-1-ND	DIGIKEY	10
C5, C9, C23	DNP				3
C6	100uF	ECASD91B107M012K00	490-5480-1-ND	DIGIKEY	1
C60, C64, C65, C67, C68, C70, C71, C73, C75, C80,					
C81, C82, C84, C86, C91, C92, C96, C101, C102,					
C103	.1uF		587-2152-1-ND	DIGIKEY	30
C77	100pF		445-4675-1-ND	DIGIKEY	1
C78, C79	4.7nF		445-13726-1-ND	DIGIKEY	2
C85, C93, C94, C95, C97, C98	10nF		445-1793-1-ND	DIGIKEY	6
C87, C90, C104	1uF		445-9091-1-ND	DIGIKEY	3
C99, C100	47pF		445-1782-1-ND	DIGIKEY	2
D1, D4	LED_0603_RED		LNJ237W82RACT-ND	DIGIKEY	2
D2, D6	LED_0603_BLUE	LTST-C193TBKT-5A	160-1827-1-ND	DIGIKEY	2
D3, D5	LED_0603_GREEN	LTST-C193KGKT-5A	160-1828-1-ND	DIGIKEY	2
J1	MICRO-FIT_3.0_2POS_RA_SMD	436500212	WM1890CT-ND	DIGIKEY	1
J2	USB_MICROAB_SMT	10104111-0001LF	609-4053-1-ND	DIGIKEY	1
L1	CHOKE_CM_ACM7060-301	ACM7060-301-2PL-TL01	445-2214-1-ND	DIGIKEY	1
L13	330	BLM18SG331TN1D	490-3997-1-ND	DIGIKEY	1
L2, L9, L10, L11, L12	26	BLM18SG260TN1D	490-3995-1-ND	DIGIKEY	5
L3, L4, L6, L7	2.2uH		541-1322-1-ND	DIGIKEY	4
L5, L8	2.2uH		541-1220-1-ND	DIGIKEY	2
R1, R2, R4, R6, R26	DNP				5
R10, R13, R14, R16, R17, R20, R23, R24, R25	523k		P523KABCT-ND	DIGIKEY	9
R11, R34	649k		P649KABCT-ND	DIGIKEY	2
R12, R19	150k		1276-3719-1-ND	DIGIKEY	2
R15	113k		P113KABCT-ND	DIGIKEY	1
R18, R28, R33	210k		P210KABCT-ND	DIGIKEY	3
R22	280k		P280KABCT-ND	DIGIKEY	1
R27, R37	270k		P270KABCT-ND	DIGIKEY	2
R29	1.15k 1%	RC1608F1151CS	1276-4649-1-ND	DIGIKEY	1
R3, R5, R8, R21, R41, R44	10k	RC0603J103CS	1276-3817-1-ND	DIGIKEY	8
R30	2k 1%	RC1608F202CS	1276-3495-1-ND	DIGIKEY	1
R31	100	RC1608J101CS	1276-5038-1-ND	DIGIKEY	1
R32	806k		P806KABCT-ND	DIGIKEY	1
R35	845k		P845KABCT-ND	DIGIKEY	1
R36	422k		P422KABCT-ND	DIGIKEY	1
R38, R45, R48, R49, R55, R56, R57, R62, R63, R64,					
R65, R66, R67	330	RC0603J331CS	1276-3787-1-ND	DIGIKEY	13
R39, R40, R50, R51, R52	50	RC0603F49R9C	1276-3590-1-ND	DIGIKEY	5
R42	2.49k		1276-4681-1-ND	DIGIKEY	1
R43, R47	887	ERJ-1GEF8870C	P887ABCT-ND	DIGIKEY	2
R46	1.69k		1276-3491-1-ND	DIGIKEY	1
R53, R54	100 0.1%	ERA-3AEB101V	P100DBDKR-ND	DIGIKEY	2
R58	0		311-0.0GRCT-ND	DIGIKEY	1
R60, R61	27		1276-3577-1-ND	DIGIKEY	2
R7	3.3k 0.1%		P3.3KDBCT-ND	DIGIKEY	1
R9, R59	4.7k	ERJ-1GNJ472C	P4.7AECT-ND	DIGIKEY	2
S1	SLIDER_SPDT_AYZ0102AGRLC	AYZ0102AGRLC	401-2012-1-ND	DIGIKEY	1
U1	ADC08D500	ADC08D500CIYB/NOPB	ADC08D500CIYB/NOPB-ND	DIGIKEY	1
U10	TMP421	TMP421AIDCNT	296-21990-1-ND	DIGIKEY	1
U11	DAC101C081	DAC101C081CIMK/NOPB	DAC101C081CIMK/NOPBCT-ND	DIGIKEY	1
U12	ADCMP553BRMZ	ADCMP553BRMZ	ADCMP553BRMZ-ND	DIGIKEY	1
U13	XCFXXS04	XCF04SVOG20C	122-1288-5-ND	DIGIKEY	1
U14	FT230XQ	FT230XQ-R	768-1130-1-ND	DIGIKEY	1
U2	XC6SLX9-3TQG144C	XC6SLX9-3TQG144C	122-1747-ND	DIGIKEY	1
U3	LTC2955-1	LTC2955CDDB-1#TRMPBF	LTC2955CDDB-1#TRMPBFCT-ND	DIGIKEY	1
U4	LT1963AEST-2.5	LT1963AEST-2.5#PBF	LT1963AEST-2.5#PBF-ND	DIGIKEY	1
U5	LT1963AEST-3.3	LT1963AEST-3.3#PBF	LT1963AEST-3.3#PBF-ND	DIGIKEY	1
U6	LT1963AEQ	LT1963AEQ#PBF	LT1963AEQ#PBF-ND	DIGIKEY	1
U7	LTC3374QFN	LTC3374EUHF#PBF	LTC3374EUHF#PBF-ND	DIGIKEY	1
U8	LMH6555	LMH6555SQ/NOPB	LMH6555SQ/NOPBCT-ND	DIGIKEY	1
U9	LMV321SC-70 .	LMV321IDCKR	296-9568-1-ND	DIGIKEY	1
X1, X2	SMA-142-0701-801/806	142-0701-801	J502-ND	DIGIKEY	2
X3	HEADER_0.1_8P_2R_SMT"	15912080	WM17450-ND	DIGIKEY	1
X4	87832-14	878321420	WM18641-ND	DIGIKEY	1
Y1	SI530-500	530FC500M000DG	530FC500M000DG	SILICON LABS	1
Y2	100MHz	DS1088LU-100+	DS1088LU-100+-ND	DIGIKEY	1
Y3	DNP	500SAAA-ACF	500SAAA-ACF-ND	DIGIKEY	1